Quaternary surface ruptures of the inherited mature Yangsan Ffault: implications for intraplate earthquakes in Southeastern Korea

Sangmin Ha[1,2], Hee-Cheol Kang[1,3], Seongjun Lee[1,4], Yeong Bae Seong[2], Jeong-Heon Choi[5], Seok-Jin Kim[5,6], Moon Son[1]

[1]Department of Geological Sciences, Pusan National University, Busan 46241, South Korea
[2]Department of Geography Education, Korea University, Seoul 02841, South Korea
[3]Institute of Geohazard Research, Pusan National University, Busan 46241, South Korea
[4]Department of Geotechnology & Infrastructure, Byucksan Engineering, Seoul 08380, South Korea
[5]Research Center of Earth and Environmental Sciences, Korea Basic Science Institute, Chungbuk 28119, South Korea
[6]Conservation Science Division, National Research Institute of Cultural Heritage, Daejeon, 34122, South Korea

Correspondence to: Moon Son (moonson@pusan.ac.kr)

Abstract. Earthquake prediction in intraplate regions, such as the Korean PeninsulaSouth Korea, is challenging due to the complexity of fault distributionszones. This study employed diverse methods and data sources to investigatedetect Quaternary surface rupturing along the Yangsan Fault, aiming to understand its long-term earthquake behaviorimprove seismic hazard assessment. Paleoseismic data of the Byeogye section (7.6 km) of the Yangsan Fault arewere analyzed to providereveal insights into earthquake parameters (i.e., timing, displacement, and recurrence intervals) as well asseismic activity, displacement, and structural patterns. Observations from five trench sites indicate at least sixthree faulting events during the Quaternary, with the most recent surface rupturing occurring approximately 3,000 years ago. These events resulted in a cumulative dhorizontal displacement of 3.1–94.076 m and a maximum estimated magnitude of 6.7–7.21. The average slip rate of 0.14–3±0.1 mm/yr suggests a quasi-periodic model with possible recurrence intervals exceeding 130,000 years. The Sstructural patterns indicateimply the reactivation of a pre-existing fault core with top-to-the--west geometry, causing a dextral-strike-slip with a minor reverse component. This study underscores the several surface ruptures with large earthquakes alongcontinuous faulting along the inherited mature fault, the Yangsan Fault, since at least the Early Pleistocene, offering critical contributing valuable insights for seismic hazard assessment in the region and offering a broader understanding of intraplate earthquake dynamics, enhancing for earthquake prediction effort.

Short summary. Unlike episodic plate boundary earthquakes, their randomness makes predicting intraplate earthquakes challenging. This study aids in understanding intraplate earthquake behaviorseismic hazard assessment by analyzing paleoearthquake records of the Yangsan Fault in Korea. Five trench sites revealed sixthree Quaternary surface rupturing

earthquakes, the latest 3,000 years ago, with M_w 6.7-7.~~2~~1. The right lateral fault has a 0.1~~4~~3 mm/yr slip rate, and a recurrence interval over 1~~0~~3,000 years, continuously active since the Quaternary.

1 Introduction

Earthquake prediction is challenging, and large earthquakes with surface ruptures significantly damage infrastructure (Geller et al., 1997; Wyss, 1997; Crampin and Gao, 2010; Woith et al., 2018). To predict large earthquakes, it is necessary to identify the pattern of earthquake occurrences, which can be periodic, quasi-periodic, and random (Shimazaki and Nakata, 1980; McCalpin, 2009). Earthquakes can be categorized as interplate (plate boundary) or intraplate (mid-continental) based on their tectonic location (England and Jackson, 2011; Liu and Stein, 2016). Numerous studies have identified relatively "predictable" cycles, patterns, causes, magnitudes, and epicentres in the interplate, where earthquakes are more frequent, leading to improved earthquake preparedness (e.g., San Andreas Fault, Nankai trough; Powell and Weldon II, 1992; Murray and Langbein, 2006; Smith and Sandwell, 2006; Uchida and Burgmann, 2019; Obara and Kato, 2024).

Large earthquakes in the intraplate occur less frequently than in the interplate but can have devastating impacts (e.g., 1556 Huaxian earthquake-M 8.0, 1976 Tangshan earthquake-M_w 7.8, 1811-1812 New Madrid earthquake, 2001 Gujarat earthquake-M_w 7.6, 2011 Virginia earthquake-M 5.8; Min et al., 1995; Johnston and Schweig, 1996; Hough et al., 2000; Hough and Page, 2011; Wolin et al., 2012). Large intraplate earthquakes have recently received considerable attention and researchers are attempting to understand them based on insights obtained from interplate earthquakes (England and Jackson, 2011; Liu and Stein, 2016; Talwani, 2017). However, intraplate earthquakes exhibit complex spatiotemporal patterns that do not follow general interplate earthquake pattern models (Liu and Stein, 2016; Talwani, 2017). This can partly be explained by the poor catalogue due to their slow slip rates (<1 mm/year) and long recurrence intervals (>1,000 yr). The faults in the intraplate region have a complex distribution rather than those in the interplate region and tend to be selectively reactivated in response to far-field stress ~~The primary reason behind the difficulty in predicting intraplate earthquakes is due to fault zone complexity and far-field stress, resulting in irregular earthquake behaviour~~ (Liu and Stein, 2016; Talwani, 2017).

To understand the unpredictable patterns of intraplate earthquakes, it is necessary not only to collect robust paleoseismic data but also to find connections between paleoseismic data and structural features such as the relationship between geometry and the in-situ stress regime, fault kinematics controlled by pre-existing structure.~~To unravel the complexity of fault zones, it is essential to understand the geometry and internal structure of fault zone, along with the relationship between geometry and the in-situ stress regime, fault kinematics controlled by structure, and the correlation of these kinematics with paleoseismic data.~~

Korea, located on the intraplate, has experienced very few ~~directly~~ damaging earthquakes since instrumented seismic monitoring began. However, medium-sized earthquakes have caused damage to people near the epicentres and raised earthquake awareness (e.g., the 2016 Gyeongju earthquake; the 2017 Pohang earthquake; Kim et al., 2018; Woo et al., 2019). Despite calls for realistic earthquake preparedness, seismic research in South Korea ~~still~~ remains at an early stage compared

to neighbouring countries on plate boundaries, such as Japan and Taiwan. Basic seismic hazard assessment requires the acquisition of robust~~reliable~~ paleoseismic data (Reiter, 1990; Gurpinar, 2005; McCalpin, 2009). The reduction of paleoseismic uncertainty necessitates an expanded dataset, which in turn demands a significant volume of data. Various methods can be employed to efficiently detect Quaternary faults and obtain robust~~reliable~~ paleoseismic parameters. Although this need has been recognized, until recently, paleoseismology studies in Korea have mostly been based on a single trench except recent a few studies~~, with a few exceptions~~ (e.g., Kim et al., 2023). Earthquakes in South Korea appear to follow the quasiperiodic behavior~~a pattern~~ of intraplate earthquakes (Kim and Lee, 2023). To unravel this quasiperiodic pattern of an intraplate fault, it is necessary to collect paleoseismic data from multiple faults with Quaternary surface rupturing to complete the puzzle. In this study, we try to provide clues to the pattern of earthquake behavior of the Yangsan Fault~~ur~~.

This study sought to trace the distribution of the Quaternary surface rupturing during the Holocene and obtain fundamental paleoseismic data on the Yangsan Fault. To achieve this, we applied multiple methods to identify traces of Quaternary surface rupture~~fault~~s with higher accuracy and interpret a highly ~~reliable~~ robust paleoseismic synthesis from the extensive~~obtained large amount of~~ data collected (e.g., five trenches and about ~30 numerical ages). We focused on the Byeokgye section (~~study area;~~ Kim et al., 2022) in the southern part of the northern Yangsan Fault, a major tectonic line in southeastern Korea, to create a geological map ~~s~~ and select trench sites through fieldwork. This study aims to reveal 1) robust paleoseismic data, filling gaps in prior surface rupture documentation, 2) Quaternary reactivation features of intraplate mature fault zones, and 3) the spatiotemporal surface rupturing pattern of the Yangsan Fault~~, a significant tectonic feature in East Asia and Korea~~. The results of this study can be used as essential inputs for seismic hazard assessment and to understand the Quaternary rupturing~~faulting~~ patterns of the Yangsan Fault~~, which is located intraplate~~.

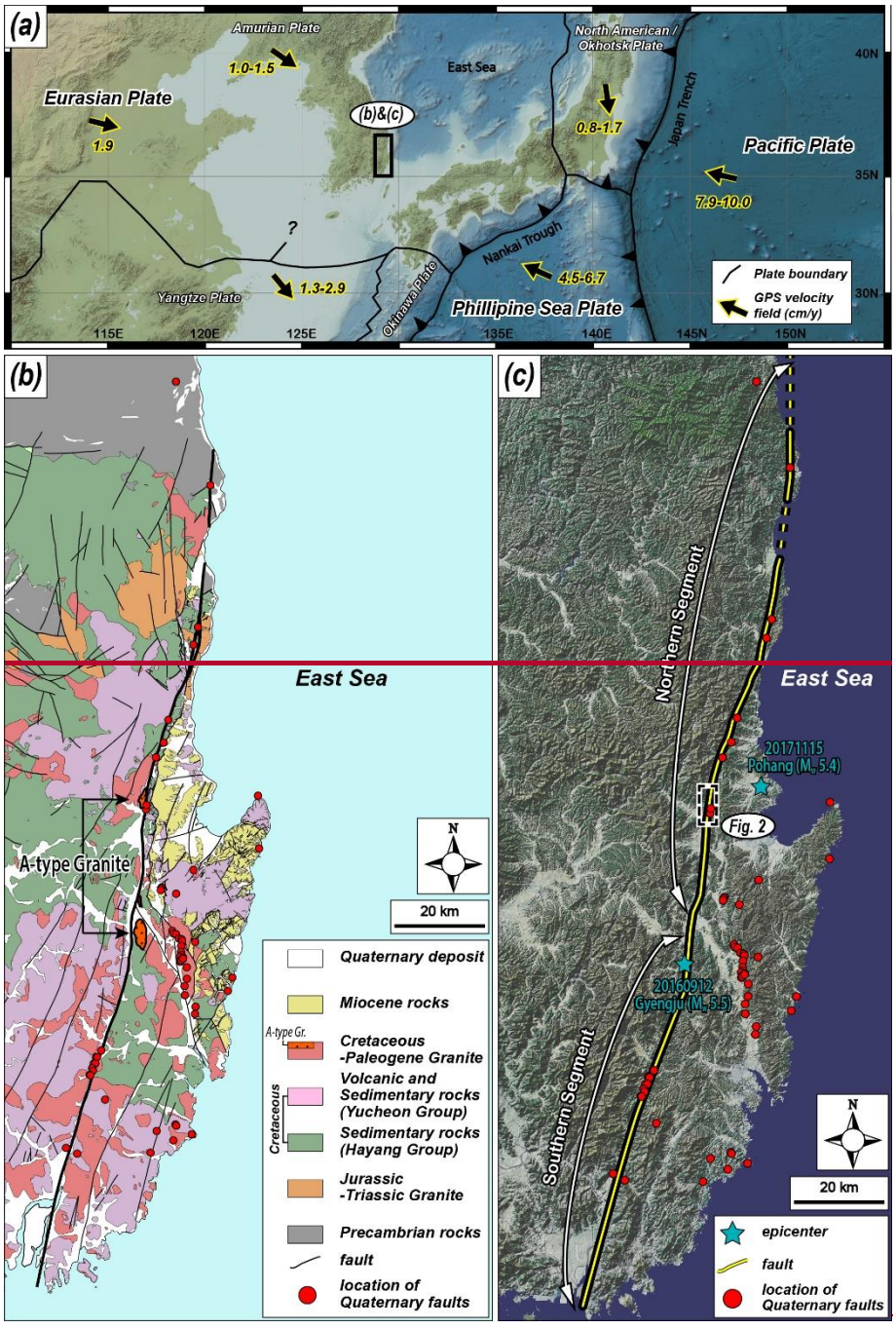
(a)
Amurian Plate
1.0-1.5
East Sea
North American / Okhotsk Plate
Eurasian Plate
1.9
(b)&(c)
0.8-1.7
Japan Trench
40N
Pacific Plate
35N
7.9-10.0
?
Nankai Trough
4.5-6.7
1.3-2.9
Yangtze Plate
Okinawa Plate
Phillipine Sea Plate
Plate boundary
GPS velocity field (cm/y)
30N
115E
120E
125E
135E
140E
145N
150N
(b)
East Sea
A-type Granite
N
20 km
Quaternary deposit
Miocene rocks
A-type Gr.
Cretaceous -Paleogene Granite
Volcanic and Sedimentary rocks (Yucheon Group)
Cretaceous
Sedimentary rocks (Hayang Group)
Jurassic -Triassic Granite
Precambrian rocks
fault
location of Quaternary faults
(c)
Northern Segment
East Sea
20171115 Pohang (M_L 5.4)
Fig. 2
20160912 Gyeongju (M_L 5.5)
Southern Segment
N
20 km
epicenter
fault
location of Quaternary faults

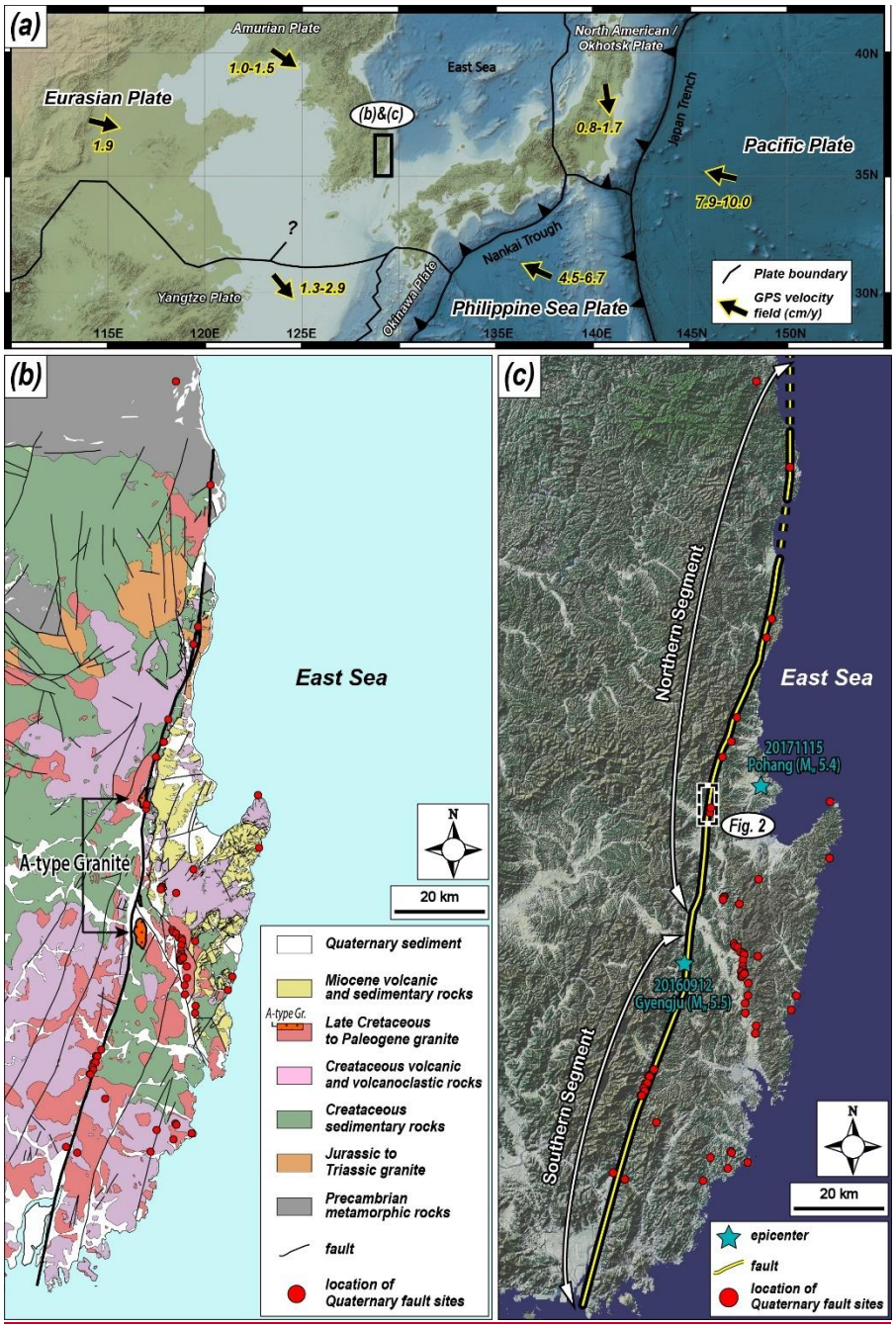

Figure 1: Regional study area maps. (a) Tectonic map of East Asia showing plate boundaries and their velocities (modified from DeMets et al., 1990, 1994; Seno et al., 1993, 1996; Heki et al., 1999; Bird, 2003; O'Nelli et al., 2005; Schellart & Rawlinson, 2010; M.-C. Kim et al., 2016). The black arrow indicates the moving direction of each plate. (b) Regional geological map of SE Korea (modified from Chang et al., 1990; Kim et al., 1998; Hwang et al., 2007a, 2007b; Son et al., 2015; Song, 2015; Kang et al., 2018). The thick black line indicates the Yangsan Fault, and the 21 km dextral offset of the Yangsan Fault is interpreted by the distribution of a-type granite. (c) Topographic satellite image map of SE Korea and recent epicentres. The Yangsan Ffault is divided into two segments (modified from Kim et al., 2022; 2023b) and the study area is located in the southern part of the northern segment.

2 Tectonic and geological settingSeismotectonic setting

2.1 Regional seismotectonic setting of Korea

The Korean Peninsula is located on the Amurian Plate, which waswas once thought to be part of the eastern margin of the Eurasian Plate (Fig. 1a; e.g., Bird, 2003; Calais et al., 2006; Argus et al., 2010; Ashurkov et al., 2011). The relative frequency of earthquakes in Korea is low compared with other countries on nearby plate boundaries, such as Japan, China, Taiwan, and the Philippines (KMA, 2022). While paleoseismology, archaeoseismology, and historical seismicity studies indicate that large (M≥7) earthquakes occurred in the past, medium-sized (M≥5) instrumental earthquakes have been repeatedlyconsistently observed since the onset of seismic instrument measurements (Lee, 1998; Lee and Yang, 2006; Han et al., 2016; Kim et al., 2016; 2018; 2020b). Currently, the Korean Peninsula is under a maximum horizontal stress ofin the E-W to ENE-WSW direction, which is the result of the combined effects of the subduction of the Pacific and Philippine Sea Plates and eastward-propagating far-field stress from India-Eurasia collision the far-field stress from the collision of the Indian and Eurasian plates (Park et al., 2006; Kim et al., 2016; Kuwahara et al., 2021). GNSS studies show that the Korean Peninsula has a velocity field of about 3 cm/yr in the WNW direction (Ansari and Bae, 2020; Sohn et al., 2021; Kim and Bae, 2023). Recent short-term (2 years) GNSS studies on the Yangsan Fault suggest that the fault appears to be stable, with blocks on both sides of the fault moving in the same direction and at the same displacement rate (Kim and Bae, 2023).

Paleoseismicological studies on the Korean Peninsula since the 1990s revealed that the most Quaternary surface ruptures were propagated along major structuresal lines in the southeastern part of the peninsula, such as the Yangsan Fault, Ulsan Fault, and Yeonil Tectonic Line (Figs. 1b and 1c; Kee et al., 2009; Kim et al., 2011; Choi et al., 2012; Kim et al., 2016). Since the 2016 Gyeongju earthquake, the Yangsan Fault has drawn increasing research attention in various fields, including tectonic geomorphology (Lee et al., 2019; Park and Lee, 2018; Kim and Oh, 2019; Kim et al., 2020d; Kim and Seong, 2021; Hong et al., 2021), structural geology (Woo et al., 2015; Choi et al., 2017; Cheon et al., 2017, 2019, 2020a; Kim et al., 2017a, b, 2020a, 2021, 2022; Ryoo and Cheon, 2019; Kwon et al., 2020), paleoseismology (Lee et al., 2015; Choi et al., 2019; Cheon et al., 2020b; Ko et al., 2020; Kim et al., 2023), and fault chronography (Yang and Lee, 2012, 2014; Song et al., 2016, 2019; Sim et al., 2017; Kim and Lee, 2020, 2023). Notably, there are many records of Quaternary surface rupturing with dextral kinematics, which were reactivated along the pre-existing mature (long-lived) Yangsan fault zoneThe reported Quaternary surface rupturing were reactivated along the pre-existing fault surface with various kinematics depending on the relationship between the stress field and the geometry of the pre-existing structure (Cheon et al., 2020a). This faultthe Yangsan Fault, one of the most significant structural lines on the Korean Peninsula, extends > 200 km on land and is several hundred meters wide, with a prevailing horizontal displacement of > 20 km (Choi et al., 2017; Cheon et al., 2017, 2019, 2020a, b). ItThe Yangsan Fault underwent multiple stages of deformations with various kinematic senses during the Cretaceous to Cenozoic (Fig. 1b; Chang et al., 1990; Kim, 1992; Chang and Chang, 1998; Chang, 2002; Hwang et al., 2004, 2007a, b; Choi et al., 2009; Cheon et al., 2017, 2019). The dextral horizontal displacement of the Yangsan fFault is approximately 25–35 km in the Cretaceous sedimentary rocks (Chang et al., 1990) and 21.3 km in A-type alkali granite on both sides of the fault (Fig. 1b; Hwang et al.,

2004, 2007a, b). ~~The most reported evidence for slip sense of Quaternary surface ruptures along the Yangsan Fault indicate that they have been reactivated with transpressional dextral slip sense under E–W to ENE–WSW oriented compressional stress fields (Kim et al., 2011; Choi et al., 2012; Jin et al., 2013; Yang and Lee, 2014; Lee et al., 2015; Kim et al., 2016; Choi et al., 2019; Cheon et al., 2020a).~~

2.2 Geological settings of the Byeokgye section of the Yangsan Fault~~detailed study area~~

The Northern Yangsan Fault, located north of Gyeongju at the junction of, the Ulsan and Yangsan Faults, has documented several Quaternary surface ruptures (Fig. 1b). These surface ruptures caused offsets in alluvial fans, river terraces, and deflected rivers with dextral displacements of 0.43-2.82 km (Kyung, 2003; Choi et al., 2012; Lee et al., 2019; Han et al., 2021; Ko et al., 2022; Lee et al., 2022; Lee, 2023). Recent significant earthquakes in Pohang and Gyeongju further underscore the seismic activity of this region. The Byeokgye section, which crosses Gyeongju and Pohang, is located in the southern part of the Northern Yangsan Fault, adjacent to the Yugye and Bangok sites to the north. In contrast, no Quaternary surface rupture has been identified in the Angang area to the south.

The rocks in the study area are composed of Cretaceous sedimentary, volcanic, and granitic rocks, Paleogene A-type alkaline granite, Middle Miocene sedimentary rocks, and Quaternary sediments (Fig. 2a). The A-type a~~A~~lkaline granite, used as a dextral offset marker for the Yangsan Fault, is distributed on the west side of the fault~~Yangsan Fault zone~~ in the center of the study area and on the east side in Gyeongju and the offset is 21.3 km (Fig. 1b, Hwang et al., 2004, 2007a, b). The Middle Miocene sedimentary rocks in the eastern part of the study area are bounded by the western marginal faults of the Miocene Pohang Basin~~faults~~ consisting of normal to dextral transfer faults~~, which form the western boundary of the Pohang Basin~~ (~~Middle Miocene;~~ Fig. 2a; Son et al., 2015; Song, 2015). The Quaternary sediments in the study area are widely distributed along streams and valleys, and stratigraphic features cut by Quaternary surface rupturing along ~~faulting of~~ the Yangsan Fault are observed in some places (Fig~~s~~. 2b~~, and~~ 2c).

In the study area, the Byeokgye (outcrop) and Dangu (trench) sites have been reported as the records of the Quaternary surface ruptures (Fig. 2; Ryoo et al., 1999; Kee et al., 2009; Choi et al., 2012; Lee et al., 2015). The NNE-striking fault splay~~surface~~ identified at the Byeokgye site cut the Cretaceous felsic dike~~acidic~~ and Quaternary sediment~~s~~. Based on the shear bands within the fault gouge, drag folds in the footwall, and sub-horizontal striations, it was interpreted that strike-slip occurred after reverse slip during the Quaternary (Ryoo et al., 1999). The most recent earthquake (MRE) of the Byeokgye site occurred after 7~~.~~5±3 ka, the optically stimulated luminescence (OSL) age of the truncated Quaternary sediments (Choi et al., 2012). ~~Dangu is a trench approximately 50 m north of Byoegye that was excavated to obtain more detailed paleoseismic data (Lee et al., 2015).~~ The surface ruptures ~~A fault surface~~ (N10–20°E/75–79°SE) of the two trenches at the Dangu site have geometric and kinematic features similar to those at the Byeokgye site (Lee et al., 2015)~~. with geometric and kinematic characteristics similar to those of Byeokgye was found in the two trenches~~. The drag fold, slickenline, and three fault gouge zones observed in the exposed walls~~cross sections~~ indicate~~d~~ that at least three strike-slip events with reverse slip occurred after the deposition of Quaternary

sediments. In addition, the MRE of the Dangu site using OSL dating, radiocarbon, and archaeological interpretation of artiefacts in the Quaternary sediments is 7.5±3 ka (Lee et al., 2015). Recently, Song et al. (2020) excavated a trench 1 km north of the Byeokgye site to identify further records on the Quaternary surface rupturing ~~Quaternary faults~~ and attempted paleoseismological interpretation. We set this trench as Trench 1 for a comprehensive interpretation and summarize the results.

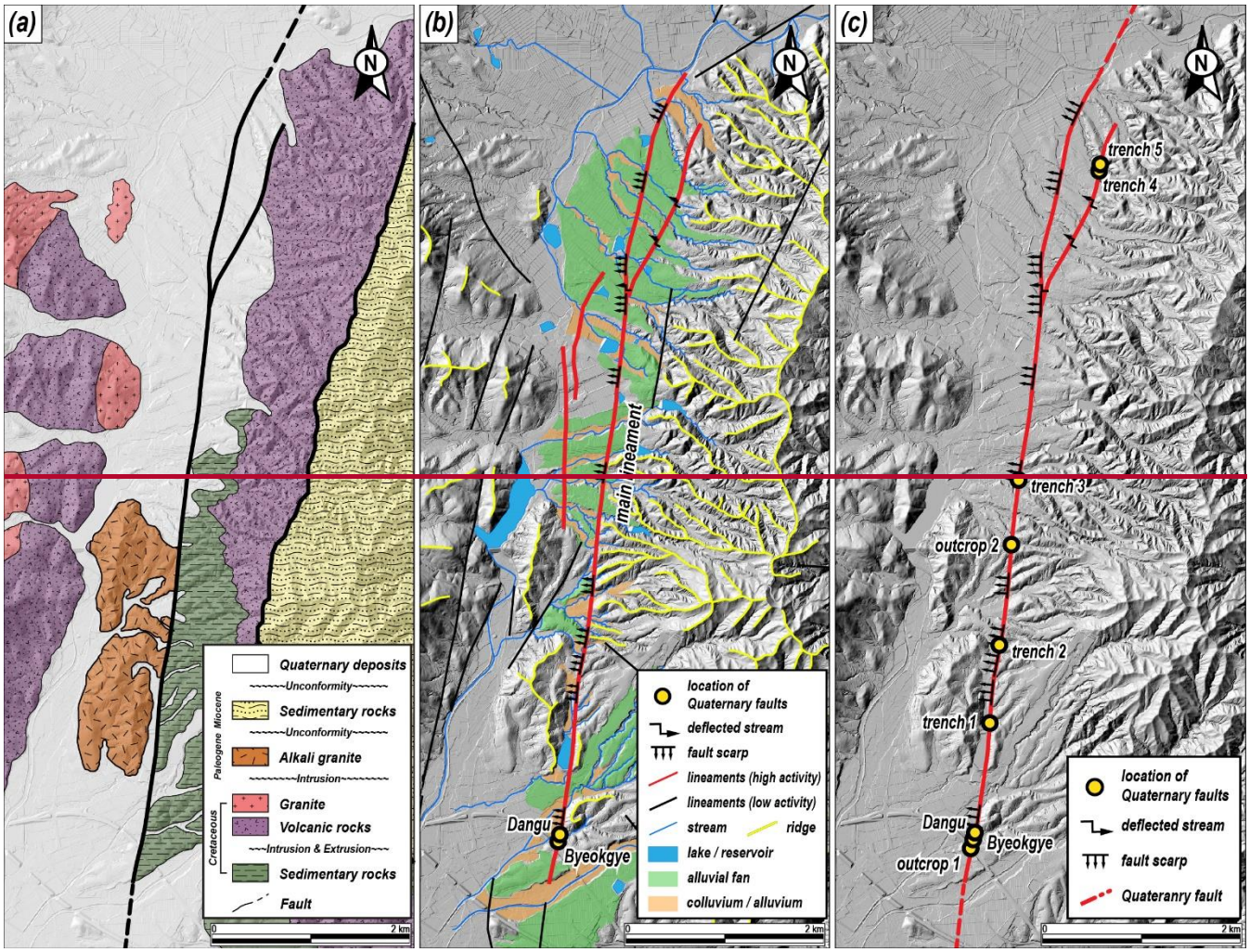
(a)
N
Quaternary deposits
~~~~~Unconformity~~~~~
Sedimentary rocks
~~~~~Unconformity~~~~~
Alkali granite
~~~~~~~~Intrusion~~~~~~~~
Granite
Volcanic rocks
~~~Intrusion & Extrusion~~~
Sedimentary rocks
Fault
Paleogene Miocene
Cretaceous
0
2 km
(b)
N
main lineament
Dangu
Byeokgye
location of Quaternary faults
deflected stream
fault scarp
lineaments (high activity)
lineaments (low activity)
stream
ridge
lake / reservoir
alluvial fan
colluvium / alluvium
0
2 km
(c)
N
trench 5
trench 4
trench 3
outcrop 2
trench 2
trench 1
Dangu
Byeokgye
outcrop 1
location of Quaternary faults
deflected stream
fault scarp
Quateranry fault
0
2 km

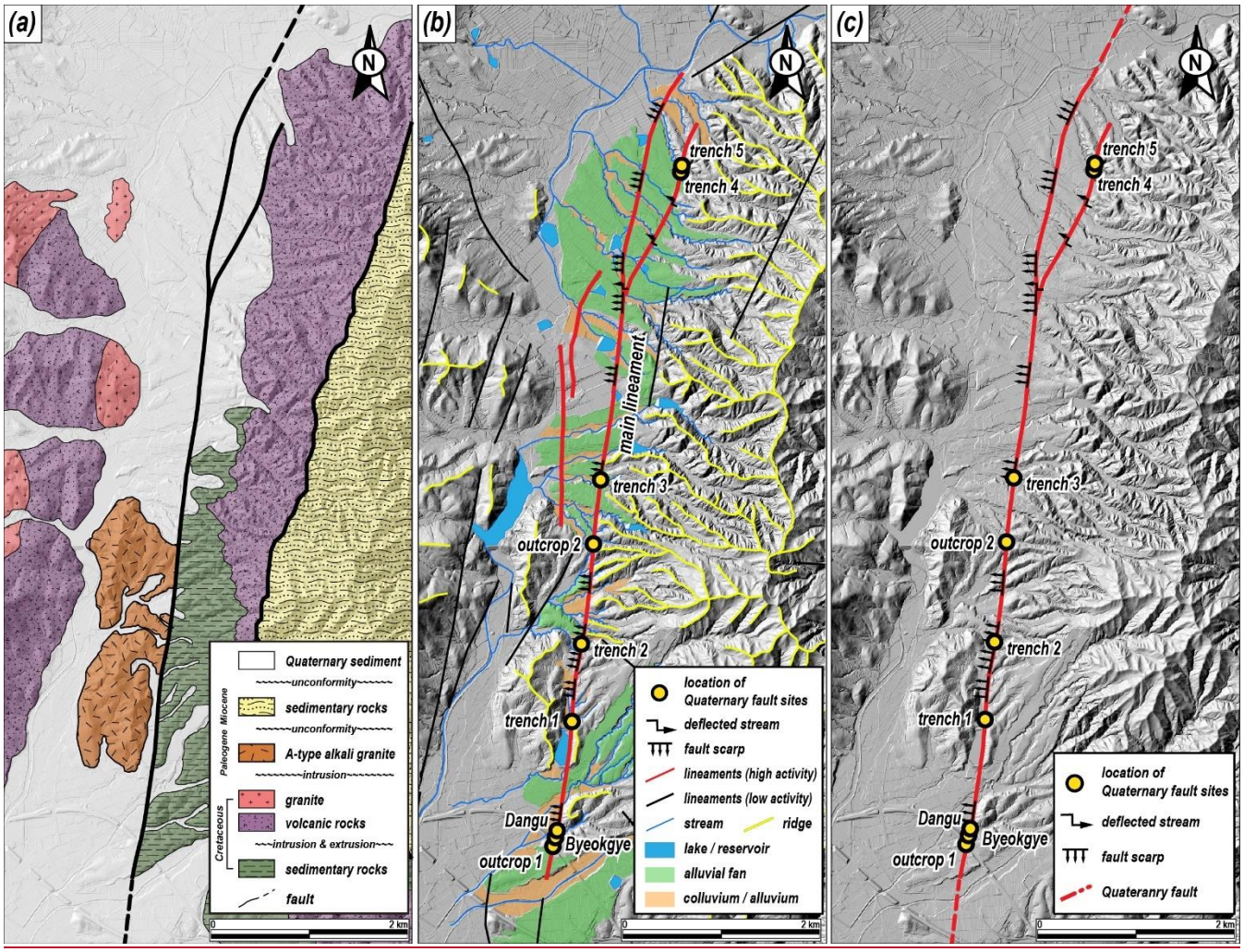

Figure 2: Detailed study area maps. (a) Geological map of the study area (modified from Hwang et al., 2007; Song, 2015). The A-type alkali granite in the study area is used as a marker of YF's dextral offset. (b) Geomorphological map of the study area (modified from Ha et al., 2022). A fault trace is recognized as an array of fault scarps and deflected streams. (c) Fault trace map of the study area. Two outcrops and five trenches are located in the fault trace.

3 Method

3.1 Fault surface rupture tracking and trench siting

Ha et al. (2022) reported a 7.6 km fault trace in the study area through detailed topographic analysis using high-resolution (<< 20 cm) LiDAR images (Fig. 2b). They interpreted the main lineament as a fault scarp with a vertical displacement of 2–4 m and a dextral refraction channel with a horizontal displacement of 50–150 m. In the trench (Trench 1) on the fault trace, the surface rupture~~fault surface~~ cuts through Quaternary sediments~~, indicating that the fault trace is Quaternary~~. The detailed

topography of the study area is described in Appendix A. We conducted fieldwork along this fault trace, trenched it at four further sites, and identified two natural exposures (described in Appendix C).

3.2 Numerical dating

3.2.1 Quartz OSL and K-feldspar IRSL dating

For luminescence dating, a total of thirty-six samples werewere collected from the five trench wallssection by inserting light-tight stainless-steel pipes (30 cm long and 5 cm diameter) into sand-rich layers. The sediment samples were then brought into a subdued darkroom to extract pure quartz and K-feldspar grains. The size fractions of 90–250 μm were first separated by wet sieving. Subsequently, these fractions were treated with 10% HCl (~ 1 h) and 10% H_2O_2 (~ 3 h) to remove carbonates and interstitial organic matter. This was followed by density separation using SPT (sodium polytungstate; ρ=2.61 g/cm^3). Pure quartz and K-feldspar extracts were finally prepared by etching the sinking (quartz-rich) and floating (K-feldspar-rich) portions with ~ 40 % and 10% HF (~ 1 h), respectively. The extracts were then rinsed with 10% HCl to dissolve any fluoride precipitates that may have formed during HF etching. The purity of quartz extracts (i.e., the absence of K-feldspar contamination) was determined by comparing infrared-stimulated luminescence (IRSL) and blue-stimulated luminescence (BSL) signals using three natural and beta-irradiated (20 Gy) aliquots. For all quartz extracts, the IRSL signals were negligible, with IRSL to BSL ratios well below 2 %, indicating that K-feldspar grains were effectively removed through the sample preparation procedure.

The luminescence signals were measured using a conventional Risø reader (Model TL/OSL-DA-20) installed at the Korea Basic Science Institute (KBSI). The stimulation light sources were Blue-LEDs (470 nm, FWHM 20 nm) for quartz and IR-LEDs (870 nm, FWHM 40 nm) for K-feldspar. The reader was equipped with a 90Sr/90Y source to deliver beta doses to the sample position at a calibrated dose rate of 0.150 ± 0.002 Gy/s (Hansen et al., 2015). The signals were detected through a UV filter (U-340) for quartz OSL and a blue filter pack (a combination of 4 mm Corning 7-59 and 2 mm Schott BG 39) for K-feldspar IRSL.

Quartz OSL equivalent dose (D_e) values were estimated using the single-aliquot regenerative-dose (SAR) procedure (Murray and Wintle, 2000), with preheat conditions for main regeneration and test doses of 260℃ for 10 s and 220℃ for 0 s, respectively. Quartz OSL signals in dose saturation (i.e., for samples older than datable age ranges of quartz OSL dating method) and K-feldspar post-IR IRSL signals, which are well known to have higher dose saturation levels than quartz OSL (Buylaert et al., 2012), were used as samples for De estimation. K-feldspar post-IR IRSL De values were estimated using the SAR procedure suggested by Buylaert et al. (2009) where, after preheating at 250℃ for 60 s, IRSL signals in K-feldspar were read at 225℃ for 100 s, immediately followed by lower temperature (50℃) IR stimulation (Hereafter, this signal is referred to as $pIRIR_{225}$). The measured fading rates (g_{2days}) of the K-feldspar $pIRIR_{225}$ signals ranged from 0–2 %/dec and fading corrections were made using the R package 'Luminescence' (Calc_FadingCorr; Kreutzer, 2023) to derive the final $pIRIR_{225}$ age estimates. The quartz OSL and fading-corrected K-feldspar $pIRIR_{225}$ ages are summarized in Table 2.

3.2.2 Radiocarbon dating

Radiocarbon dating was performed to obtain independent ages and to cross-validate the ages of the sediments. Eight charcoal samples ~~were~~are collected from sediment profiles of trenches 1, 2, and 4 and analyzed using accelerator mass spectrometry at the Beta Analytic Radiocarbon Dating Laboratory. The ^{14}C age was calibrated to calendar years using the OxCal 4.3 (Bronk Ramsey, 2017) and IntCal 20 (Reimer et al., 2020) atmospheric curves.

3.2.3 ^{10}Be-^{26}Al isochron burial dating

Isochron-burial dating is a variation of conventional burial dating methods that constrains the time elapsed since the sediment burial and has been widely used for dating the alluvial sediments of ~~0.2~~ 5.0-0.2 Ma (Granger & Muzikar, 2001). The burial duration was calculated from the difference between the initial $^{26}Al/^{10}Be$ ratio at the time of burial and the measured ratio of $^{26}Al/^{10}Be$ (Balco & Rovey, 2008; Erlanger et al., 2012). Unlike traditional simple burial dating, which assumes that the initial ratio is known or the same as the surface production ratio of 6.8, isochron-burial dating requires multiple samples with their pre-burial histories (i.e., various initial ratios of $^{26}Al/^{10}Be$) to construct an isochron. The initial ratio of $^{26}Al/^{10}Be$ of the samples at burial depended on the erosion and production rates in the source basin. Thus, we assumed that all the analyzed samples originated from the same basin under steady-state erosion. The pre-burial (i.e., inherited) concentrations of the gravel at the time of burial accumulated with a surface production ratio of 6.8 so that it falls on a line in the plot of ^{26}Al-^{10}Be (Lal, 1991; Granger, 2006; Balco and Rovey, 2008). We used the conventional value of 6.8 for the surface production ratio of $^{26}Al/^{10}Be$ for the current study, which can vary depending on longitude, latitude, and altitude (Balco and Rovey, 2008). Without considering the pre-burial exposure history, the measured nuclide concentrations of gravels at the same depth should fall again on a line in the plot of ^{26}Al-^{10}Be with a mean life ($\tau_{pb} = (1/ (\lambda_{26} - \lambda_{10}))$; ~ 2.07 Ma) because they have the same post-burial production of ^{26}Al (C_{26}) and ^{10}Be (C_{10}). Thus, the post-burial component can be treated as a constant so that it can be modeled, and the initial ratio of $^{26}Al/^{10}Be$ (R_{inh}) can be calculated as

$$\boldsymbol{N_{26} = (N_{10} R_{inh} e^{-t/\tau_{pb}} + C_{10} R_{inh} e^{t/\tau_{pb}} + C_{26})} \quad (1)$$

The final time (t_b) elapsed since burial can be calculated from the decay of the initial isochron (R_{inh}) to the isochron of the measured samples (R_m):

$$\boldsymbol{t_b = \tau_{pb} \ln(R_m / R_{inh})} \quad (2)$$

3.2.4 ESR dating

Electron Spin Resonance (ESR) dating of fault rocks is a method used to derive the timing of faulting by measuring the ESR signal in the quartz of a fault gouge (Ikeya et al., 1982; Lee & Schwarcz, 1994). In general, ESR dating has an age detection limit of up to several thousands of ka (e.g., Lee and Yang, 2003) and is thus helpful for direct dating the timing of faulting. The ESR signal of quartz grains can be reset when the fault surface is subjected to normal stress of more than 3 MPa and displacements of more than 0.3 m (Kim and Lee, 2020; 2023). These conditions are usually easier to meet at a depth of more

than ~100 m than at the surface. Therefore, it is likely that ESR signals from fault gouges currently exposed at the surface ~~were~~are reset at depths and then brought up to the surface (i.e., current position) via uplift. In addition, in the case that the ESR signals ~~were~~are not completely reset during faulting, the ESR ages may indicate the maximum age of MRE. In our study, we use the ESR ages of samples from trenches and fault sites in the study area reported by Kim and Lee (2023) to estimate the number of earthquakes.

3.3 Paleo-stress reconstruction

Pal~~a~~eo-stress reconstruction of Quaternary rupturing is carried out using 20 slickenlines obtained from five trenches~~faulting was conducted using fault-slip data from 23 slickenlines in cross-sections~~. The data were~~were~~ analyzed using Wintensor S/W (v.5.8.5; Delvaux and~~&~~ Sperner, 2003). The type of stress regime is expressed quantitatively using the R' value: R′=R (σ_1 is vertical), or 2-R (σ_2 is vertical), or 2+R (σ_3 is vertical); $R=(\sigma_2-\sigma_3)/(\sigma_1-\sigma_3)$ (Delvaux et al., 1997).

3.4 Displacement and earthquake magnitude estimation

The slickenlines of the main ~~fault~~surface rupture ~~surface~~ and the vertical separation of the ~~q~~Quaternary sediments in the trench wall~~section~~ are~~were~~ used to determine the horizontal~~true~~ displacement of the MRE and the displacement per event. In general, for strike-slip faults like the study area, horizontal displacements must be obtained from 3D trenches or from topography that preserves the displacements almost intact (e.g., Kim et al., 2024; Naik et al., 2024). Using only 2D trenches to obtain displacements or slip rates is uncertain because the sedimentary layers are unlikely to have recorded all earthquakes. Furthermore, ~~D~~deriving the horizontal~~true~~ displacement is challenging when exposed walls~~sections~~ are inclined, markers are inclined, or the slip sense is not purely dip-slip or strike-slip (which is almost always the case). In addition, displacements based on fragmentary information, such as bedrock separation and thickness of Quaternary sediments, can be over- or underestimated by fault slip motion and the possibility of paleo-topographic relief cannot be ignored. Despite these uncertainties, fault displacement is a necessary factor in earthquake magnitude estimation and key paleoseismological information, and the displacement obtained from the 2D trench can be used as a minimum value; therefore, the process of collecting or estimating fault displacement is indispensable in paleoseismology. Therefore, correlations based on vertical separation, marker dip angle, angle of ~~outcrop~~ slope wall~~cross-section~~, fault dip angle, rake of slickenline, etc. are important for estimating the horizontal~~true~~ displacement of a fault (Fig. ~~A~~B1; Xu et al., 2009; Jin et al., 2013; Lee et al., 2017; Gwon et al., 2021). The method of using their relationship to find the ~~true~~ horizontal displacement is described in detail in Appendix ~~A~~B.

Variables used for earthquake magnitude estimation include average displacement (Kanamori, 1977), maximum displacement (MD; Bonilla et al., 1984; Wells and Coppersmith, 1994), surface rupture length (Bonilla et al., 1984; Khromovskikh, 1989; Wells and Coppersmith, 1994), rupture area (Wells and Coppersmith, 1994), and surface rupture length × MD (Bonilla et al., 1984; Mason, 1996). However, in Korea, where rupture traces are difficult to find, it is difficult to use surface rupture length or rupture area owing to large uncertainties. Thus, we used MD (horizontal displacement), which is relatively easy to obtain

from outcrops and trenches and more reliable. Many previous studies within in intraplate~~Korea~~ have applied the empirical relationship of the MD-moment magnitude (M_w) presented by Wells and Coppersmith (1994) (e.g., Patyniak et al., 2017 in Kyrgyzstan; Suzuki et al., 2021 in Mongolia; Ge et al., 2024., in China~~Kyung, 2010; Kim & Jin, 2006; Jin et al., 2013; Lee et al., 2017~~). We also estimated the maximum earthquake magnitude by applying the MD obtained from the trench to the empirical formula. The rake of slickenlines on the Quaternary slip~~fault~~ surface that underwent ~~Quaternary~~ faulting averages 20° and strike-slip motion ~~wa~~is dominant; therefore, we used a corresponding strike-slip fault type M_w-MD empirical relationship. ~~In addition, we used the MD-surface rupture length (SRL) empirical relationship to determine the extent to which the derived MD differed from the true displacement.~~

4 Results

4.1 Characteristics of Quaternary faulting in the trench

4.1.1 Trench 1

Trench 1, previously ~~was~~ reported by Song et al. (2020) and Ha et al. (2022), is~~and the findings are~~ summarized as follows: It~~Trench 1~~ i~~was~~s located on the main lineament, approximately 1 km north of the Byeokgye site (Fig. 2c),~~.~~ within a cultivated field where a narrow 50 m wide N-S trending valley and a 20 m wide NE-trending valley meet, through which the main lineament passes. To the east of Trench 1, a NE-trending ridge develops, although this is currently difficult to identify due to human modification, while to the west, a hill with a N-S trending ridge is formed (Fig. A2). Fault scarps are distinctly visible along the main lineament, both to the south and north of Trench 1, with small fluvial and colluvial deposits observed on the surface. Nine Quaternary sedimentary units and seven east-dipping splay slip surfaces (F1–F7) cutting the units ~~were~~are found in the E-W trending trench wall~~section~~ (Fig. 3). The hanging wall of F6 is the western boundary of pre-existing fault core more than 2.5 m wide and the footwall of F6 is a 4 m thick Quaternary sedimentary unit overlying the A-type alkali granite. The pre-existing fault core is divided into two zones based on whether it is related to rupturing. ~~Fault~~ Between F6 and F7, the fault core ~~core 1~~ had a 40 cm wide blue fault gouge cutting Quaternary sediments and a weakly developed shear band within the fault gouge. ~~F~~The fault core ~~2~~, eastern side of F7~~east of fault core 1~~, did not cut the Quaternary sediments and consisted of a brown to dark ~~gray~~grey ~~fault~~ brecciated zone and a ~~fault~~ gouge zone more than 2 m wide. ~~White, light grey, and dark grey fault gouge bands developed anastomosingly within the fault brecciated zone. Slickenlines, observed at the boundary of the fault brecciated and fault gouge zones, indicate a dextral strike-slip.~~ The stratigraphic features of the nine units are listed in Table 1, and there are two noteworthy observations: First, the triangular-shaped unit D, characterized by ~~has~~ a light brown sandy matrix with better ~~good~~ sorting and roundness compared to the surrounding units, ~~despite it~~ is surrounded by the slip surfaces (Fig. 3). It indicates that unit D may have been captured by the horizontal displacement of nearby sediments during the faulting event. Second, various types of seismogenic soft-sediment deformation structures (SSDs) are developed in units E and G (Fig. 3, Fig. 10 in Ha et al., 2022). The orientations of slip surfaces ranged from N60°W to N28°E, changing from

NW-to NE-striking to the east. The F6 fault splay (N01°E/69°SE) cut through unit B and the F7 ~~fault~~ splay (N28°E/86°SE) is terminated in unit C. ~~Each of~~ F3, F4~~–~~ and F5 cut~~s~~ through units D, E, and F, respectively, and are~~is~~ terminated under unit C. F1 and F2 cut through units G, H, and I but not through unit F. The rakes of the slickenline observed on F6 measured 15–55°, indicating a dextral ~~strike-~~slip with a reverse component. Three faulting events are interpreted based on ~~can be analyzed in terms of~~ the geometry of the sediments and the kinematics of the slip surface: (1) ~~.~~The first faulting event involves the rupture of all F1-F7 after the deposition of units G, H, and I before the deposition of unit F, marking the event 1 horizon. (2) The second faulting event occurred after the deposition of units E and F prior to the deposition of unit C, defining the event 2 horizon, with ruptures affecting faults F3 through F7. During this event, dextral slip along faults F5 and F6 displaced unit D. (3) The third faulting event took place after the deposition of units B and C, with rupture limited to faults F6 and F7.

OSL/pIRIR$_{225}$ ages are presented in Table 1~~2~~. We also conducted ^{14}C and ESR dating on the trench. Three charcoal samples (1803BYG-01-C, 1803BYG-02-C, and 1803BYG-03-C) ar~~were~~e collected from unit E and one charcoal sample (1803BYG-04-C) i~~wa~~s collected from unit I for radiocarbon dating. The results of samples 1803BYG-01-C and 1803BYG-02-C are ~~36,897~~ 38,420–36,897 and ~~43,802~~ 45,670–43,802 Cal yr BP, respectively (Table 2~~3~~). However, the ages of these two samples ~~were~~are near the upper limit of the radiocarbon dates and ~~were~~are stratigraphically contradictory, with the lower layer being younger than the upper layer. The age of 1803BYG-03-C (~~7,675~~ 7,821–7,675 cal yr BP) from the upper part of unit E i~~wa~~s inconsistent with the OSL age (1803BYG-10-O: ~164 ka). It is possible that liquefaction in unit E caused a disturbance in the sediments and that the radiocarbon and OSL dates do not indicate the exact depositional timing. In addition, the radiocarbon age of ~~41,955~~ 43,292–41,955 cal yr BP for the sample from unit I i~~wa~~s near the upper limit of the radiocarbon ages and i~~wa~~s thus subject to error. In particular, it ~~wa~~is younger than K-feldspar pIRIR$_{\text{~~225~~225}}$ (177±7 ka (1803BYG-07-O)) from unit H, making it unlikely that this age ~~was~~ is indicative of the depositional age of unit I. The main surface rupture cut unit B and the MRE using the OSL age of unit B is >3.2±0.2 ka (1803BYG-06-O; Table 1, Fig. 3). The geometry and cross-cutting relationship between the Quaternary sediments and the seven surface ruptures indicated that a pre-existing fault core is reactivated during the Quaternary, resulting in at least three faulting events (Fig.3; Fig. 9 in Song et al., 2020): the first (antepenultimate earthquake, AE) occurring at <142±4 ka (1803BYG-12-O), the second (penultimate earthquake, PE) at >17±1 ka (1803BYG-13-O), and the third at the MRE (Table 1, Fig. 3). For ESR dating, 36 fault gouge samples ~~were~~are collected from eastern side~~fault core 2 adjacent t~~ of F7, and ESR dating i~~wa~~s performed on 10 of them (1810BYG-01 to 10-E) (Fig. 3). The dates of each sample are presented in Table ~~4~~3. The weighted average ESR ages of the samples from the same fault viscose band ~~were~~are 245±37 ka (1810BYG-02-E, 1810BYG-10-E), 406±35 ka (1810BYG-01-E, 1810BYG-05-E, 1810BYG-06-E), 387±26 ka (1810BYG-04-E), and 335±53 ka (1810BYG-04-E) (Table 3~~4~~). Samples with dose-saturated ESR signals (1810BYG-03-E, -07-E, and -08-E) ~~were~~are excluded from the weighted average age calculations. Considering the error, the timing of faulting events using ESR ages at these sites can be determined to be ~~245±37 and~~ 406±35 and 245±37 ka. ~~The main fault surface cut unit B and the MRE using the OSL age of unit B was >3.2±0.2 ka (1803BYG-06-O; Table 2, Fig. 3). The geometry and cross-cutting relationship between the Quaternary sediments and the seven fault surfaces indicated that a pre-existing fault core was reactivated during the Quaternary, resulting in at least three faulting events (Fig.3; Fig. 9 in~~

~~Song et al., 2020): the first (antepenultimate earthquake, AE) occurring at <142±4 ka (1803BYG-12-O), the second (penultimate earthquake, PE) at >17±1 ka (1803BYG-13-O), and the third at the MRE (Table 2, Fig. 3).~~

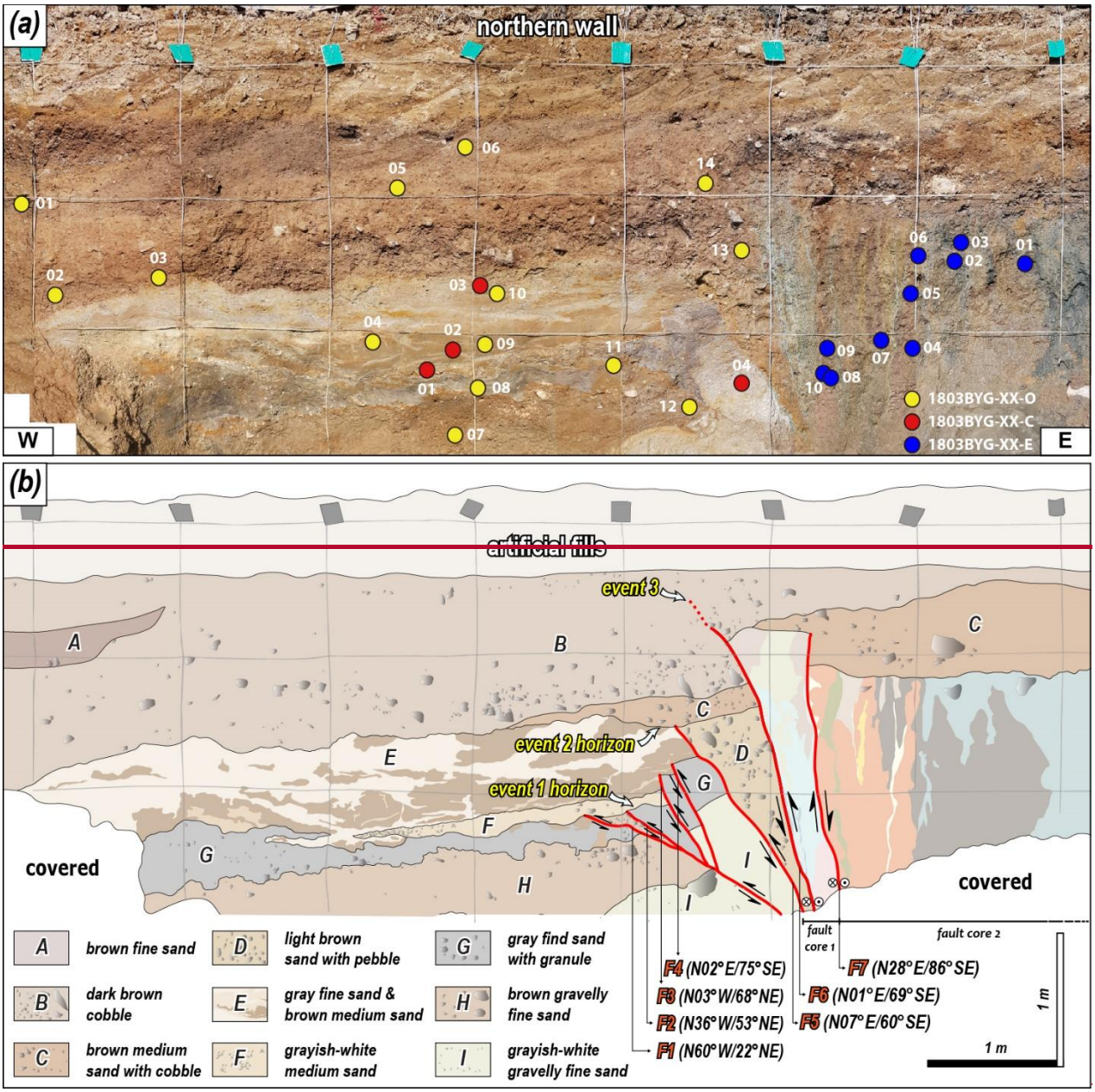
(a)
northern wall
W
E
1803BYG-XX-O
1803BYG-XX-C
1803BYG-XX-E
(b)
artificial fill
event 3
event 2 horizon
event 1 horizon
covered
covered
A
B
C
D
E
F
G
H
I
fault core 1
fault core 2
F4 (N02°E/75°SE)
F8 (N03°W/68°NE)
F2 (N36°W/53°NE)
F1 (N60°W/22°NE)
F7 (N28°E/86°SE)
F6 (N01°E/69°SE)
F5 (N07°E/60°SE)
1 m
1 m
brown fine sand
dark brown cobble
brown medium sand with cobble
light brown sand with pebble
gray fine sand & brown medium sand
grayish-white medium sand
gray find sand with granule
brown gravelly fine sand
grayish-white gravelly fine sand

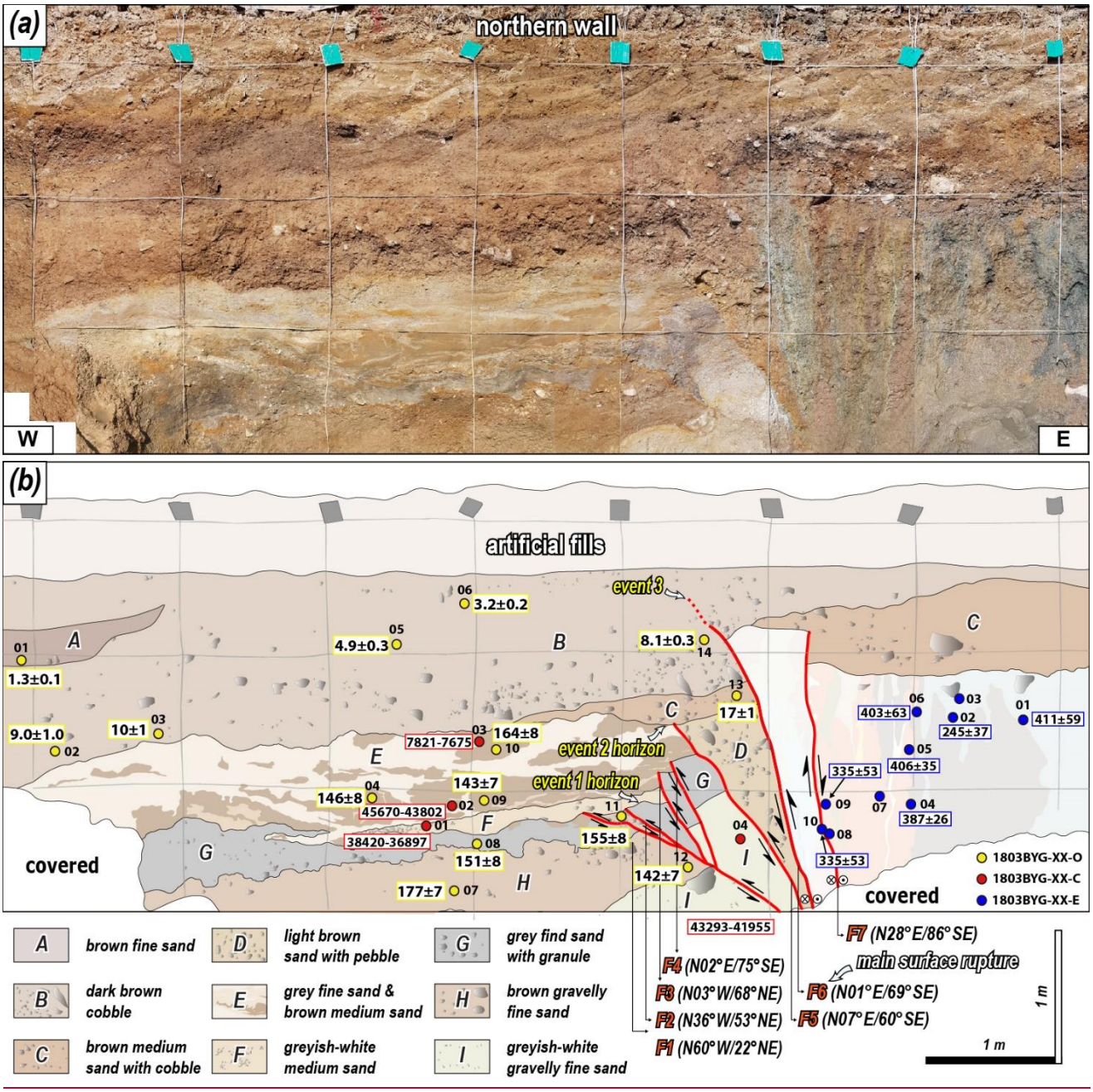

Figure 3: (a) Photomosaic of the trench 1 wall~~section~~ of the northern wall. The colored circles represent samples for age dating. (b) Detailed sketch of the trench 1 ~~section~~exposed wall. Light grey lines indicate a 1 × 1 m grid. The numbers in the yellow, red, and blue boxes represent OSL and IRSL (ka), radiocarbon (cal yr BP), and ESR (ka) dating results, respectively.

Table 1. Description and OSL/pIRIR$_{225}$ dating results of the units in each trench

Unit	Features	Age		
		Age (ka)	Dating method	Sample number
Trench 1				
A	Brown fine sand, lens shape in unit B, coarsening upward in the bottom (silt to fine sand)	1.3 ± 0.1	OSL	01
B	Dark brown cobble, fine sand matrix, poor roundness, fining upward in clast (cobble to pebble) and matrix (sand to fine sand), the youngest unit cut by rupture	9.0 ± 1.0	OSL	02
		10 ± 1	OSL	03
		4.9 ± 0.3	OSL	05
		3.2 ± 0.2	OSL	06
		8.1 ± 0.3	OSL	14
C	Brown medium sand with cobble, good roundness and sorting compared to unit b, pinch out in footwall, cover the pre-existing fault core	17 ± 1	OSL	13
D	Light brown sand with pebble, good roundness and sorting despite adjacent rupture, captured by a triangular shape, with ruptures		-	
E	Grey fine sand & brown medium sand, mixing with grey and brown parts, SSDS (load structure dominated; load cats, pillar structure, sand dike, disturbed structure, structureless sediments)	146 ± 8	pIRIR$_{225}$	04
		143 ± 7	pIRIR$_{225}$	09
		164 ± 8	pIRIR$_{225}$	10
F	Greyish-white medium sand		-	
G	Grey fine sand with granule, SSDS (intrusive structure dominated; ball and pillow, flame structure, sand dike)	151 ± 8	pIRIR$_{225}$	08
		155 ± 8	pIRIR$_{225}$	11
H	Brown gravelly fine sand, moderate roundness and sorting	177 ± 7	pIRIR$_{225}$	07
		142 ± 7	pIRIR$_{225}$	12
I	Greyish-white gravelly fine sand, matrix derived from granite that basement rock		-	
Trench 2				
A	Reddish brown cobble deposits, A subangular clast composed of granitic and sedimentary rocks with a maximum diameter of 40 cm, poor sorting, charcoal in the bottom, cover the pre-existing fault core	3.2 ± 0.3	OSL	05
		3.4 ± 0.4	OSL	06
		19 ± 1	OSL	07
B	Light grey silt-light yellowish brown fine sand, interbedded two layers, cut by surface rupture		-	
Trench 3				
A	Dark brown fine sand-silt		-	
B	Light brown boulder-cobble deposits, colluvial deposits from mountain slopes, moderate roundness, decreasing the clast size toward the west, cover the Quaternary slip zone	6.4 ± 0.4	OSL	10
C	Brown pebble deposits, poor roundness and sorting, brown sand matrix, the youngest unit cut by fault splays		-	
D	Yellowish-brown pebble deposits, colluvial wedge, triangular shaped, angular to subangular clast, poor sorting in bottom, fining upward, sand content increases with distance from the main Quaternary slip zone	137 ± 3	pIRIR$_{225}$	08
E	Brown cobble-pebble deposits, subangular clast, poor sorting, intercalated fine sand to silt	173 ± 6	pIRIR$_{225}$	02
		175 ± 5	pIRIR$_{225}$	03
F	Brown sand-fine sand		-	
G	Brown pebble deposits, subangular clast, poor sorting, clast composed of granitic, volcanic, sedimentary rocks		-	
H	Brown sand-fine sand		-	
Trench 4				
A	Brown fine sand, have a charcoal	0.15±0.01	OSL	07
		0.15±0.01	OSL	08
B	Dark brown cobble deposits-sand, colluvial deposits from mountain slopes, subangular clast, poor sorting, the youngest unit cut by surface rupture	1.3 ± 0.1	OSL	05
		1.2 ± 0.1	OSL	06
		5.9 ± 0.4	OSL	09
C	Light brown boulder deposits-sand, matrix is coarse sand to sand, angular clast, poor sorting, clast mainly composed of granite, the maximum diameter of a clast is ~ 120 cm		-	
D	Brown sand-fine sand, fining upward		-	
E	Brown cobble deposits-coarse sand, alternating sand and gravel, average diameter of clast is 2-5 cm, subangular to angular, moderate sorting		-	
F	Light brown sand-fine sand		-	
Trench 5				
A	Reddish brown pebble deposits, A subangular clast composed of granitic, sedimentary, volcanic rocks with a maximum diameter of 15 cm, good sorting, matrix-supported	-		
B	Reddish brown fine sand-slit, weak horizontal bedding, the youngest unit cut by surface rupture, no truncation or deformation after MRE.	2.8 ± 0.1	OSL	03
		2.6 ± 0.1	OSL	04
C	Reddish brown cobble-pebble deposits, fine sand matrix, clast composed of granitic, sedimentary, volcanic rocks, angular to sub-angular clast, poor sorting, containing clasts almost 40%.	10 ± 1	OSL	01
		4.8 ± 0.2	OSL	02
D	Light bluish-grey pebble deposits, light grey fine sand matrix, the maximum diameter of a clast is ~ 20 cm, clast composed of sedimentary, volcanic rocks, angular to sub-angular clast, poor sorting	-		
E	Light yellowish brown pebble deposits, A slit near the rupture gradually increases in grain size as it moves away, changing to a pebble deposit, angular to sub-angular clast, good sorting	-		
~~Unit~~	~~Trench 1~~ ~~Trench 2~~ ~~Trench 3~~ ~~Trench 4~~ ~~Trench 5~~			

A	Brown fine sand, lens shape in unit B, coarsening upward in the bottom (silt to fine sand)	Reddish brown cobble deposits, A subangular clast composed of granitic and sedimentary rocks with a maximum diameter of 40 cm, poor sorting, charcoal in the bottom, cover the pre-existing fault core	Dark brown fine sand-silt	Brown fine sand, have a charcoal	Reddish brown pebble deposits, A subangular clast composed of granitic, sedimentary, volcanic rocks with a maximum diameter of 15 cm, good sorting, matrix-supported
B	Dark brown cobble, fine sand matrix, poor roundness, fining upward in clast (cobble to pebble) and matrix (sand to fine sand), the youngest unit cut by fault	Light grey silt-light yellowish brown fine sand, interbedded two layers, cut by main fault surface	Light brown boulder-cobble deposits, colluvial deposits from mountain slopes, moderate roundness, decreasing the clast size toward the west, cover the main fault surface	Dark brown cobble deposits-sand, colluvial deposits from mountain slopes, subangular clast, poor sorting, the youngest unit cut by fault	Reddish brown fine sand-slit, weak horizontal bedding, the youngest unit cut by fault, no truncation or deformation after MRE.
C	Brown medium sand with cobble, good roundness and sorting compared to unit b, pinch out in footwall, cover the pre-existing fault core		Brown pebble deposits, poor roundness and sorting, brown sand matrix, the youngest unit cut by fault	Light brown boulder deposits-sand, matrix is coarse sand to sand, angular clast, poor sorting, clast mainly composed of granite, the maximum diameter of a clast is ~ 120 cm	Reddish brown cobble-pebble deposits, fine sand matrix, clast composed of granitic, sedimentary, volcanic rocks, angular to sub-angular clast, poor sorting, containing clasts almost 40%. **Holocene †**
D	Light brown sand with pebble, good roundness and sorting despite adjacent fault, captured by a triangular shape, with fault surface		Yellowish-brown pebble deposits, colluvial wedge, triangular shaped, angular to subangular clast, poor sorting in bottom, fining upward, sand content increases with distance from the main fault surface	Brown sand-fine sand, fining upward	**Pleistocene ↓** Light bluish-grey pebble deposits, light grey fine sand matrix, the maximum diameter of a clast is ~ 20 cm, clast composed of sedimentary, volcanic rocks, angular to sub-angular clast, poor sorting
E	Gray fine sand & brown medium sand, mixing with gray and brown parts, SSDS (load structure dominated; load cats, pillar structure, sand dike, disturbed structure, structureless sediments)		Brown cobble-pebble deposits, subangular clast, poor sorting, intercalated fine sand to silt	Brown cobble deposits-coarse sand, alternating sand and gravel, average diameter of clast is 2-5 cm, subangular to angular, moderate sorting	Light yellowish brown pebble deposits, A slit near the fault surface gradually increases in grain size as it moves away, changing to a pebble deposit, angular to sub-angular clast, good sorting
F	Grayish-white medium sand		Brown sand-fine sand	Light brown sand-fine sand	
G	Gray fine sand with granule, SSDS (intrusive structure dominated; ball and pillow, flame structure, sand dike)		Brown pebble deposits, subangular clast, poor sorting, clast composed of granitic, volcanic, sedimentary rocks		

H	Brown gravelly fine sand, moderate roundness and sorting	Brown sand fine sand
I	Grayish-white gravelly fine sand, matrix derived from granite that basement rock	

Table 2. OSL/pIRIR$_{225}$ dating results

Trench number	Dating method	Sample number													
		01	02	03	04	05	06	07	08	09	10	11	12	13	14
Trench 1	OSL (ka)	1.3 ± 0.1	9.0 ± 1.0	10 ± 1		4.9 ± 0.3	3.2 ± 0.2							17 ± 1	8.1 ± 0.3
	pIRIR$_{225}$ (ka)				146 ± 8			177 ± 7	151 ± 8	143 ± 7	164 ± 8	155 ± 8	142 ± 7		
	Target unit	A	B	B	E	B	B	H	G	E	E	G	H	C	B
Trench 2	OSL (ka)					3.2 ± 0.3	3.4 ± 0.4	19 ± 1							
	pIRIR$_{225}$ (ka)														
	Target unit					A	A	A							
Trench 3	OSL (ka)										6.4 ± 0.4				
	pIRIR$_{225}$ (ka)		173 ± 6	175 ± 5					137 ± 3						
	Target unit		E	E					D		B				
Trench 4	OSL (ka)					1.3 ± 0.1	1.2 ± 0.1	0.15±0.01	0.15±0.01	5.9 ± 0.4					
	pIRIR$_{225}$ (ka)														
	Target unit					B	B	A	A	B					
Trench 5	OSL (ka)	10 ± 1	4.8 ± 0.2	2.8 ± 0.1	2.6 ± 0.1										
	pIRIR$_{225}$ (ka)														
	Target unit	C	C	B	B										

345

Table 23. ^{14}C dating results

Sample name	Material dated	$\delta^{13}C$ (‰)	^{14}C age (yr)	Calibrated age (cal yr BP)[a]	Probability (%)[b]
1803BYG-01-C	Charcoal	-25.1	33400±220	38420-36897	95.4
1803BYG-02-C	Charcoal	-27.4	41250±500	45670-43802	95.4
1803BYG-03-C	Sediment	-24.7	6910±30	7821-7675	95.4
1803BYG-04-C	Charcoal	Not analyzed	38560±480	43293-41955	95.4
1810NSR-01-C	Charcoal	-27.8	170±30	0-291-0	95.4
1810NSR-02-C	Charcoal	-26.3	210±30	0-304-0	95.4
2009UGR-01-C	Sediment	-24.2	25230±100	29,576-28,966	95.4
2009UGR-02-C	Charcoal	-26.9	160±30	286-0	95.4
2009UGR-03-C	Sediment	-22.5	540±30	634-513	95.4

[a] Calibration used the database INTCAL13 (Reimer et al., 2013)

[b] Probability Method (Bronk Ramsey, 2009)

Table 34. ESR dating results (from Kim and Lee, 2023)

Trench	Sample number									
	01	02	03	04	05	06	07	08	09	10
Byeokgye	421±27	396±24	871±63	1886±319						
Trench 1	411±59	245±37	n.d.	387±26	406±35	403±63	n.d.	n.d.	335±53	248±40
Trench 2	790±60	409±41	405±32	n.d.	369±53	330±44	n.d.	n.d.	261±48	
Trench 3	425±66	409±52	702±123	n.d.						

n.d. = Not Determined

The details of all data are in Kim and Lee (2023)

4.2.2 Trench 2

Trench 2 iwas located on the main lineament 01.8 km north of the Trench 1Byeokgye site (Fig. 2c),. within a colluvial area where fault scarp extend continuously along the main lineament to the south and north. Just north of Trench 2, the transition to an alluvial fan is clearly visible where the mountain ridge meets the main lineament. The 25-m wide valley surface contains partially developed colluvial sediments and deposits from small streams and gullies. Two Quaternary deposits are observed in Trench 2, along Aa low-angle Quaternary slip surfacefault surface (N02°E/38°SE) intersectingcutting the Quaternary deposits onwas observed in the trench sectionexposed wall (Fig. 4). The minimum 6-m-wide fault core of the hanging wall iwas composed of mature fault rocks. The fault core iwas divided into yellow and bluish-grey fault cores 1 and 2 from the west, with the yellowish brown fault core 1 overlaying unit B (Fig. 4). Foliation developed within the yellow fault core, which abutted the Quaternaryfault core 1, which abutted the main faultslip surface in the upper part of the wallsection. The strikes of the foliation within fault core 1 showed a wide range from NE to E-W striking in shallow dip parts but were more consistently N-S or NNE striking where the dip increased. The main fault surface that cut the Quaternary sediments showed a similar change from strike to foliation. The main fault surface had an N-S strike in the lower part of the section and changed to an E-W strike as the dip became shallower. Toward the top of the section, the dip deepened to regain the N-S striking. This indicated warping of the main fault surface along the pre-existing structural grains and foliation (Figs. 4b and 4d). Fault core 1, without foliation, was a yellowish brown fault brecciated zone composed of granitic rock breccia and a clayey matrix. The bluish gray fault core 2 was bounded by a high angle N-S striking slip surface with fault core 1. The internal structure of the bluish gray fault core was divided into four to six alternating gouge and brecciated zones, each of which was bounded by an NNE- or N-S striking slip surface. Numerous slickenlines (rake ≤ 10°) were observed on the slip surfaces in fault core 2, indicating dextral strike-slip movements. The Quaternary slip surface cuts unit B, displaying thrusting of the hanging wall's pre-existing fault core, while unit A overlies both features. Unit A has a loose matrix and relatively low consolidation compared to the underlying unit B and overlies the pre-existing fault core (Table 1). The main fault surface cut the yellowish fault core and unit B and tThe slickenline on the Quaternary slip surface showsrevealed a dextral strike- slip with a minor reverse component. Only Unit A had a loose matrix and relatively low consolidation compared to the underlying unit B and had an irregular boundary with the pre-existing fault core (Table 1). one faulting event is recognized, in which the Quaternary slip surface cuts through unit B, and unit A overlies it At least one faulting event was identified on the cross-section, which did not reach unit A or the surface (Figs 5cb and 5d).

The OSL ages of unit A, which covers the rupturefault, werare 3.4±0.4 ka (1810NSR-06) and 3.2±0.3 ka (1810NSR-05) and 3.4±0.4 ka (1810NSR-06)) at the southern wall and 19±1 ka (1810NSR-07) at the northern wall (Table 12). The radiocarbon ages of the charcoal in unit A werare 291–0 291 and 0–304–0 cal yr BP (Table 32), making them much younger than the OSL age from unit A. Radiocarbon dates do not indicate when the charcoal iwas deposited with the sediment but when the tree died after being rooted in the ground. The OSL results indicate a depositional age of 3.4±0.4 ka for unit A, which is not cut by the rupture, so the MRE of the surface rupture in Trench 2 is interpreted to be before 3.4±0.4 ka. The ESR ages obtained from the

fault gouge ~~were~~are higher than the depositional ages of the sediments cut by the rupture~~fault~~ (Table ~~4~~3). The ESR ages suggest that the quartz ESR signal in the fault gouge ~~i~~~~was~~ not fully initialized during faulting. Nevertheless, the ESR ages roughly cluster into four periods: 790±60 ka (1810NSR-01-E), 407±37 ka (1810NSR-02, 03-E), 350±49 ka (1810NSR-05, 06-E), and 261±48 ka (1810NSR-09-E). ~~Therefore, we interpreted the faulting event to have occurred after the ESR date of 261±48 ka (1810NSR-09-E). Taken together, these results indicate a depositional age of 3.4±0.4 ka for unit A, which was not cut by the fault, and an ESR age for the fault gouge indicating a faulting event after 261±48 ka, so the MRE of the fault in Trench 2 was interpreted to be before 3.4±0.4 ka.~~

To estimate the thickness of the Quaternary sediments and the cumulative vertical displacement of the Quaternary slip~~fault~~, drilled~~cored~~ sediments ~~were~~are sampled from the footwall along the ~~main fault~~Quaternary slip surface (Fig. ~~C~~D1). The Quaternary sediments extend to a depth of approximately 32.8 m, underlain by a granite wash (1.2 m thick) of Paleogene A-type alkali granite, and a subsequent fault damage zone of the granite exists at its base (Fig. D~~C~~1). Therefore, the vertical separation caused by the Quaternary ~~faulting~~ rupture in Trench 2 ~~i~~~~was~~ at least 34 m. However, the vertical separation is a paleo-topographic relief difference that may have been caused by the strike-slip movement of the Quaternary slip~~fault~~. Cosmogenic ^{10}Be-^{26}Al isochron dating of the granite wash underlying the Quaternary sediments yielded a burial age of 2,871±593 ka, indicating that the thick Quaternary sediments started to be deposited after 2,871±593 ka (Table ~~5~~4).

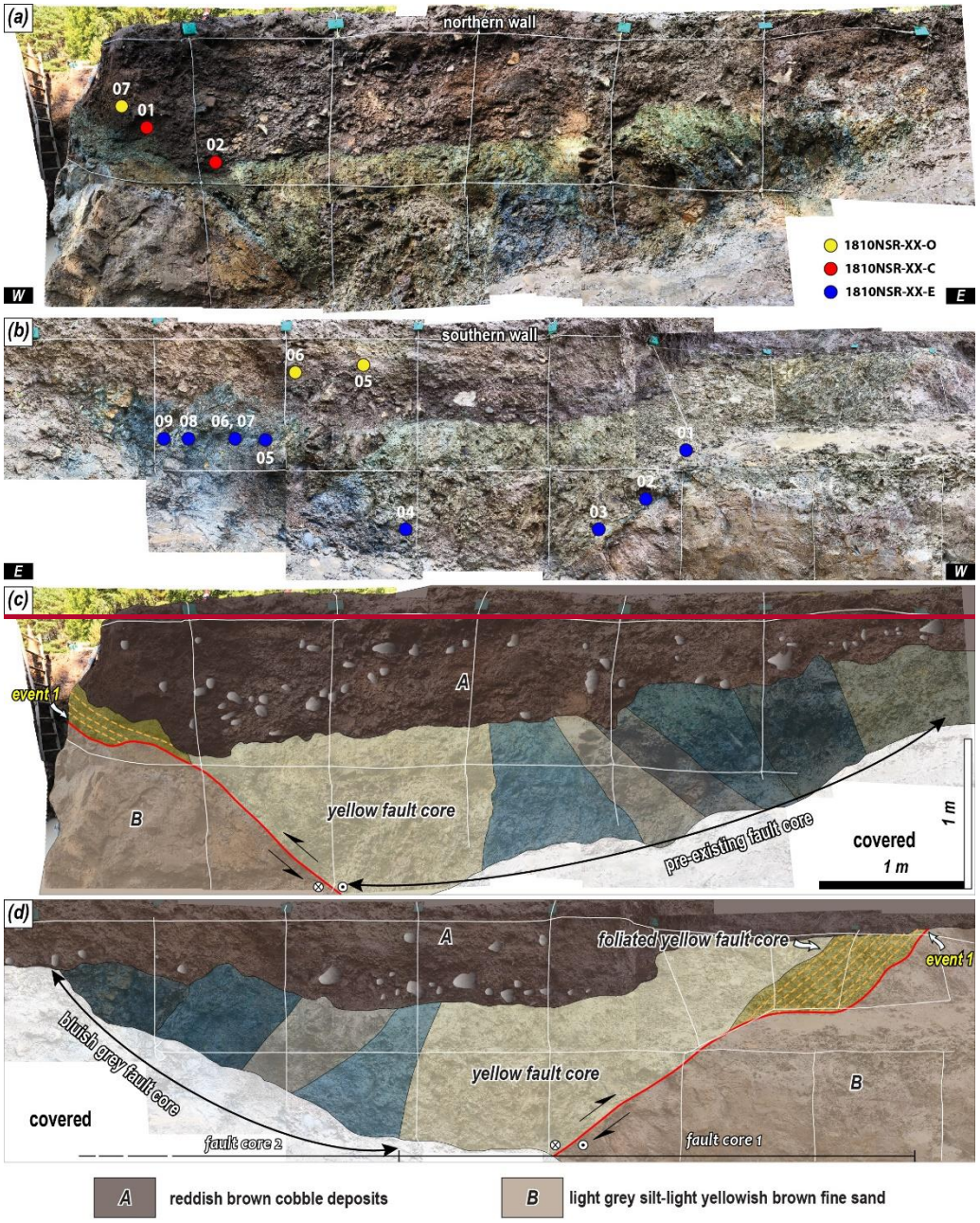
(a)
northern wall
07
01
02
1810NSR-XX-O
1810NSR-XX-C
1810NSR-XX-E
W
E
(b)
southern wall
06
05
09
08
06
07
05
01
02
03
04
E
W
(c)
event 1
A
B
yellow fault core
pre-existing fault core
covered
1 m
1 m
(d)
A
foliated yellow fault core
event 1
bluish grey fault core
yellow fault core
B
covered
fault core 2
fault core 1
A
reddish brown cobble deposits
B
light grey silt-light yellowish brown fine sand

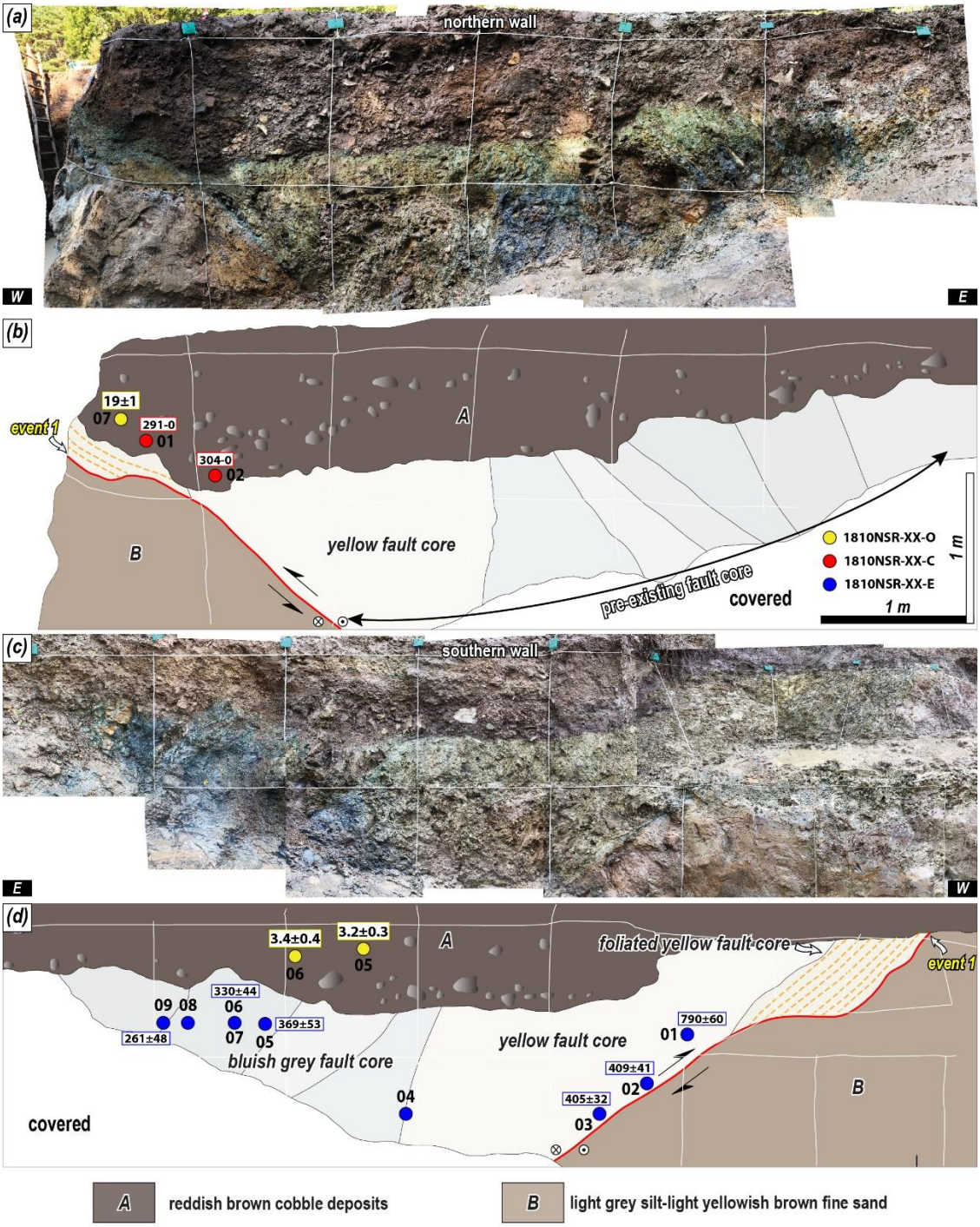

Figure 4: Photomosaic of the trench 2 ~~section~~exposed wall of the (a) northern and (~~c~~b) southern walls. The colored circles represent samples for age dating. Detailed sketch of the trench 2 ~~section~~exposed wall of the (~~c~~b) northern wall and (d) southern wall. White lines indicate a 1 m × 1 m grid. The numbers in the yellow, red, and blue boxes represent OSL and IRSL (ka), radiocarbon (cal yr BP), and ESR (ka) dating results, respectively.

Table 4~~5~~. Cosmogenic ^{10}Be-^{26}Al isochron burial dating results of granite wash at Trench 2

Name	Latitude (˚N, DD)	Longitude (˚E, DD)	Elevation (m asl)	Depth[a] (m)	Density[b] (g·cm^{-3})	^{10}Be Conc. (10^4 atoms g^{-1})	^{27}Al Conc. (10^4 atoms g^{-1})	$^{26}Al/^{10}Be$[c]	Isochron Age[d,e] (Ma)
NAN001	36.075519	129.256658	104	28	2.0	12.12 ± 0.53	23.39 ± 2.16	1.93	
NAN002	36.075519	129.256658	104	28	2.0	2.08 ± 0.08	6.89 ± 0.83	3.31	
NAN003	36.075519	129.256658	104	28	2.0	2.41 ± 0.10	10.39 ± 1.08	4.30	
									2.87 ± 0.59

[a] Relative depth from the surface.

[b] Density of unconsolidated sediment.

[c] Production ratio for the surface is 6.75.

[d] Uncertainties are calculated at the 1σ confidence interval.

[e] All errors are propagated.

4.2.3 Trench 3

Trench 3 iwas located on the main lineament extending 1.73.5 km north of the Trench 2 Byeokgye site (Fig. 2c),. within a cultivated field next to a wide road at the mouth of a broad basin. Fault scarps along the main lineament extend both south and north of the Trench 3. This trench marks the northernmost point where the transition to the alluvial fan is observed where the mountain ridge meets the main lineament; beyond this point, fault scarps continue to develop on the alluvial fan surface. Eight Quaternary sedimentary units and three fault planesfault splays arewere identified in the trench wallsection (Fig. 5, Table 1). The hanging wall of the Quaternary slip zonemain fault surface, which cut through Quaternary sediments, iwas composed of a pre-existing fault core. Excavation revealed a fault core at least 20 m wide. The pre-existing fault core was divided into gouge and brecciated zones and the brecciated zone was further divided into black-brown and gray by color. The fault gouge zone that cut the Quaternary sediments iwas narrower than 5 cm at the bottom of the wallsection and widened to 40 cm at the top of the wallsection; it iwas divided into an greyishoff-white gougefault zone and a red gougefault zone by color and slip surface. The red fault gouge zone iwas almost entirely composed of clay; however, there wereare numerous uncrushed quartz and rock fragments within the graeyish-white gouge zone. The fault brecciated zones were all crushed, with numerous NE-striking veins embedded within the black-brown fault brecciated zones. The slip surfaces separating each zone within the fault core were all N-S- to NE-striking. The characteristics of the eight units are shown in Table 1. Unit D iswas a colluvial wedge that indicates a paleo-earthquake (Fig. 5, Table 1). Brown sand to fine (units F and H) and brown gravel (units C, E, and G) deposits wereare in the trench sectionwall. These features can be attributed to environmental factors, such as deposition due to repeated rainfall, flooding, or seismic events due to repeated seismic motion. The Quaternary slip zone cuts through unit C, including unit D, a colluvial wedge, and is covered by unit B. The slickenline observed on the main fault surfacefault splays indicateindicatess a dextral strike-slip with a small reverse component. There wereare at least two estimated faulting events in this exposedcross wall section: event 1, which formed a colluvial wedge, and event 2, which cut the colluvial wedge (Fig. 5). The $pIRIR_{225}$ ages of sample 1903NR1R-02 and 03-O from unit E at the southern wall wereare 173±6 ka and 175±5 ka, respectively.. In contrastwhile, the $pIRIR_{225}$ age of 1903NR1R-08-O from unit D, which is the colluvial wedge that directly indicatesd the timing of athe faulting event, showsrevealed that the deposit formed at 137±3 ka (Table 12). AdditionallMeanwhile,y sample 1903NR1R-10-O from unit B, which coversed the rupturefault, iwas dated as 6.4±0.4 ka. These findings suggest that the first surface rupture occurred at 137±3 ka, as indicated by the colluvial wedge, and the next surface rupture occurred before 6.4±0.4 ka indicated by event 2 horizon. The youngest ESR age for the fault gouge wasis 409±52 ka (1903NR1R-02-E, Table 34). However, sinceconsidering that the quartz ESR signal in the fault zone may not fully reset during faulting, this age implies that the last faulting event occurred at or after 409±52 ka. The ESR ages cluster into two time periods: 417±59 ka (1903NR1R-01, 02-E), 702±123 ka (1903NR1R-03-E).The combination of descriptive features and ages suggests a paleo-earthquake that formed the colluvial wedge at 137±3 ka, followed by MRE that cut the wedge between 137±3 and 6.4±0.4 ka.

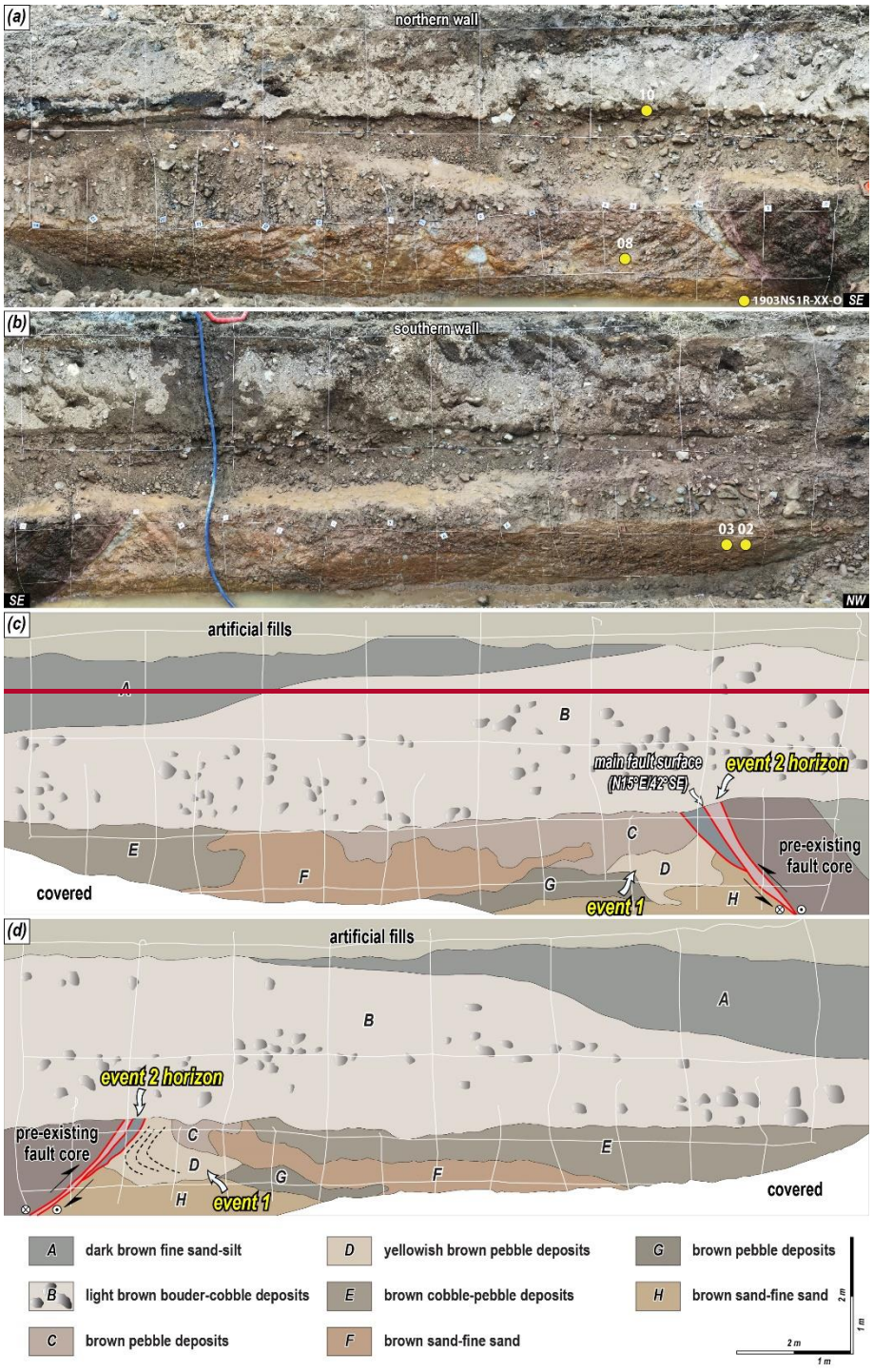
(a)
northern wall
10
08
1903NS1R-XX-O
SE
(b)
southern wall
03 02
SE
NW
(c)
artificial fills
A
B
main fault surface
(N15°E/42°SE)
event 2 horizon
C
E
F
G
D
pre-existing
fault core
covered
event 1
H
(d)
artificial fills
A
B
event 2 horizon
pre-existing
fault core
C
D
G
H
event 1
E
F
covered
A dark brown fine sand-silt
B light brown bouder-cobble deposits
C brown pebble deposits
D yellowish brown pebble deposits
E brown cobble-pebble deposits
F brown sand-fine sand
G brown pebble deposits
H brown sand-fine sand
2 m
1 m
2 m
1 m

445

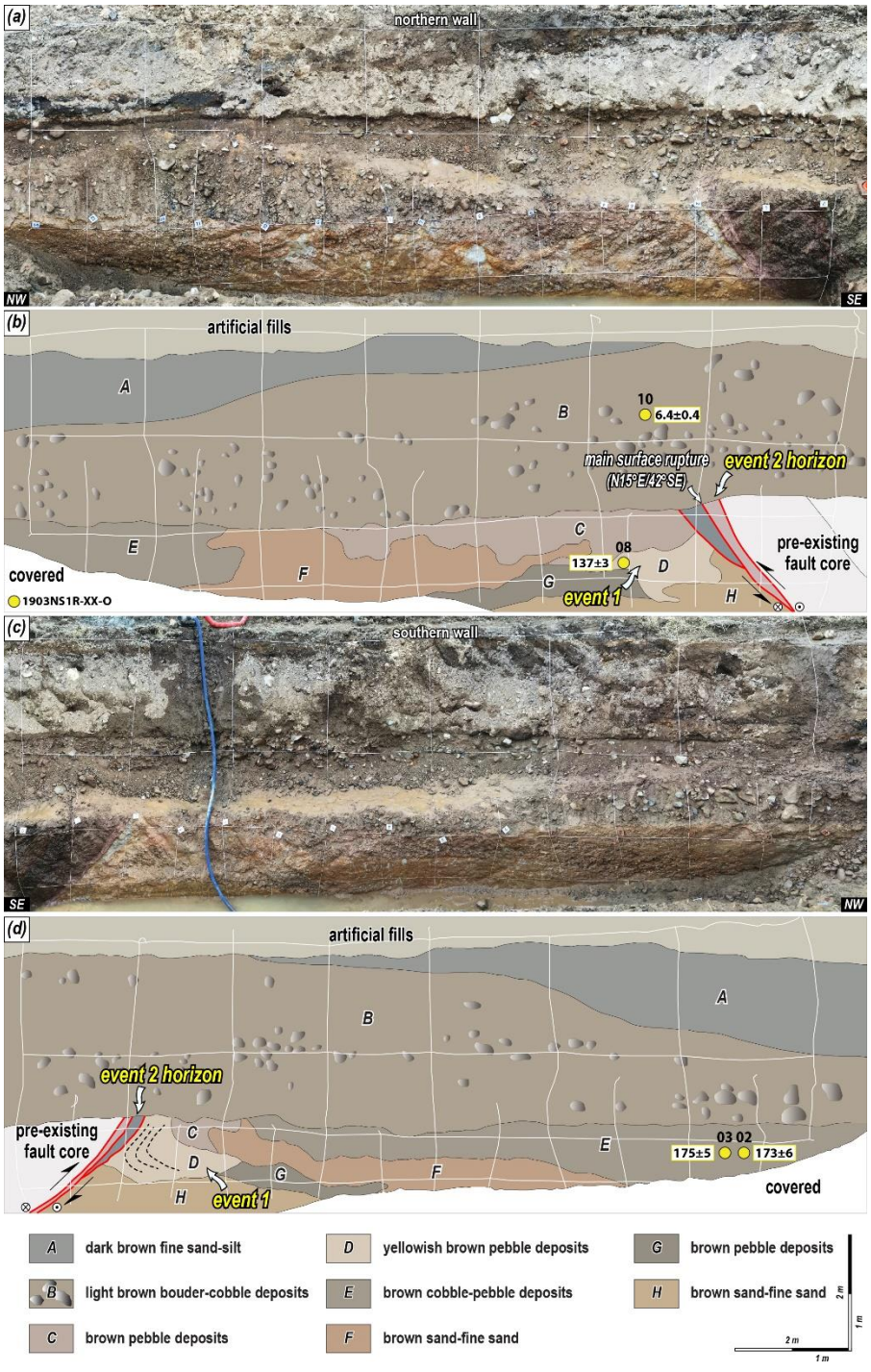

Figure 5: Photomosaic of the trench 3 ~~section~~wall of the (a) northern wall and (~~c~~b) southern wall. The colored circles represent samples for age dating. Detailed sketch of the trench 3 ~~section~~wall of the (~~c~~b) northern and (d) southern walls. White lines indicate a 1 × 1 m grid. Black dot line reveals bedding trace. The numbers in the yellow, red, and blue boxes represent OSL and IRSL (ka), radiocarbon (cal yr BP), and ESR (ka) dating results, respectively.

4.2.4 Trench 4

Trench 4 iwas situatedlocated on an NE-strikingtrending eastern branch lineament from the main lineament, which stretchesthat extends 2.86.3 km north of the Trench 3Bycokgye site (Fig. 2c). South of Trench 4, a continuous dextrally deflected stream follows the branching lineament, with smaller displacements identified further north. Trench 4 lies at the edge of an alluvial fan near a hillslope, with two features separated by a stream. WithIin the trench sectionwall, there were five Quaternary sedimentary units are cut by a surface ruptureone main fault surface (Fig. 6, Table 1). The hanging wall of the Quaternary fault splay includes main fault surface that cut the Quaternary sediments contained a pre-existing fault core that was at least 5 meters wide at the time ofduring excavation. The pre-existing fault core was divided into two zones based on the color and type of fault rock. Fault core 1 is likely of alkaline granite origin and consisted of a reddish-brown gouge zone and a light yellow breccia zone cutting through Quaternary sediments. The fault gouge zone was an equal mixture of gouge and breccia and the breccia was mostly composed of alkaline granite. In the area Aadjacent to the Quaternary sediments, a 20-cm-wide fault gouge zone developed, characterized by which was distinguished by yellowish-brown and reddish-brown gouges. The fault breccia zone was dominated by 30–50 cm alkaline granite breccias with dark gray to black fault gouges along both edges of the zone. Fault core 2, shown in gray, was dominated by a mixture of fault gouge and fault breccia. Slip surfaces of the N–S strike were developed within the fault core. In some sections within the fault core, a 30 cm wide, dark gray fault gouge zone developed and the boundary of the fault gouge zone consisted of N–S striking slip surfaces containing slickenlines indicating dextral strike slip. Units A and B exhibitshowed horizontal to sub-horizontal bedding, whilewhereas the bedding of units C-F tiltsed to the westward, with dips of up to 50° nearadjacent to the surface rupture, main fault surface and becoming shallower toward the west (Fig. 6, Table 1). The difference in bedding orientations indicatesd an angular unconformity between unit B and units C–F. A surface rupture, covered by unit A, cuts through all of units C-F, including the unconformity, but does not extend through all of unit B. The slickenlines observed on the main fault surfacefault splay indicatingindicates a dextral strike slip with a minorsmall reverse component. At least two faulting events wereare inferred from the exposed wallcross section: the first faulting event 1 (PE), which caused the tilting of units C–F to tilt after they were depositioned (event 1 horizon), and MRE, occurred during the deposition of unit B, following the formation of after anthe angular unconformity (Fig. 6).

We collected five samples from the northern wall of units A and B and four from units D and F for dating. The OSL age of 5.9±0.4 ka waswas obtained from 2009UGR-09-O, which wasis cut by the rupturefault. For the remaining four samples that wereare not cut by the rupturefault, the oldest OSL age wasis 1.3±0.1 ka, recorded obtained for 2009UGR-05-O (Table 21). Additionally, The fault event occurred during the continuous deposition of unit B. Ssamples werewere collected from units F (2009UGR-01-C) and A (2009UGR-02-C) for radiocarbon dating (Table 23). The radiocarbon age of the charcoal from 2009UGR-02-C wasis 160±30 cal yr BP, which alignsagreed with the OSL age of 0.15±0.01 ka ofor the sediment containing the charcoal (2009UGR-07-O), and strongly indicatinged that unit A waswas deposited at this time. Based on the The MRE

~~for this trench, derived from~~ the comprehensive dating analyses, the MRE for this trench occurred between~~indicates~~ ~~1.3±0.1~~ 5.9±0.4 ~~–~~ 1.3±0.1 ka, as the faulting event took place during the continuous deposition of unit B.~~.~~

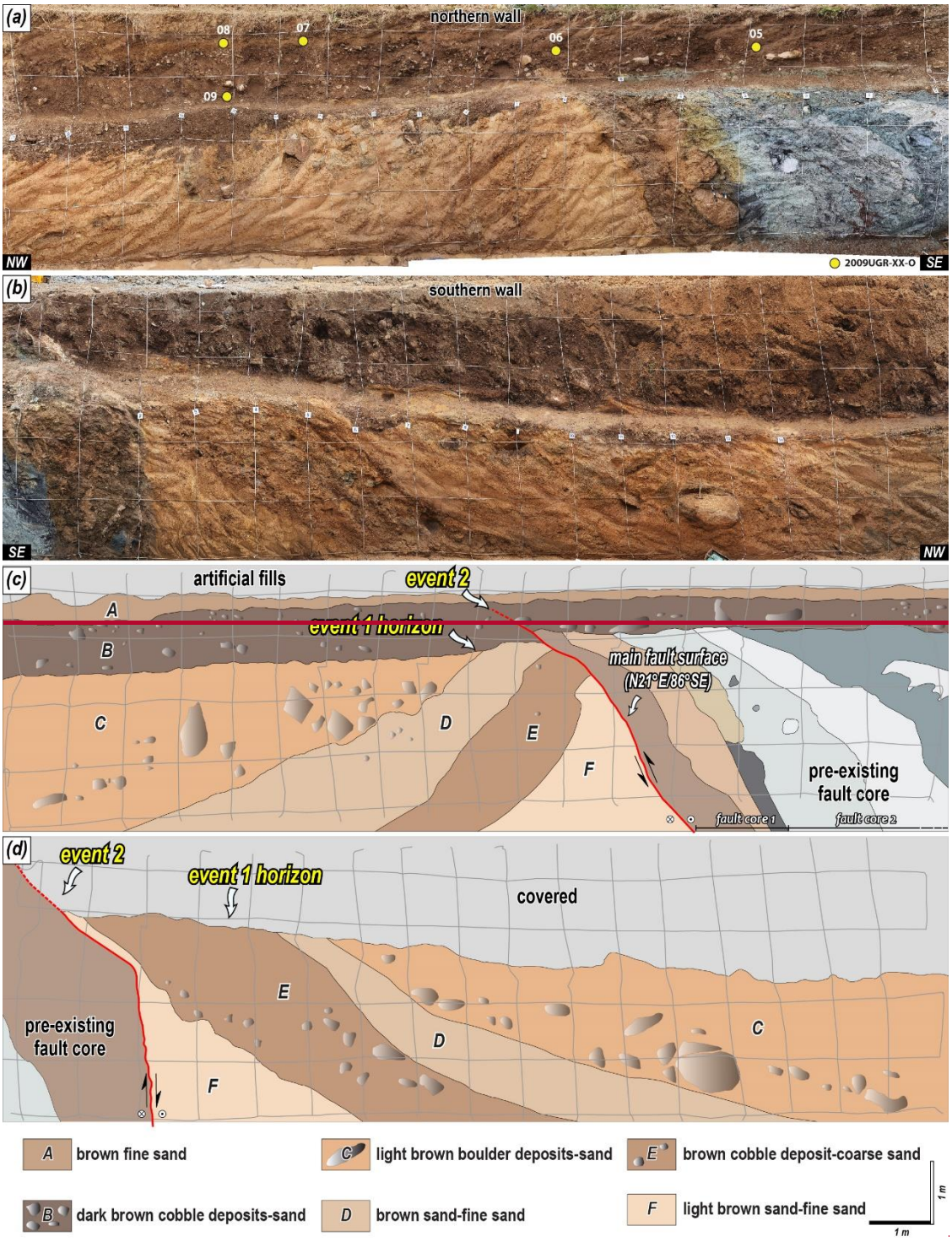
(a)
northern wall
08
07
06
05
09
NW
2009UGR-XX-O
SE
(b)
southern wall
SE
NW
(c)
artificial fills
event 2
event 1 horizon
A
B
C
D
E
F
main fault surface
(N21°E/86°SE)
pre-existing
fault core
fault core 1
fault core 2
(d)
event 2
event 1 horizon
covered
E
D
C
pre-existing
fault core
F
A brown fine sand
B dark brown cobble deposits-sand
C light brown boulder deposits-sand
D brown sand-fine sand
E brown cobble deposit-coarse sand
F light brown sand-fine sand
1 m
1 m

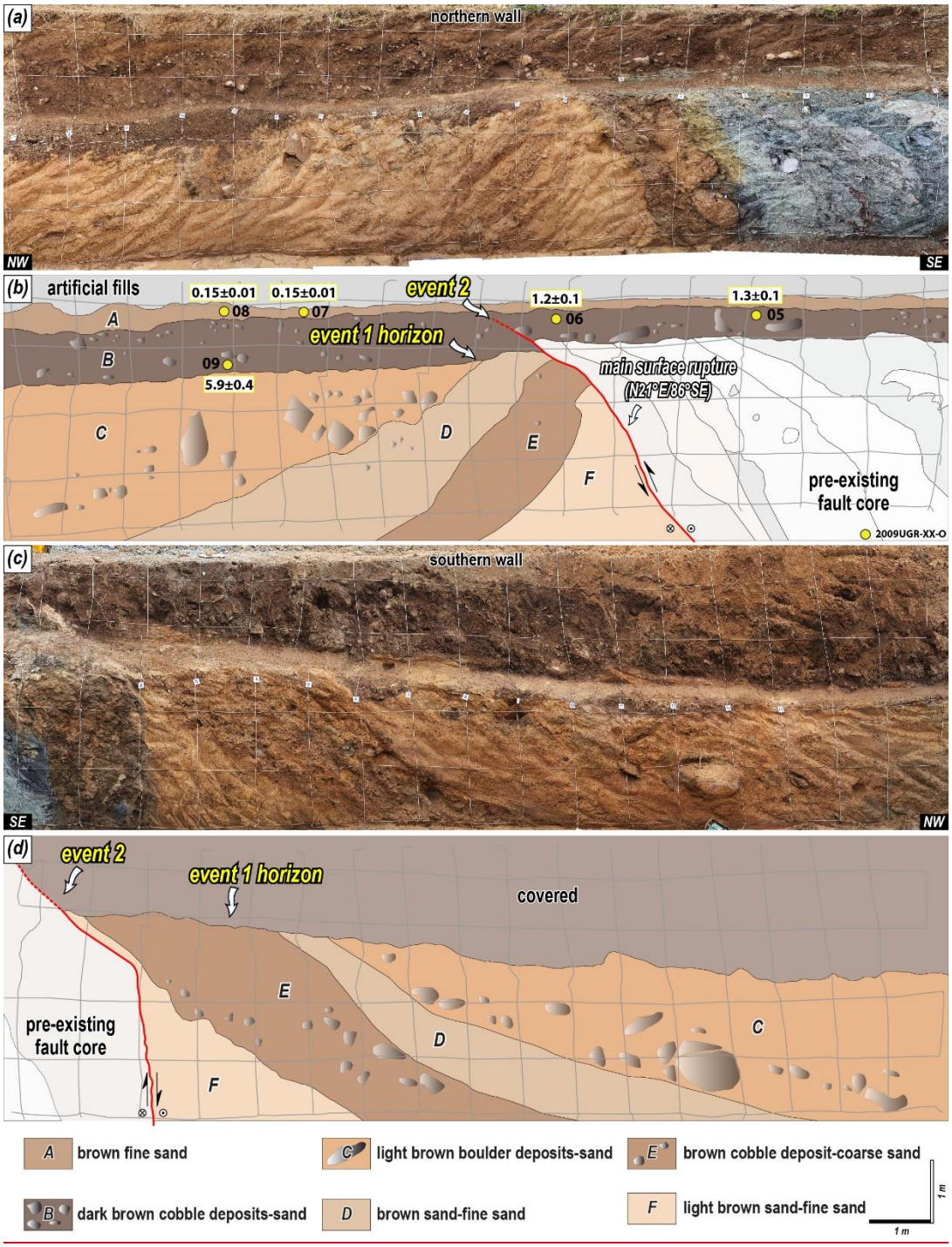

Figure 6: Photomosaic of the trench 4 ~~section~~wall of the (a) northern and (~~c~~b) southern walls. The colored circles represent samples for age dating. Detailed sketch of the trench 4 ~~section~~wall of the (~~c~~b) northern and (d) southern walls. Grey lines indicate a 1 × 1 m grid. The numbers in the yellow, red, and blue boxes represent OSL and IRSL (ka), radiocarbon (cal yr BP), and ESR (ka) dating results, respectively.

4.2.5 Trench 5

Trench 5 ~~was~~is located 40 m north of Trench 4. Because of its proximity, Trench 5 shares identical topographic characteristics with Trench 4, except that it lies on the margins of a hillslope instead of on an alluvial fan. The trench ~~section~~wall contained five quaternary sedimentary units, cut by one ~~main fault surface~~ fault splay (Fig. 7). The overall appearance of the exposed wall~~cross section~~ ~~was~~is similar to that of Trench 4. The hanging wall of the fault splay that cut the Quaternary sediments consisted of a pre-existing fault core at least 20 m wide. ~~The pre-existing fault core was derived from alkaline granite, as shown in Fig. 6. The fault core was divided into a fault gouge zone and a fault breccia zone bounded by an N-S to NNE striking slip surface. The host rock of the light-yellow fault breccia zone was interpreted as alkaline granite and contained a 5–10 cm wide black fault gouge.~~ Where it abuts the Quaternary sediments, a 10 cm wide light ~~gray~~grey fault gouge developed, which changed to a yellowish grey fault gouge with yellow clay mixed toward the top. ~~A 20-cm-wide fissure filling was unveiled near the main fault surface and the slip surface within the fault core showed multiple slickenlines, indicative of dextral strike-slips. Compared to Trench 4, units A–C in Trench 5 were considered to have the same deposits as units A and B in Trench 4 and units D and E in Trench 5 were interpreted to have the same deposits as units C–F in Trench 4. Units D and E in Trench 5 showed westward-dipping bedding like units C–F in Trench 4, whereas units A–C had subhorizontal bedding. The reddish-brown sediments in the upper part of Trench 5 were thicker than those in Trench 4, indicating that a more accurate MRE could be identified compared with Trench 4.~~Units A-C show subhorizontal bedding, units D and E show westward-dipping bedding, and there is an angular disconformity between units C and D. Trenches 4 and 5 are almost the same because they are adjacent, with units A-C in Trench 5 matching units A, B in Trench 4 and units D, E in Trench 5 matching units C-F in Trench 4. The reddish-brown sediments in the upper part of Trench 5 appear to be thicker than in Trench 4 because it is the tip of a hillslope. The Quaternary fault splay cut unit C but failed to cut unit B. The slickenline observed on the high-angle Quaternary fault splay ~~main fault surface~~ indicated a dextral ~~strike~~ slip with a small reverse component. At least two~~The number of~~ faulting events are~~was~~ estimated~~, at least two~~ based on the same angular unconformity as in Trench 4. Event 1 caused units D and E ~~tilting~~to tilt, which cut them (event 1 horizon, Fig 7). Event 2 occurred during the deposition of unit C, which failed to cut into unit B.

The OSL ages on the southern wall of 2010UGR-03-O and 04-O from unit B ~~on the south slope were~~are 2.8±0.1 and 2.6±0.1 ka, respectively, and those of 2010UGR-01-O and 02-O from ~~the fault cut~~ unit C ~~were~~are 10±1 and 4.8±0.2 ka, respectively (Table 1~~2~~). The fault splay is cutting through unit C and failing to cut through unit B. Therefore, ~~T~~trench 5 yielded a tighter MRE range of ~~2.8±0.1~~ 4.8±0.2 – 2.8±0.1ka than the MRE of Trench 4.

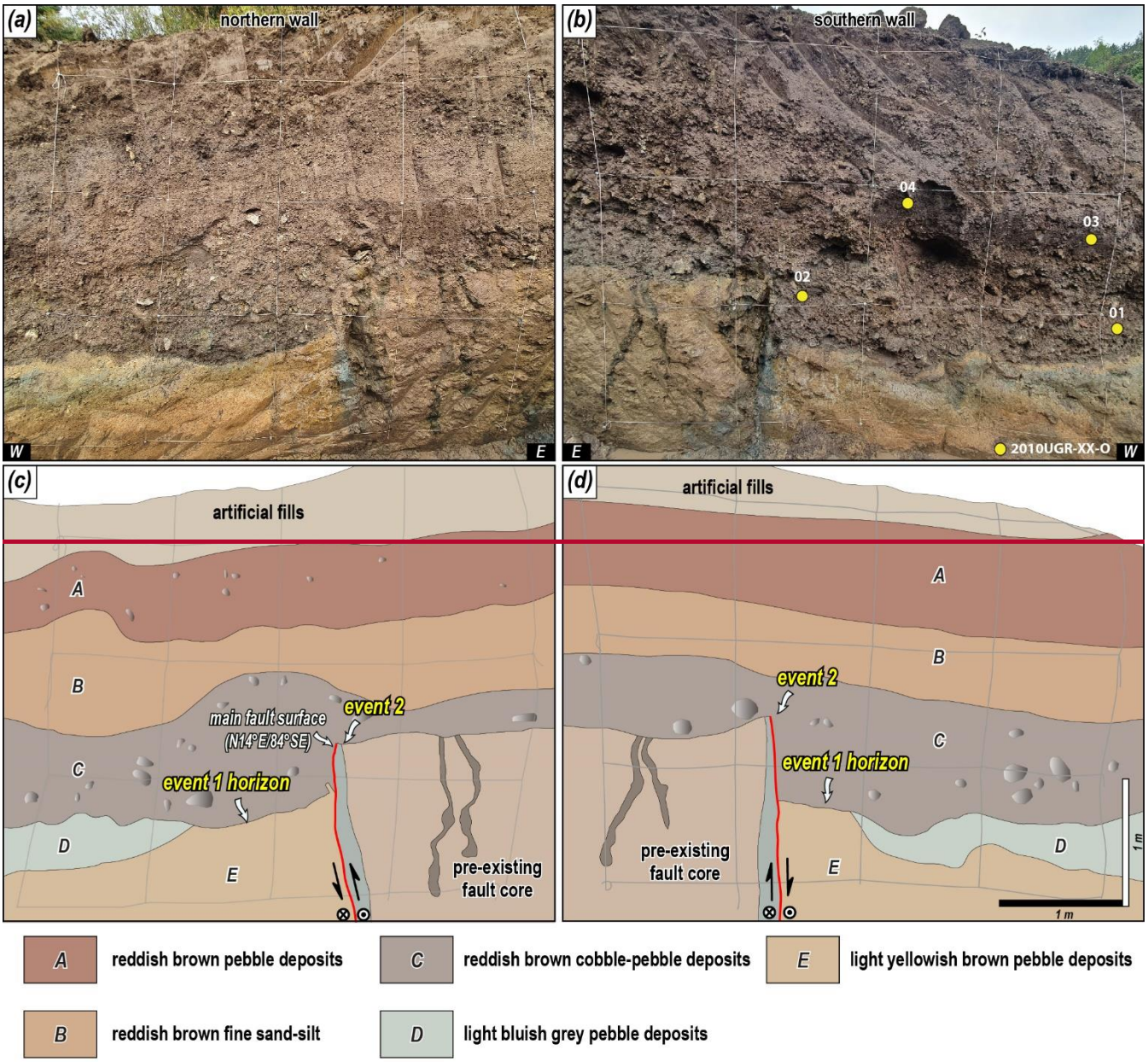
(a)
northern wall
W
E
(b)
southern wall
04
03
02
01
E
2010UGR-XX-O
W
(c)
artificial fills
A
B
C
D
E
main fault surface
(N14°E/84°SE)
event 2
event 1 horizon
pre-existing
fault core
(d)
artificial fills
A
B
C
D
E
event 2
event 1 horizon
pre-existing
fault core
1 m
1 m
A
reddish brown pebble deposits
B
reddish brown fine sand-silt
C
reddish brown cobble-pebble deposits
D
light bluish grey pebble deposits
E
light yellowish brown pebble deposits

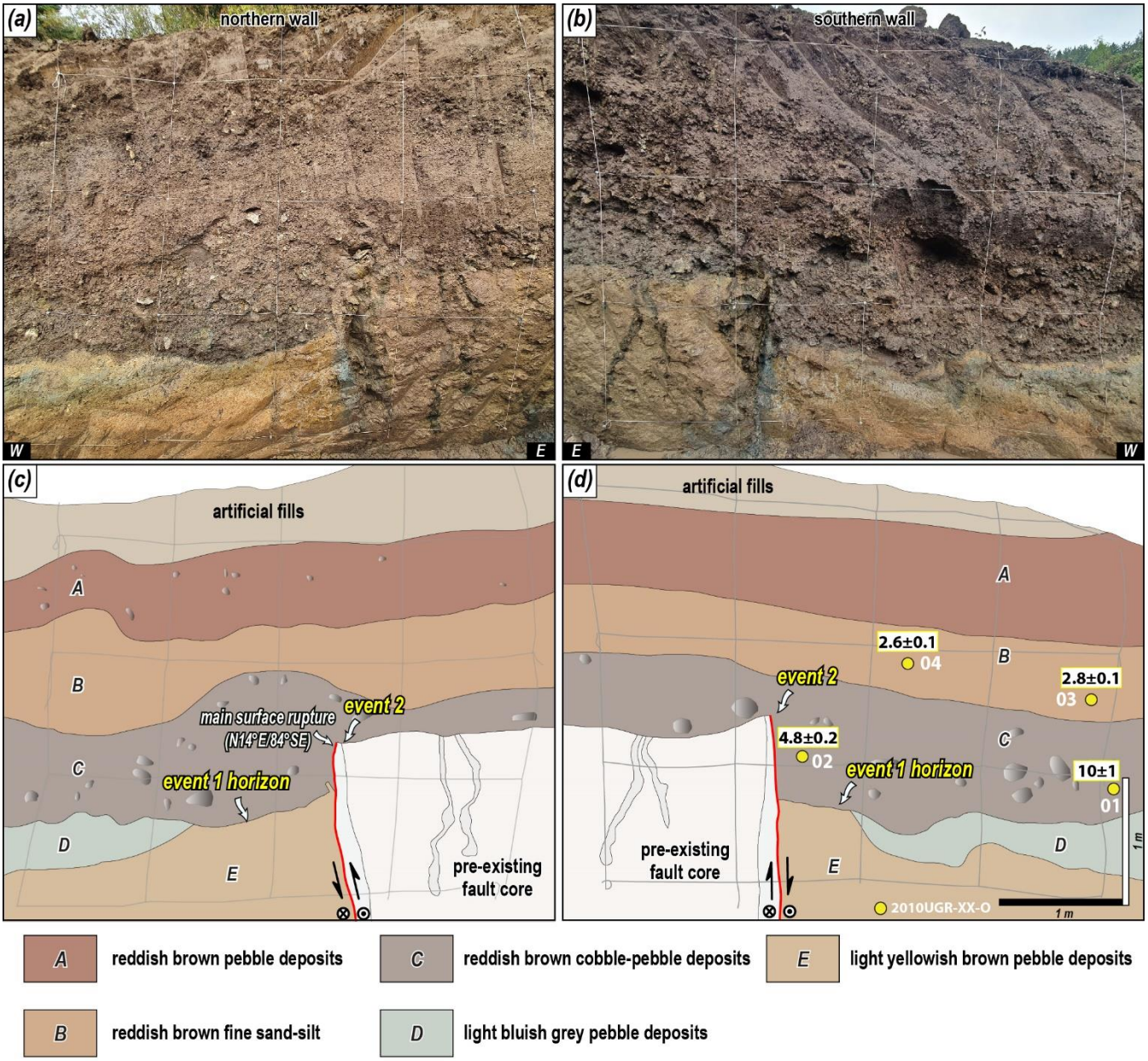

Figure 7: Photomosaic of ~~the trench 5 section of the~~ (a) northern and (b) southern walls of the Trench 5. The colored circles represent samples for age dating. Detailed sketch of ~~the trench 5 section of the~~ (c) northern and (d) southern walls of the Trench 5. Grey lines indicate a 1 × 1 m grid. The numbers in the yellow, red, and blue boxes represent OSL and IRSL (ka), radiocarbon (cal yr BP), and ESR (ka) dating results, respectively.

4.3 Paleo-stress reconstruction

The 20 slickenlines found in the trench ~~were~~are divided into those in the ~~main fault surface~~Quaternary slip surface that cut the Quaternary sediments and those in the pre-existing fault core. For the reconstruction of the paleo-stress field, twenty kinematic data along with the geometry of the fault planes and slickenlines ~~were~~were collected and analyzed using Wintensor S/W (v.5.8.5) (Delvaux & Sperner, 2003). Based on the slickenlines of the Quaternary slip surface~~main fault surface~~, the analysis yielded a maximum horizontal stress (σ_{Hmax}) in the ENE-WNW direction (R´=1.62; Delvaux et al., 1997; Fig. 8), which agrees with the current stress field on the Korean Peninsula (Kim et al., 2016). ~~The slickenlines in the pre-existing fault core indicated NE-SW compression, which was consistent with the stress field that causes dextral strike-slip deformation, which is one of the major movements of the Yangsan Fault (Cheon et al., 2019, 2020a).~~ The reconstructed paleo-stress indicated that the dextral ~~strike-~~slip with a small reverse component identified in the Quaternary slip surface ~~main fault surface~~ occurred in an ENE-WSW strike-slip~~compressional~~ stress regime.

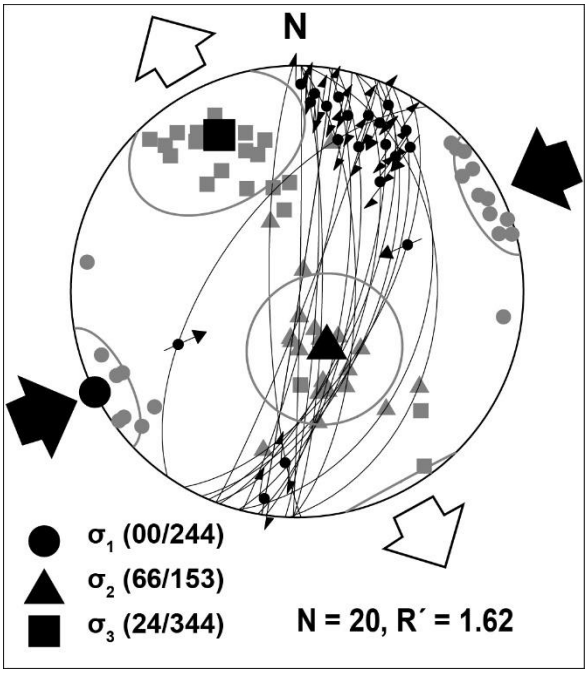

Figure 8: Fault slip data in the Quaternary slip surface~~fault zone~~ (lower-hemisphere, equal-area projection). Convergent and divergent arrowheads represent contraction (σ_{Hmax}) and horizontal stretching (σ_{Hmin}) directions, respectively. The principal stress axes σ_1 (circles), σ_2 (triangles), and σ_3 (squares) are projected. R´=2-R (σ_2 is vertical) [Delvaux et al., 1997; R=(σ_2-σ_3)/(σ_1-σ_3)].

4.4 Displacement and ~~m~~Magnitude ~~e~~estimation

The results calculated using the marker, vertical separation of each trench, and Eq. (B~~A~~1) are listed in Table 5~~6~~. In the~~our~~ previous study by Lee et al. (2016), the horizontal~~true~~ displacement of the MRE at the Dangu site ~~was~~is determined to be 2.~~64~~55 m ~~(Lee et al., 2016)~~. For each surface rupturing~~faulting~~ event in Trench 1, the horizontal displacement per event according to the event horizon i~~was~~ 0.~~339 1.8~~1.05~~1~~ m, and the horizontal~~true~~ displacement of the MRE ~~was~~is 1.72~~0.61 2.81~~

m., and the cumulative displacement based on the unconformity of the bedrock and Quaternary sediments was 3.1–8.8 m. Using the bedrock and Quaternary sediments unconformity identified by corings in Trench 2 as a marker, the cumulative horizontaltrue displacement wais 7694 m. The MRE cutting the colluvial wedge in Trench 3 hased a horizontaltrue displacement of 2.853.29 m. However, when considering the overall interpretation, only the MRE and AE, but not the PE, are recognized in Trench 3 (Figs. 5 and 9). The displacement cutting the colluvial wedge likely reflects the displacement of the missing PE as well as the MRE, which is supported by the long interval between the wedge (unit D) and the deposit covering the wedge (unit B). Thus, it is reasonable to exclude the calculated displacement as it is unlikely to be the displacement of the MRE. The horizontaltrue displacement of the MRE in Trench 4 and 5 arewas 0.862 m and 2.211.17–2.34 m, respectively, using the lower boundary of units B and C as markers. Combining the results from each trench, the horizontaltrue displacement of MRE in the study area wasis 0.820.64–2.812.55 m and the cumulative horizontal displacement wasis 763.1–94 m. The horizontal displacement per event iwas similar, between 0.339–1.051 m for PE and AE (event 1, 2), but the trench showsed a higher displacement for the MRE (event 3).

We estimatedassumed the maximum earthquake magnitude by applying the MD (horizontal displacement: 0.64–2.81.82-2.55 m) of the MRE,. resulting in a The maximum magnitude estimate of the MRE was estimated to be 6.7–7.12. Seismic SSDs such as the 20-50 clastic dike and 30 cm ball-and-pillow structure observed in the exposed wall (units E and G in Trench 1; unit F in Trench 3), serve as indirect evidence indicating an earthquake of at least magnitude 5.5 (Atkinson et al., 1984).Furthermore, the surface rupture length (SRL) of 7.6 km obtained from the topographic analysis (Ha et al., 2022) was applied to the MD-SRL empirical relationship. The calculated MD was 0.21 m, which was smaller than the true displacement of the MRE (0.64–2.81 m), suggesting that the actual surface rupture length in the study area exceeds 7.6 km, although this was not confirmed by the current topography. The earthquake magnitude was estimated from the seismic SSDs in the trench cross-sections (units E and G in Trench 1; unit F in Trench 3). In unit E, the clastic dike varied in size from approximately 20 to 50 cm, whereas in unit G, a ball-and-pillow structure of more than 30 cm developed (Song et al., 2020; Ha et al., 2022). Atkinson et al. (1984) reported that liquefaction phenomena, including SSDs above a certain size in sediments of shallow lake or fluvial origin, occur when the minimum earthquake magnitude exceeds 5.5. Based on this, the estimated earthquake magnitude of these SSDs structures may vary depending on the depositional environment and substrate characteristics. However, it was estimated to be at least 5.5, which is consistent with the magnitude of the inferred empirical relationship.

Table 56. Fault displacement of study area

		S_v (m)	α (˚)	γ (˚)	S_t (m)	**S_h (m)**
Dangu[a]	MRE (event 3)	0.67	79	15	2.64	**2.55**
	Marker	Unit D				
Trench 1[b]	MRE (event 3)	0.49	69	17	1.8	**1.72**
	Marker	Unit C				
	PE (event 2)	0.31	75	17	1.1	**1.05**
	Marker	Unit G				
	AE (event 1)	0.22	53	17	0.94	**0.9**
	Marker	Unit H				
Trench 2	Cumulative displacement	34	38	36	94	**76**
	Marker	Quaternary deposits thickness				
Trench 3	MRE (event 3)	1.1	42	30	3.29	**2.85**
	Marker	Unit D				
Trench 4	MRE (event 3)	0.25	86	17	0.86	**0.82**
	Marker	Unit B				
Trench 5	MRE (event 3)	0.8	84	20	2.35	**2.21**
	Marker	Unit C				

	Dangu[a]				Trench 1[b]				Trench 2				Trench 3				Trench 4				Trench 5			
	S_v (m)	α (˚)	γ (˚)	**S_t (m)**	S_v (m)	α (˚)	γ (˚)	**S_t (m)**	S_v (m)	α (˚)	γ (˚)	**S_t (m)**	S_v (m)	α (˚)	γ (˚)	**S_t (m)**	S_v (m)	α (˚)	γ (˚)	**S_t (m)**	S_v (m)	α (˚)	γ (˚)	**S_t (m)**
MRE	0.67	79	15	**2.64**	0.49	69	17-56	**0.64-1.81**					1.1	42	30	**3.29**	0.25	86	17	**0.86**	0.4-0.8	84	20	**1.17-2.34**
Marker	Unit D				Unit C								Unit D				Unit B				Unit C			
PE (event 2)					0.31	75	17-56	**0.39-1.1**																
Marker					Unit G																			
AE (event 3)					0.22	53	17-56	**0.33-0.94**																
Marker					Unit H																			
Cumulative displacement					2.4	69	17-56	**3.1-8.8**	34	38	36	**94**												
Marker					Quaternary deposit thickness																			

[a]modified from Lee et al., 2015

[b]modified from Song et al., 2020

5 Discussion

5.1 Interpretation of Paleoseismic Ddata

5.1.1 MRE and number of surface faulting

We determinedd the MRE and number of faulting events of the study area based on each trench site, considering previous studies, the age of Quaternary deposits and fault gouges, the geometry and cross-cutting relationship between fault splays and sediments, and the kinematics in the each trench section (see the heading 4.1). The results for each trench arewere synthesized to estimate the MRE, number of earthquakes (faulting events), and timing of earthquakes along the Byeokgye sectionin the study area (Fig. 9). First, the MRE wais 2.8±0.1 3.2±0.2 2.8±0.1 ka, which is the time of overlap in several trenches. Considering the error range, the surface rupture must have occurred approximately 3,000 years ago. Considering the minimum number of earthquakes estimated for each trench as the maximum, at least three faulting events may have occurred along the studied sectionin the study area, as determined from the Dangu site and Trench 1. The timings of the remaining two prior earthquakes, excluding the MRE, were quantified by combining the age and interpretation of each trench. Furthermore, The penultimate earthquake (PE) occurred in 17±1 75±3 17±1ka, based onwhich was determined using the youngest age of the PE (unit C) from Trench 1 and the MRE from the Byeokgye site (Fig. 9). The antepenultimate earthquake (AE) waiis from 137±3 142±4 137±3ka, constrained by the paleoseismic interpretationthe age of the lowermost sediments cut by the fault in Trench 1 and the colluvial wedge in Trench 3. On the other hand, clustering the ESR ages at each trench with an error range suggestsed at least three separate older earthquakes at 245±37, 404±10, and 817±10, 404±10, and 245±37 ka (Fig. 9). These ages indicate the time elapsed since the ESR signal waisis set to zero by the faulting at depth, but it needs much care to use as a timing indicator of the faulting event because of the possibility thatas the ESR signal waisis not completely bleached. Nevertheless, clustered faulting patterns at seven sites suggest that the study area had at least six earthquakes during the Quaternary. Nevertheless, the faulting patterns recognized from clustering in several trenches indicated that the study area experienced at least three earthquakes in addition to those that cut Quaternary sediments.

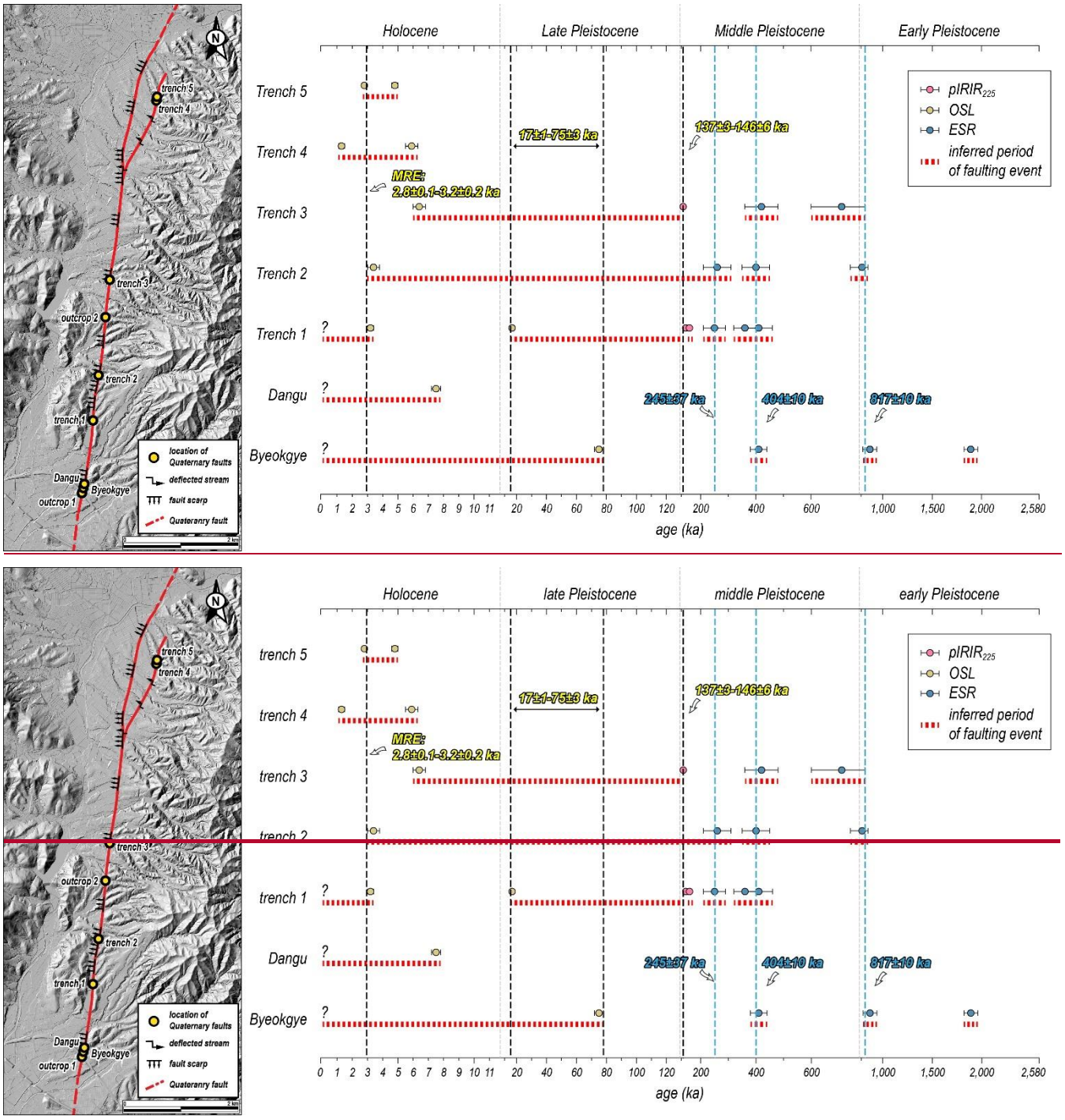

Figure 9: Age distribution graph of the study area. The graph reveals the timing of the paleo earthquake based on trench interpretation and age overlap. The most recent earthquake in the study area occurred probably around 3,000 years ago.

605

5.1.2 Quaternary slip rate and recurrence interval

The slip rate is an expression of the average displacement of a fault over a certain period, which numerically shows how quickly energy (stress) accumulates in a fault zone and is used as an important input parameter in seismic hazard assessment (Liu et al., 2021). The horizontal slip rate in the study area ~~was~~is calculated based on the earthquake timing~~age~~ and horizontal displacement of each trench. We calculated slip rates from three trenches spanning different periods: Late Pleistocene to Holocene (Trench 1), Quaternary (Trench 2), and Middle Pleistocene to Holocene (Trench 3). In Trench 1, we derived a slip rate of 0.12-0.14 mm/yr based on the horizontal displacement of event 3 (MRE) of 1.72 m and the 13.8±1.2 ka time interval between events 3 and 2 (time gap between units B and C; Table 1). For Trench 2, borehole data revealed a slip rate of 0.02-0.03 mm/yr, calculated from the cumulative horizontal displacement of 76 m and the cosmogenic ^{10}Be-^{26}Al isochron burial age of 2.87±0.59 Ma from the lowermost Quaternary deposits. In Trench 3, we calculated a slip rate of 0.02 mm/yr using the 2.85 m horizontal displacement of the event that cut the colluvial wedge (unit D) and the 130.6±3.4 ka time interval between events (time gap between units B and D).

Considering the age of the deposits, the slip rate of 0.12-0.14 mm/yr from Trench 1 represents movement during the Holocene, while the rates from Trenches 2 and 3 may represent cumulative slip rate (0.02 mm/yr) throughout the Quaternary. As noted in the method section (3.3), there are uncertainties in obtaining slip rates from 2D trenches alone on strike-slip faults such as the study area. ~~The slip rate was calculated using the MRE and MRE displacement only, and the cumulative slip rate was calculated using the cumulative displacement and the oldest age in the trench section and drilling core. The slip rate calculated using the MRE can be considered maximum because it uses the shortest time for the last earthquake. The cumulative slip rate reflects trends over a relatively longer period than the MRE; therefore, it may show a slip rate closer to the mean but is likely to be an underestimate. The minimum overall slip rate was 0.02 mm/yr, maximum was 0.38 mm/yr, and average was 0.14 mm/yr (Fig. 10). The most reliable slip rate of each trench was 0.04–0.11 mm/yr, which is equal to the slip rate of the MRE obtained for Trench 1, where the second and third of the three earthquakes were identified. The long time interval and displacement of Trench 3 included the MRE from the AE so it is reasonable to consider the slip rate of Trench 3 to be a cumulative slip rate (Fig. 10). The slip rates from the MRE ranged from 0.20–0.35 mm/yr, suggesting a maximum slip rate that can be derived for the study area. The cumulative slip rates derived for each trench indicate a range of 0.02–0.06 mm/yr. The difference in slip rates can be inferred in two ways. First, slip rates during the Quaternary in the study area averaged 0.02–0.06 mm/yr but may have accelerated in the recent Holocene due to changes in the surrounding tectonic setting, such as changes in the thickness of the subducting plates and increases or decreases in far field stress, but also due to local factors such as seasonal climate, fluid inflow, and increased stress accumulation on faults.~~ In particular~~Second~~, the discontinuous distribution of Quaternary sediments may have led to ~~an~~ a mis~~over~~estimation of the slip rate ~~using the MRE~~. There are two distinct types of sediments in the trench wall~~section~~: (1) light brown, relatively coarse-grained sediments of mid-to-late Pleistocene age, which tend~~were observed~~ to be tilted in the vicinity of the surface rupture~~fault~~, and (2) dark brown, relatively coarse-grained, nearly horizontal Holocene sediments (Table 1, Figs. 3-7). The exact absolute time interval between these two deposits is

unknown; however, there ~~was~~is unconformity, and the MRE mostly cut Holocene sediments (<10,000 years). A depositional gap, such as an unconformity, causes earthquake records to be missed during that time, leading to a misestimation of the slip rate. For this reason, in strike-slip fault settings, 3D trenching should be used because the slip rate using displacement from 2D trenches is underestimated compared to the slip rate using topography, which preserves most of the displacement.~~The unconformity in deposition is likely to have missed the earthquakes between the two periods and the MRE cut through younger sediments (Sadler effect; Sadler, 1999), causing the maximum slip rate to be overestimated.~~ The slip rates in this study (0.12-0.14 mm/yr) are lower compared to the slip rates derived from the topography and 3D-trench reported in the study area of 0.38-0.57, 0.5 mm/yr, respectively (Kim et al., 2024; Naik et al., 2024). Nevertheless, the slip rates in our study are meaningful as a minimum value that establishes a lower boundary for the slip rates in the study area.

The recurrence interval in the study area ~~was~~is also estimated. Based on the minimum of three earthquakes estimated from the number of faulting events, the interval between the MRE and PE ~~was~~is 14–72 ka and between the PE and AE ~~was~~is 62–129 ka (Fig. 9). The recurrence interval inversely calculated using the slip rate (RI=event per displacement/slip rate; Wallace, 1970) ~~was~~is approximately 13~~9.5~~ ka using the slip rate of the MRE (average 0.~~21~~13 mm/yr) and the event per displacement (~~average 2~~1.72 m in Trench 1) and approximately ~~23~~ 49 ka using the long-term slip rate (0.0~~31~~2 mm/yr) and the displacement per event (average 0.~~7~~98 m) of the PE and AE. The recurrence interval between MRE and PE is similar to the minimum value of the time gap shown in Figure 9 and the value estimated by the slip rate. Between PE and AE, the recurrence interval calculated from the slip rate is smaller than the time gap obtained in Figure 9. It suggests that the earthquake records in the trench are not complete. Therefore, we can make a conservative estimate that the recurrence interval of the study area is over 13,000 years.

Although no clear recurrence interval has been presented in Korean paleoseismic~~ological~~ studies, Kim and Lee (2023) used ESR ages to suggest that the Yangsan Fault follows a quasiperiodic model and has a recurrence interval of approximately 100 ka, which is closely related to the interval of interglacial sea-level loading over the Late Quaternary~~. Determining the recurrence interval and earthquake periodicity model of the intraplate is difficult. Earthquakes occur in a regular pattern along the boundary in an interplate; however, in an intraplate, they often occur randomly, depending on the heterogeneous and complex interior structure (Liu and Stein, 2016). Long recurrence intervals of 400 ka have been reported for intraplate (Williams et al., 2017); therefore, we can make a conservative estimate that the recurrence interval of the study area is over 10,000 years.~~. However, the recurrence interval may be shorter if the complexity of the fault ~~zone~~ distribution is combined with external factors, such as increased seismicity on the Korean Peninsula after the Tohoku Earthquake (Hong et al., 2015; 2018) or changes in slip rates.

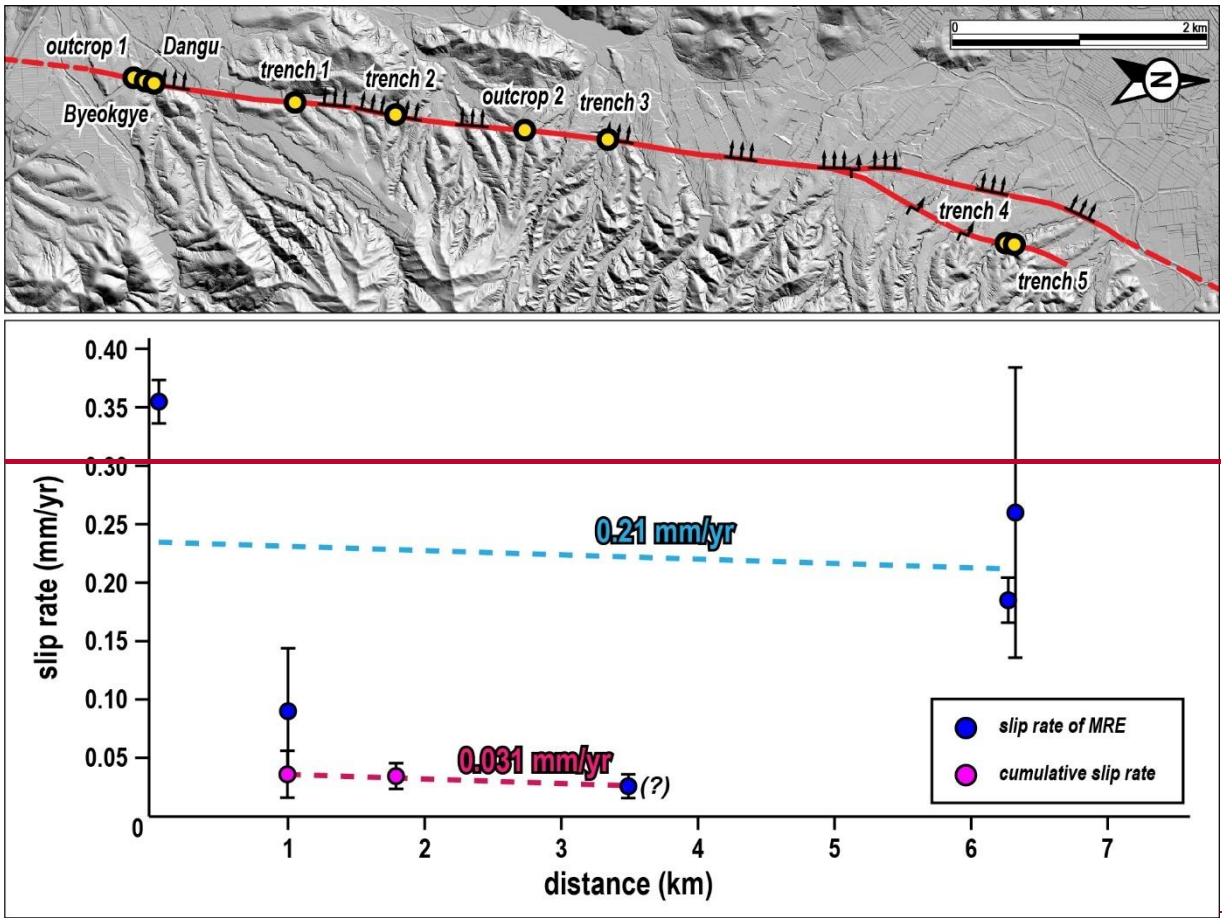

Figure 10: Slip rate graph of the study area. Blue circles indicate slip rate using displacement and age of MRE. Pink circles represent the slip rate using cumulative displacement and age. Dash lines show the trend line and average value of each slip rate. The slip rate in the study area is expected to be between 0.031 and 0.21 mm/yr.

5.2 Structural patterns of Quaternary reactivation of the Yangsan Fault

The trenches revealed the following common features. In all trenches of the study area, the hanging wall of the main fault surface maintained a pre-existing fault core. The exposure of the fault core varied from trench to trench but showed several common features. First, the hanging wall of the Quaternary slip surface is mostly deposited with Holocene sediments only, with no Middle Pleistocene sediments present. only Holocene sediments were present in the hanging wall of the fault core, with no Middle Pleistocene sediments observed. This indicates that reverse faulting has occurred continuously since at least the Middle Pleistocene. Second, NNE to N-S striking Quaternary slip surfaces with high-angle dip have rakes of 20˚ or less, indicating dextral slip with a minor reverse component, NNE-to-N-S striking slip surfaces with high-angle dips were present within the fault core, and slickenlines developed on these slip surfaces, indicating dextral strike-slip with rakes of 10° or less. The main fault surface, which cut Quaternary sediments, dictated E-W compression; however, most shear fractures and slip surfaces in the fault core indicated NE-SW compression. Third, the main surface rupture has a top-to-the-west geometry, and

its hanging wall consists of a pre-existing fault core in all trenches. ~~the internal structure of the fault core was composed of two or more zones delimited by the slip surface, each showing different types of fault rocks and colors depending on the host rock. Fault rocks of the Cretaceous sedimentary origin were mainly composed of thick, purple-colored fault gouge zones and the captured sandstones were greyish-white lenticular fault breccia or brecciated zones. The Cretaceous volcanic rocks mainly comprised dark blue-grey fault breccia zones and fault gouges with a thickness of over 10 cm on both sides of the fault breccia zone. Fault rocks of the Cretaceous granite origin were mainly observed as white fault breccia zones characterized by numerous veins and a clayey matrix due to hydrothermal alteration. In the case of alkaline granites, bright orange fault breccia mainly developed, and a 2–3 cm fault gouge was observed surrounding the lenticular fault breccia. The descriptive features of the fault core internal structure and the occurrence of slickenlines and shear surfaces indicative of NE–SW compression within the fault core are similar to the reported fault core features of the Yangsan Fault (Cheon et al., 2017, 2019; Kim et al., 2022).~~ Fieldwork and previous studies revealed that the A-type alkaline granite in the study area is a dextral offset marker of the Yangsan Fault (Hwang et al., 2004, 2007a, b), and ~~vertical~~ vertically drilled borehole~~cores~~ from the footwall of Trench 2 revealed that the basement rock is A-type alkali~~ne~~ granite. In addition, Kim et al. (2022) conducted inclined borehole drilling~~corings~~ and microstructural studies in the vicinity of Trench 1 and identified a fault damage zone, undeformed wall rock, and a fault core approximately 25 m wide on the eastern side of the A-type alkali granite~~within the alkaline granite of the footwall~~. Multiple lines of evidence demonstrate that the pre-existing fault core distributed on the trenches is the main fault core zone of the Yangsan Fault cutting the A-type alkali granite and that the western boundary of the main fault core i~~was~~s reactivated during the Quaternary. The ~~fault~~ slip surface where the A-type alkali granite contacts the main fault core suggests that it ~~was~~is in a more slip-prone state (e.g., l~~L~~ow coefficient of friction, foliated smectite-rich slip zone; Woo et al., 2015; Kim et al., 2022) during the Quaternary than other slip surfaces within the fault core. ~~The NE–SW compression shown by the slip surfaces and shear fractures within the pre-existing fault core is also consistent with a stress field that generates dextral strike-slip movement, which is the major deformation of the Yangsan Fault (Cheon et al., 2017, 2019).~~ Taken together, these results demonstrate that the western boundary of the fault core within the Yangsan F~~f~~ault zone has been reactivated as a dextral ~~strike-~~ slip with a small reverse component since at least the Early Pleistocene, causing surface rupture in the study area.

A Quaternary surface rupture with a top to the west geometry and its hanging wall composed of fault core is characterized not only in the study area but also throughout the Yangsan Fault. All Quaternary fault sites on the Yangsan Fault, except for the Bogyeongsa site (top-to-the-east, BGS in Fig. 10; Lee et al., 2022), show the top-to-the-west geometry of the main surface rupture (Kyung, 2003; Choi et al., 2012; Cheon et al., 2020a; Han et al., 2021; Ko et al., 2022; Lim et al., 2022; ~~Lee et al., 2022;~~ Kim et al., 2023). At the Quaternary fault sites north of the study area, pre-existing fault cores are observed on the hanging wall of the main slip surface (Kyung, 2003; Choi et al., 2012; Han et al., 2021; Lee et al., 2022; Ko et al., 2022; Lee, 2023). ~~(Kyung, 2003; Ko et al., 2022; Lee et al., 2022; Kim et al., 2023)~~

~~Given that the present-day ENE–WSW stress field acting on the Korean Peninsula has existed since 5 Ma (Kim et al., 2016), it is reasonable to infer that the study area has been continuously faulted with the same kinematics since the beginning of the Quaternary. The hanging wall of the main fault surface that cuts the Quaternary sediments is composed of a pre-existing fault~~

~~core not only in the study area but also in other Quaternary fault sites along the Yangsan Fault. In all reported Quaternary fault sites, except for one (Bogyeongsa site) north of the study area, the fault core was distributed in the hanging wall and had a top-to-the-west geometry (Kyung, 2003; Ko et al., 2022; Lee et al., 2022; Kim et al., 2023). The top-to-west geometry is also confirmed topographically. Where the Quaternary faults are located north of the study area, the average elevation is higher, and the relief is more mountainous on the east side where the hanging wall is located. In the Bogyeongsa section, which does not have this similarity, the topography is uplifted to the west and is the only Quaternary fault of the Yangsan Fault with a top-to-the-east geometry.~~ In the southern part of the study area, the pre-existing fault core constitutes a hanging wall up to Miho (MH in Fig. 10) and Inbo-N site~~ri, Ulju-gun~~ (IBN in Fig. 10~~MH, IBN trench in~~) ~~Kim et al., 2023)~~, located in southern Yangsan Fault (Kim et al., 2023). However, the Quaternary fault sites south of Inbo-N site~~Mihori~~ show different deformation patterns from those to the north. In the Inbo site~~trench~~ (IB in Fig.10), which is closest to the IBN trench, ~~fault planes~~surface rupture developed between unconsolidated sediments (Cheon et al., 2020a), these features are also present in other fault sites of the southern Yangsan Fault (Choi et al., 2012; Lim et al., 2022). The deformation pattern of the Quaternary faulting of the northern Yangsan Fault is top to the west, with the main fault core and unconsolidated sedimentary layers abutting the main surface rupture~~fault surface~~, while the Quaternary faulting of the southern Yangsan Fault is characterized by the development of the ~~main fault surface~~ surface rupturing between unconsolidated sedimentary layers. ~~The Mihori area, which has been suggested as the boundary between the central and southern Yangsan faults (Choi et al., 2017), is a point location where the trend of the Yangsan Fault changes on the surface. The fault-line valley was relatively wide south of Mihori and narrowed as it passed through the Mihori area. In addition, the distribution of aftershocks was concentrated in this area during the 2016 Gyeongju earthquake and the geometry of surface geological surveys and faults suggests that this area is prone to deformation (Kim et al., 2017). Taken together, the topographic, structural, seismic, and paleoseismic features of the Mihori area suggest a high probability of large earthquakes or future earthquakes.~~

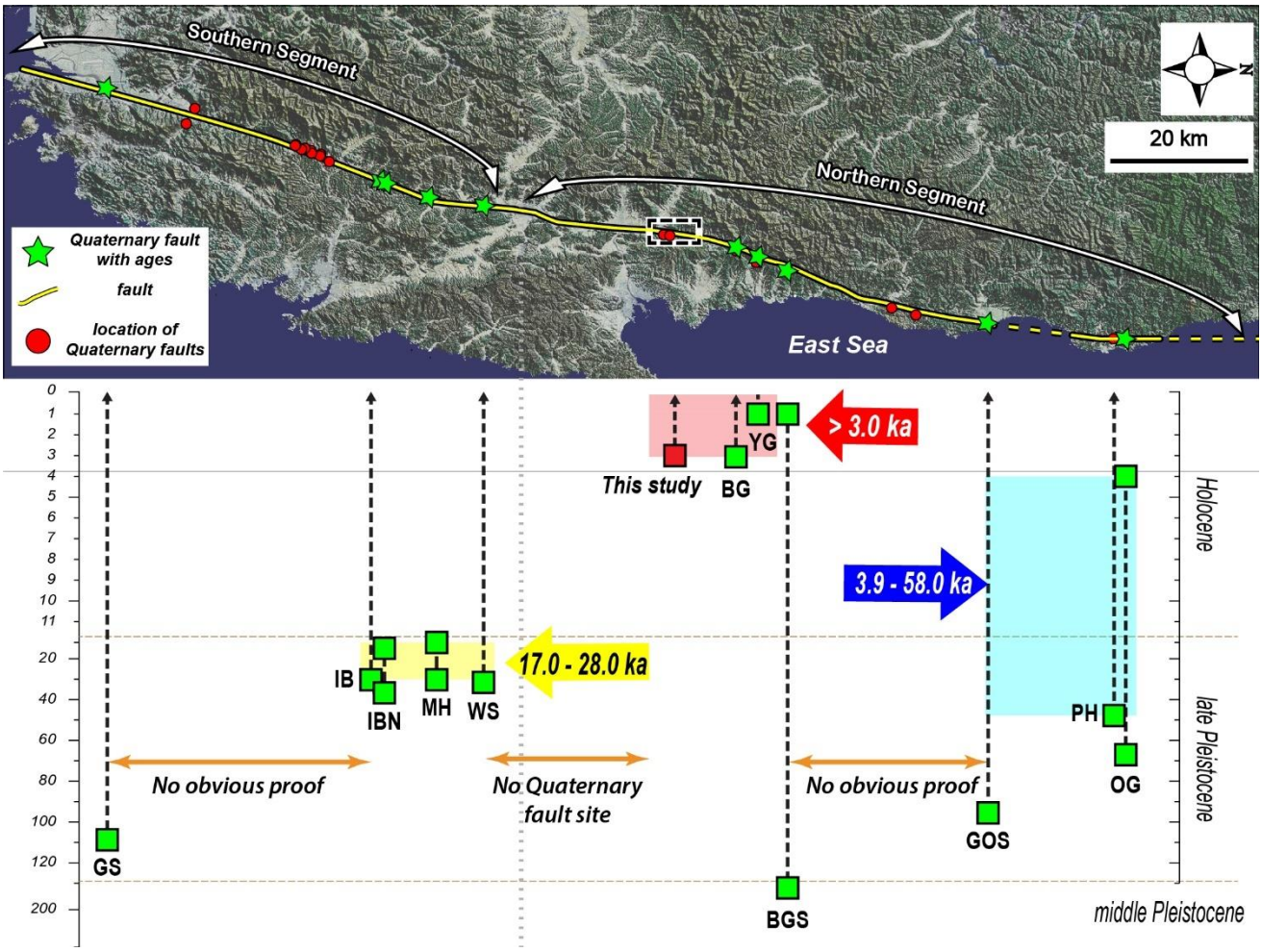

Figure 10: MRE of Yangsan Fault. Green stars indicate where MREs have been identified due to the presence of Quaternary sediment ages. GS: Gasan (Lim et al., 2022), IB: Inbo (Cheon et al., 2020a), IBN: Inbonorth, MH: Miho, WS: Wolsan (Kim et al., 2023), BG: Bangok (Lee, 2023), YG: Yugye (Kyung, 2003), BGS: Bogyeongsa (Lee et al., 2022), GOS: Goesi (Ko et al., 2022), PH: Pyoenghae (Choi et al., 2012), OG: Ogok (Han et al., 2021). "No obvious proof" refers to areas where sites that cut unconsolidated sediments are present but not dated.

5.3 MRE and activity for each segment of the Yangsan Fault

The MRE of the Yangsan Fault ~~was~~is analyzed~~examined~~ section-by-section by synthesizing previous studies (Fig. 10). The Bangok (BG) and Yugye (YG) sites adjacent to the north of the study area have similar MREs. The Bangok site, which is closest to the study area, shares the same MRE, after 3,000 years ago (Lee, 2023), while the Yugye site has the youngest MRE along the entire Yangsan Fault, after AD 646 (Kyung, 2003). It is clear that the section from the study area to the Yugye site, including the Bangok site, is the most recently ruptured section of the Yangsan Fault, with the last surface rupture occurring approximately 3,000 years ago (red arrow in Fig. 10). The Bogyeongsa (BGS) site, north of the Yugye site, has an MRE of Middle Pleistocene and Holocene (Lee et al., 2022). The Yeongdeok area, which extends from the northern part of the

Bogyeongsa site to Goesi (GOS) site, has several reported Quaternary fault sites though no conclusive evidence of Quaternary faulting exists. This is due to either the cutting of unconsolidated sediments without age constraint or the lack of displacement of unconsolidated sediments, with only ESR ages available for the fault gouge (Choi et al., 2012). ~~First, t~~The MREs at ~~of~~ the Ogok (OG), Pyeonghae (PH), and Goesi sites in the northernmost region of the northern Yangsan Fault date to ~~were~~ both Late Pleistocene and Holocene (Choi et al., 2012; Han et al., 2021; Ko et al., 2022). Overall, the northern part of the Bogyeongsa site (the northern part of the Northern Yangsan Fault) experienced MREs between the Late Pleistocene and the Holocene. ~~The Yeongdeok area, which extends from the Goesi trench to the northern part of the Bogyeongsa site, has several reported Quaternary fault sites but no clear evidence of Quaternary faulting because they either cut unconsolidated sediments with no age constraint or do not cut unconsolidated sediments and have only ESR ages of the fault gouge (Choi et al., 2012). The Bogyeongsa site is between the Middle Pleistocene and Holocene (154±13–0.9±0.1 ka; Lee et al., 2022) and the MRE of the Yugye site located at the northern Yangsan faults is after Holocene (AD 646), making it the youngest MRE in the entire Yangsan fault (Kyung, 2003). The MRE of the Bangok site, closest to the study area, and the study area both occurred after the Holocene (Lee, 2023).~~ The Angang area beyond the south of the study area has no reports of Quaternary faulting and at the Wolsan (WS) site, in the northernmost part of the southern Yangsan Fault, the MRE is Late Pleistocene. The Miho (MH), Inbonorth (IBN), and Inbo (IB) sites of the southern Yangsan Fault are all Late Pleistocene and the southernmost part of the Yangsan Fault, the Gasan (GS) site, is after the Late Pleistocene (Lim et al., 2021). ~~Looking at the MRE trends by area, the northern part of the Bogyeongsa site experienced MREs after the Late Pleistocene, the section between Yugye and Byeokgye experienced surface rupture in the Holocene, and t~~The ~~S~~southern Yangsan ~~F~~fault from the Wolsan site to the Gasan site experienced MREs mostly in the Late Pliocene. At first glance, it may appear that the section between Yugye and the study area ~~was~~is more active with Holocene MREs but the timing of the MREs alone ~~was~~is inadequate to assess which zone ~~was~~is more active. For example, Holocene surface rupture may indicate that the fault has a short recurrence interval; conversely, a fault with an older MRE may have a higher potential for future earthquakes because recent faulting events may have released stress accumulation. Deviation in the timing of MREs at different sites or sections can be a direct indication of the fault motion that caused the surface rupture; however, uncertainty in age constraints due to the presence or absence of sediments must be considered. The MRE is an important factor in activity assessment because if it has a recurrence interval, the elapsed time can be calculated, which can be used to predict future earthquakes. However, the activity considered using MRE alone can be misleading; therefore, it is necessary to derive recurrence intervals and elapsed time to accurately predict earthquakes based on paleoseismic data. Ultimately, activity assessment should consider not only paleoseismic data but also topographic, structural, seismic, and geodetic aspects.

6 Conclusion

We conducted surface geological surveys, trenching, coring, OSL/IRSL dating, radiocarbon dating, ESR dating, and cosmogenic nuclides dating along the lineament extracted from topographic analysis using high-resolution LiDAR imagery at

the Yangsan Fault. The primary aim ~~was~~is to identify the surface ruptures that occurred during the Quaternary period, derive structural features, and gather paleoseismic data for the Quaternary surface rupture~~fault~~. The main conclusions are as follows: (1) A comprehensive analysis, combining two previously reported Quaternary fault sites (Byeokgye and Dangu), two newly discovered natural outcrop sites, five trenches, coring surveys, and dating of unconsolidated sediments, charcoal, and fault rocks, revealed a 7.6 km Quaternary surface rupture along the Yangsan Fault. (2) The Quaternary surface rupture~~fault~~s in the study area exhibited an east-dipping geometry with an N-S to NNE strike and moved as a dextral ~~strike~~ slip with a reverse slip component during the Quaternary. (3) At least ~~three~~ six faulting events ~~were~~are interpreted from the trench wall~~section~~s, with an MRE of approximately 3,000 years ago. The MRE horizontal displacement ranged from 0.~~64~~82 to 2.55~~3.29~~ m, cumulative horizontal displacement from ~~3.1 to 94~~76 m, horizontal displacement per event before the MRE from 0.~~33~~9 to 1.~~1~~05 m, and maximum magnitude using the MD from M_w 6.7–7.1~~2~~. The slip rate ~~was~~is 0.12~~03~~ 0.~~21~~14 mm/yr, with a recurrence interval of at least 1~~0~~3~~0~~,000 years. (4) The Quaternary structural features indicate that during the Quaternary period, the western boundary of the main fault core of the Yangsan Fault ~~was~~is reactivated under ENE-WSW compressional stress. The top-to-west geometry is consistent with that observed throughout the Yangsan Fault. (5) The southern part of the northern Yangsan Fault, including the study area, documents a Holocene MRE that is younger than those documented in the southern Yangsan Fault~~s~~.

Surface rupturing has been observed along most sections of the Yangsan F~~f~~ault and in the study area, and basic paleoseismic studies continue to be reported (Fig. 1~~1~~0; Lee et al., 2022; Kim et al., 2023). The challenge is that Korea's geologic diversity results in a large number of faults that need to be studied (e.g., Chugaryeong Fault). Only then will it be possible to properly understand the seismicity pattern of Korea and the earthquakes in the low active intraplate regions. Although the study results are only for a small 10 km section of the Yangsan F~~f~~ault with a 200 km extension, the San Andreas F~~f~~ault, which has high-resolution paleoseismic data from more than 200 trenches, also started out in the same way. In particular, studying seismic hazards on the Korean Peninsula, with its urbanization, cultivated land, slow slip rates, long recurrence intervals, and fast erosion rates, is a challenge. This research will hopefully contribute to the research on earthquake hazards in Korea, which is just beginning to advance. Furthermore, this study contributes valuable insights for seismic hazard assessment in the region and offers a broader understanding of intraplate earthquake dynamics, thereby aiding earthquake prediction efforts.

Appendices

Appendix A. Geomorphic map of the study area

The topography of the study area in Ha et al. (2022) is summarized as follows:

The study area's topography is divided into a lowland area to the west and a mountainous region to the east (Fig. A1). The eastern mountains, the ridges extending from the summit are cut off by a lineament heading west, which influences the drainage system, with streams flowing from the high elevations east to the west. Alluvial fans, formed from sediments from the eastern mountains, are found at the base of the slopes. Twelve lineaments are identified, with the main lineament, which extends for 7.6 km, displaying high activity through the northern part of the Byeokgye site. Subsidiary high-activity lineaments and low-activity lineaments, mainly following N–S or NNE directions, are present, though many are valleys formed by erosion rather than rupturing. The main lineament exhibits continuous fault scarps and deflected streams, with reservoirs often located along it due to impermeable fault gouges that enable water storage. Topographic analysis revealed fault scarps, knickpoints, and displacement features along the main lineament, particularly visible in LiDAR data. Fault scarps are continuously and distinctly visible in the main lineament of the southern region (Fig. A2). In the cross-section, the fault scarps are recognized as knickpoints, and on the topographical map, the ridges on the east side of the lineament are cut by the surface rupture and merged with the alluvial fans. The main lineament of the northern region is identified as a linear arrangement of deflected streams and fault scarps (Fig. A3). Unlike in the south, the fault scarps in the north show surface uplift estimated at a vertical offset of between 2–4.2 m of the same alluvial fan surface cross-section. Differences between the southern and northern regions are observed, with the north showing vertical offsets of 2–4.2 m and more pronounced faulting. The horizontal offsets calculated based on the three deflected streams are 92 m, 98 m, and 150 m. The tendency for the offset to decrease as the distance from the main lineament increases indicates that the fault offset branching from the main surface rupture gradually decreases.

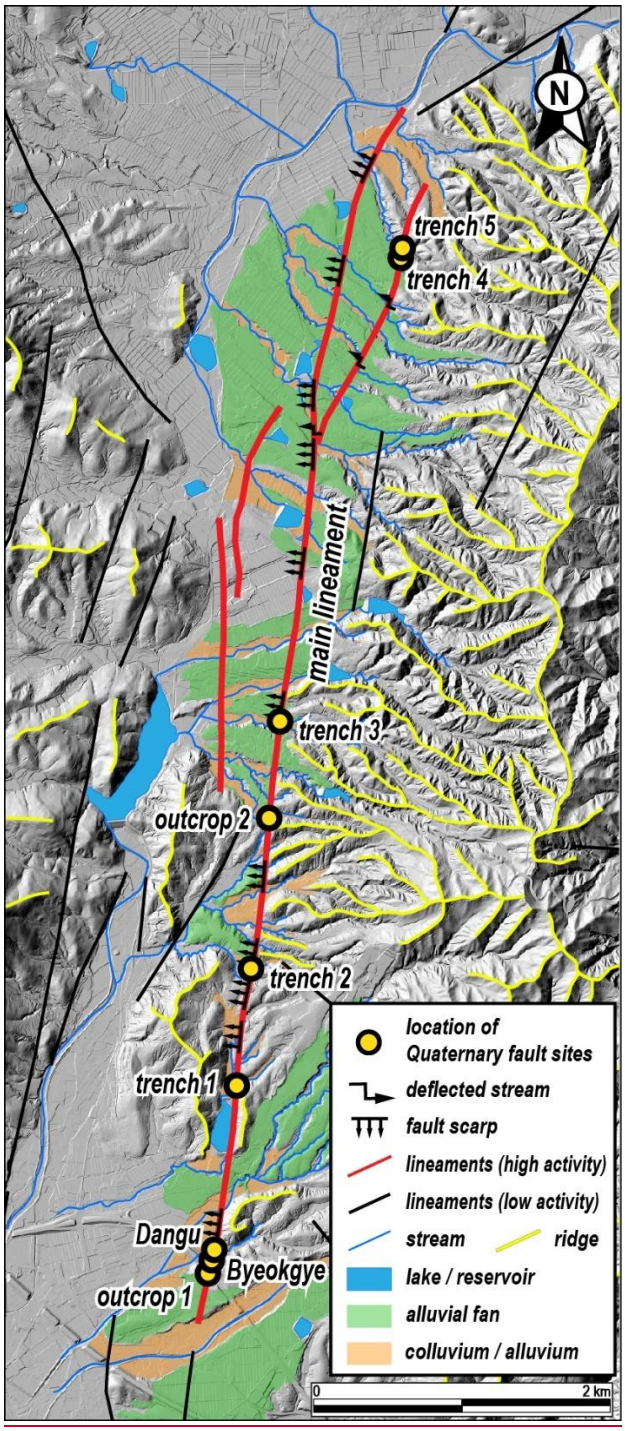

Figure A1: The geomorphic map of the study area (modified from Ha et al., 2022).

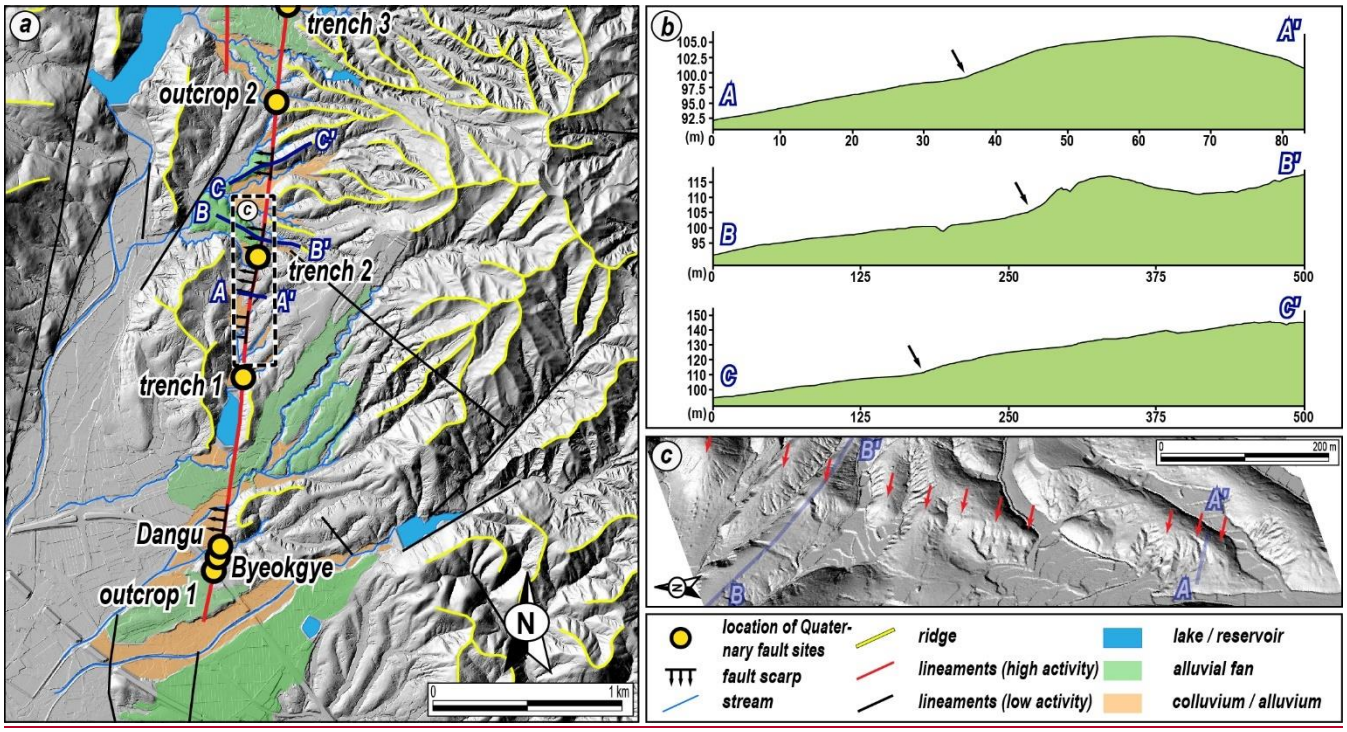

Figure A2: (a) A detailed topographic map of the southern region. (b) Topographic profiles along the main lineament (blue line in (a)) crossing the fault scarps. Black arrows mark knickpoints identified as fault scarps. (c) A 3D hillshade image. The red arrows highlight the fault scarp, which is clearly visible to the unaided eye (modified from Ha et al., 2022).

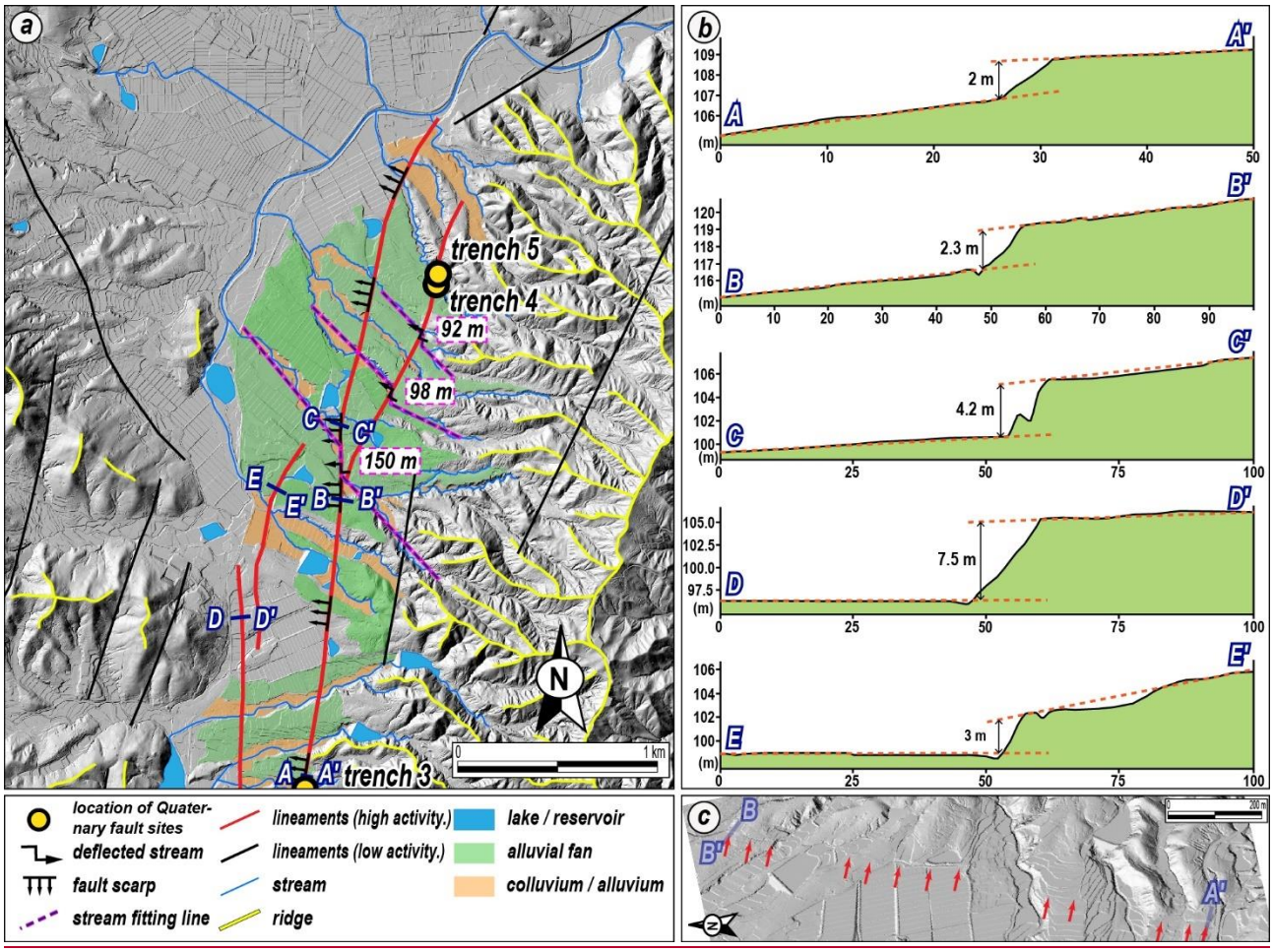

Figure A3: (a) A detailed topographic map of the northern region. An NNE lineament branching off from the main lineament is shown by the dextrally deflected stream. (b) Topographic profiles along the line (blue line in (a)) crossing the fault scarps. Fault scarps in the northern region are evident due to the elevation difference in the alluvial fan surfaces. (c) A 3D hillshade image. Red arrows highlight the fault scarp (modified from Ha et al., 2022).

Appendix B~~A~~. Calculation of horizontal~~true~~ displacement

The horizontal ~~true~~ displacement (S_{ht}) can be calculated using a trigonometric function that considers the vertical displacement (S_v), fault dip angle (α), rake (γ), true displacement (S_t) and their relationships (Fig. ~~A~~B1; Eq. ~~A~~B1). Assume that the attitude of the marker in the ~~cross-section~~exposed wall at each trench is nearly horizontal in three dimensions and the angle (β) of the ~~cross-section~~exposed wall is nearly vertical, then the two factors are perfectly horizontal and vertical, respectively. Thus, the vertical separation (S_{vm}) and vertical displacement (S_v) measured in the ~~cross-section~~exposed wall are equal.

Therefore,

$$\boldsymbol{S_{vm} = S_v, S_m = \frac{S_v}{\sin \alpha}, S_t = \frac{S_m}{\sin \gamma}, S_h = \cos \gamma * S_t} \quad \text{———(B~~A~~1)}$$

We calculate ~~true~~ horizontal displacement (S_{th}) using Eq. (B~~A~~1) for vertical separation (S_{vm}) of the marker measured in the ~~trench section~~exposed wall, as shown in Table 5~~6~~.

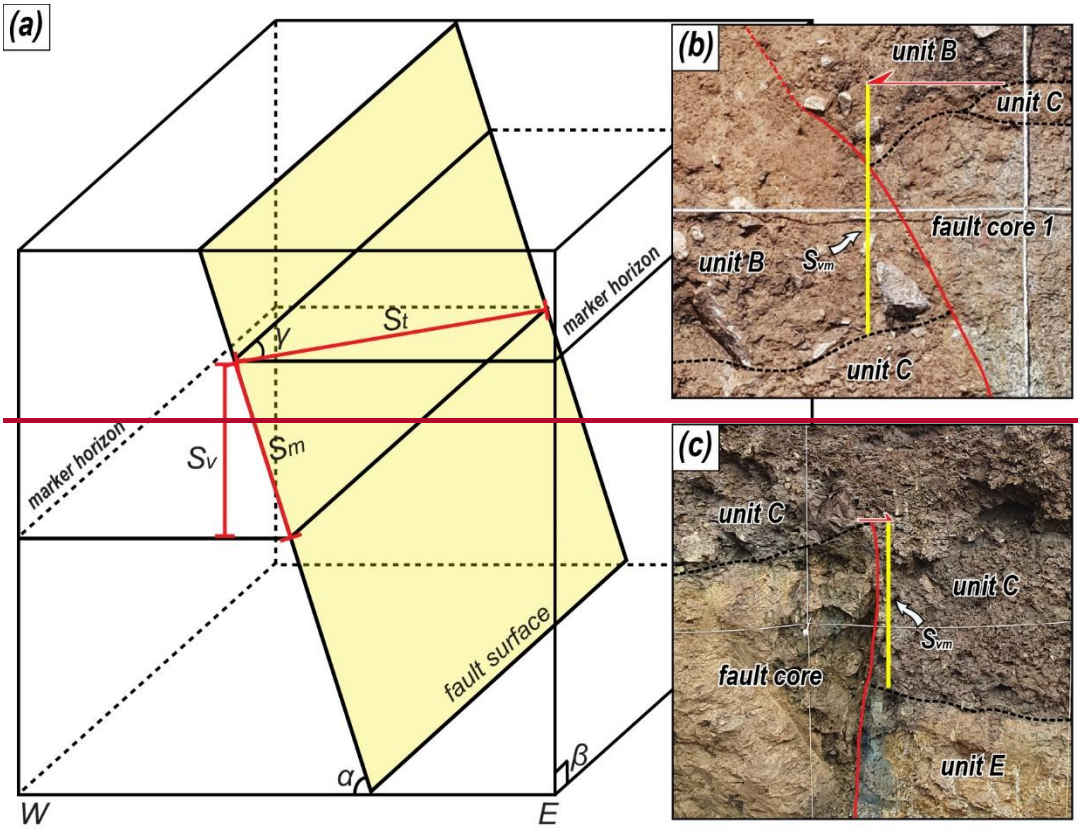
(a)
(b)
(c)
unit B
unit C
fault core 1
unit B
S_{vm}
unit C
unit C
unit C
S_{vm}
fault core
unit E
marker horizon
S_t
γ
S_v
S_m
marker horizon
fault surface
α
β
W
E

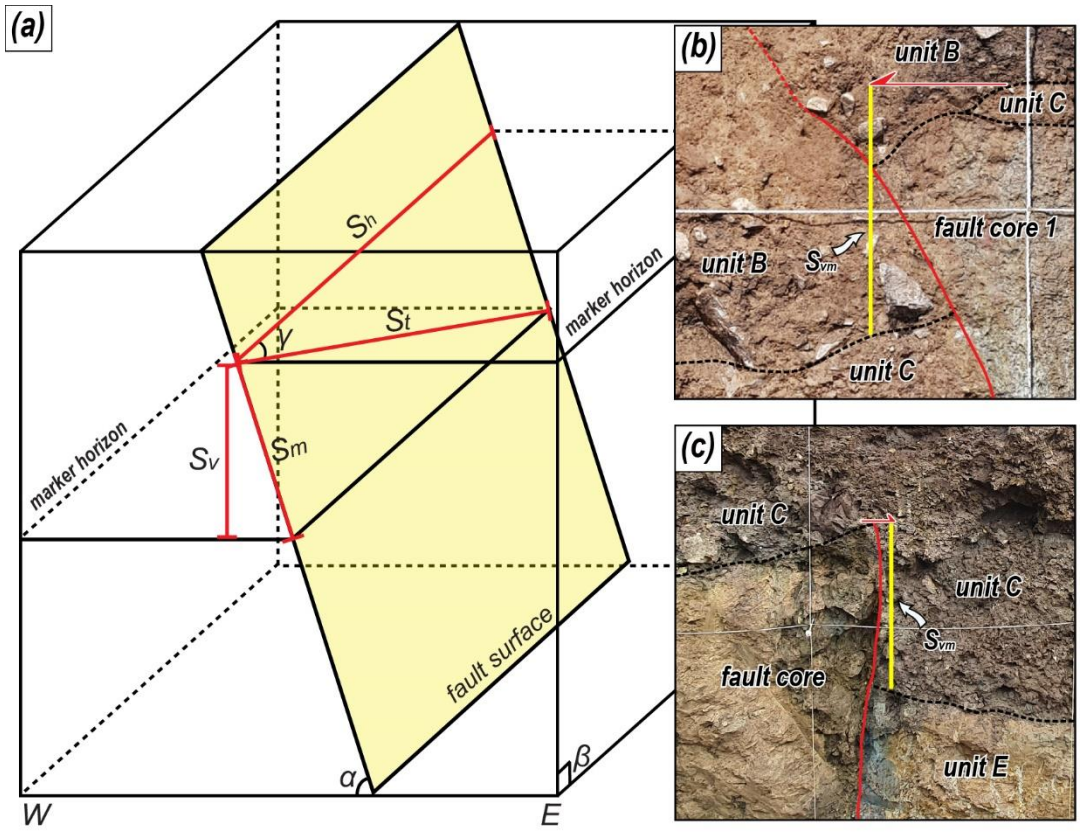

Figure BA1: (a) Schematic diagram showing how to calculate true displacement. S_h: horizontal displacement S_t: true displacement, S_v: vertical displacement, S_m: dip separation, α: dip of fault surface, β: dip of cut slope, γ: rake of the striation (modified from Xu et al., 2009). (b and c) Photographs showing the measured vertical separation of the trenches 1 and 5. S_{vm}: vertical separation.

Appendix CB. Description of the Outcrop 1 and 2

Outcrop 1 is located 30 m south of the Byeokgye site (Fig. 2c). A high-angle rupturefault cut the Cretaceous volcanic rocks and unconsolidated sediments interbedded with gravel deposits and sand layers (Fig. CB1a). The fault rupture trace wasis partially recognized on the surface based on the lithological distribution. The fault core consisted of a 20 cm-wide fault breccia with a fault Quaternary slip surface attitude of N12°E/84°NW, and no clear slickening wasis observed (Fig. CB1b). Outcrop 2, on the extension of the main lineament, is located 2.7 km north of the Byeokgye site (Fig. 2c). The outcrop contained highly weathered purple sedimentary rock overlying unconsolidated sediments (Fig. CB1c). The NNE-striking fault splaysurface dipped toward the east with a low angle. The purple sedimentary rock of the hanging wall wasis mostly clayey and may be either a pre-existing purple fault gouge or weathered purple Cretaceous sedimentary rock. The fault core adjacent to the unconsolidated deposits consisted of a 2–3 cm thick foliated fault gouge (Fig. BC1d). The foliation is subparallel to the slip surface. The unconsolidated gravel deposits have poor sorting, and angular clasts consist of sandstone, granitic, and volcanic rocks. No clear slickenlines wereare observed, owing to highly weathered outcrop conditions. We could not date either outcrop because the clast-rich sediments wereare not suitable for OSL dating and did not include organic material for ^{14}C dating.

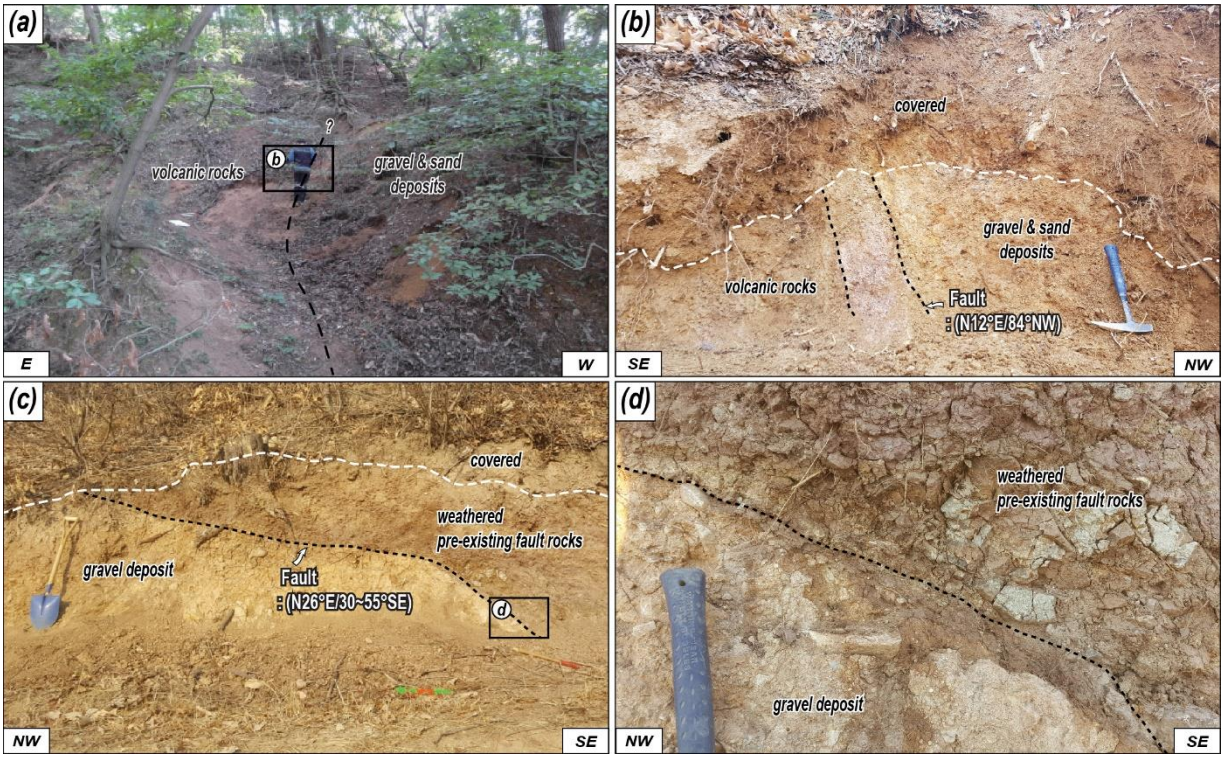

Figure CB1: Photographs showing the outcrops of the rupturefault which that cut the unconsolidated sediments. (a) RuptureFault trace on the surface. (b) NNE striking rupture fault cut the boundary between volcanic rocks and gravel and sand deposits. The fault rock is composed of breccia. (c) Weathered pre-existing fault rocks thrust gravel deposits along the low-angle surface rupturingfault surface. (d) Close-up photograph of the rupturefault surface. A 2-3 cm thick fault gouge forms a boundary between two different rocks.

Appendix ~~C~~D. Coring at the Trench 2

We cored the footwall of Trench 2. Unconsolidated sand and gravel deposits alternated up to 24 m below the surface. From 24 m to 32.8 m, the material consisted of a granite wash, at the base of which a 1.2 m thick weathering zone ~~was~~is recognized. From 34 m onwards, the bedrock is clearly identified as A-type alkaline granite (Fig. D~~C~~1). We performed ^{10}Be-^{26}Al isochron burial dating on the granite wash immediately above the basement rock.

Figure D~~C~~1: Photograph showing drilled core. The lowermost of the unconsolidated sediments, the granite wash, directly overlies bedrock. Cosmogenic ^{10}Be-^{26}Al isochron dating samples ~~were~~are taken from this granite wash.

Appendix E~~D~~. Detailed quartz OSL, K-feldspar pIRIR$_{225}$~~IRSL~~, and ^{10}Be-^{26}Al isochron burial age dating results

The graphs of the detailed results of 1-2 representative samples per trench for quartz OSL and pIRIR$_{255}$~~IRSL~~. We selected samples from sediments cut into the MRE and from sediments overlying the MRE. The graphs include decay curves, probability density graphs, and ^{10}Be-^{26}Al isochron graphs. The tables also include dose rates, equivalent doses, and luminescence ages of the samples from each trench.

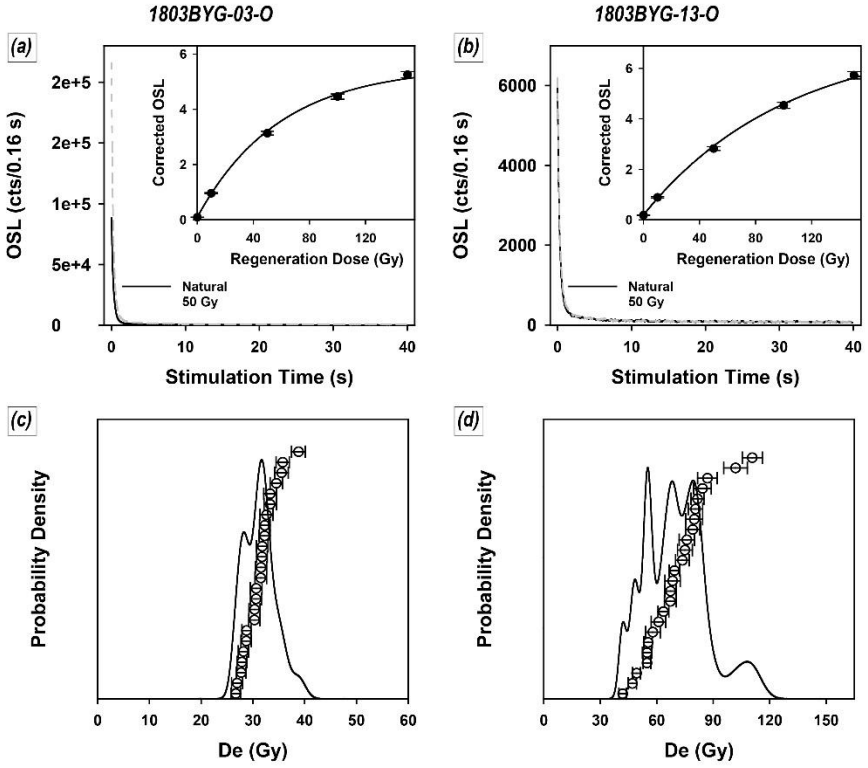

Figure E~~D~~1: Representative quartz OSL decay curves (a, b) and probability density graph (c, d) of Trench 1.

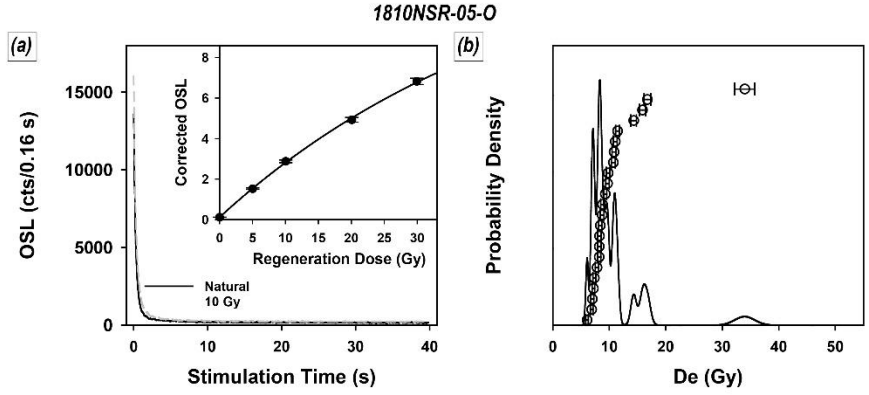

Figure E~~D~~2: Representative quartz OSL decay curves (a, b) and probability density graph (c, d) of Trench 2.

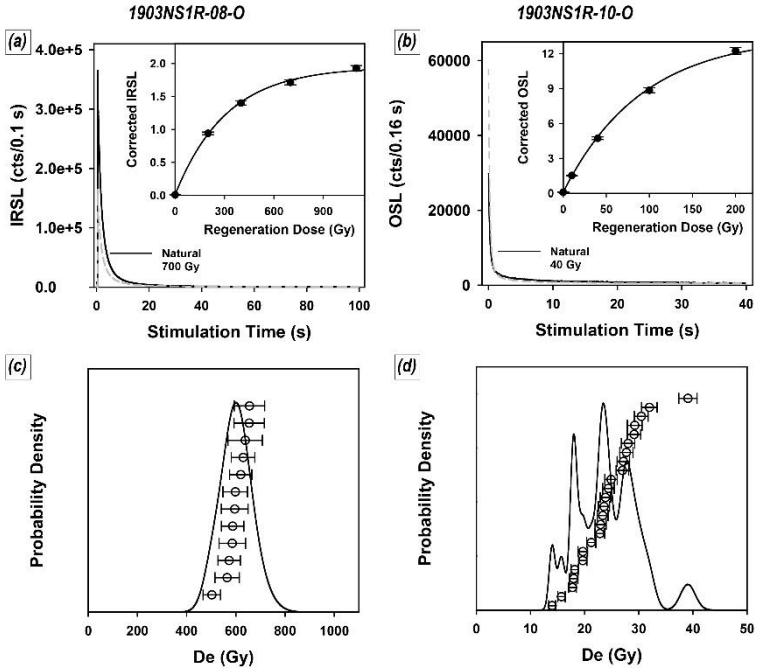

Figure ED3: Representative quartz OSL/IRSL decay curves (a, b) and probability density graph (c, d) of Trench 3.

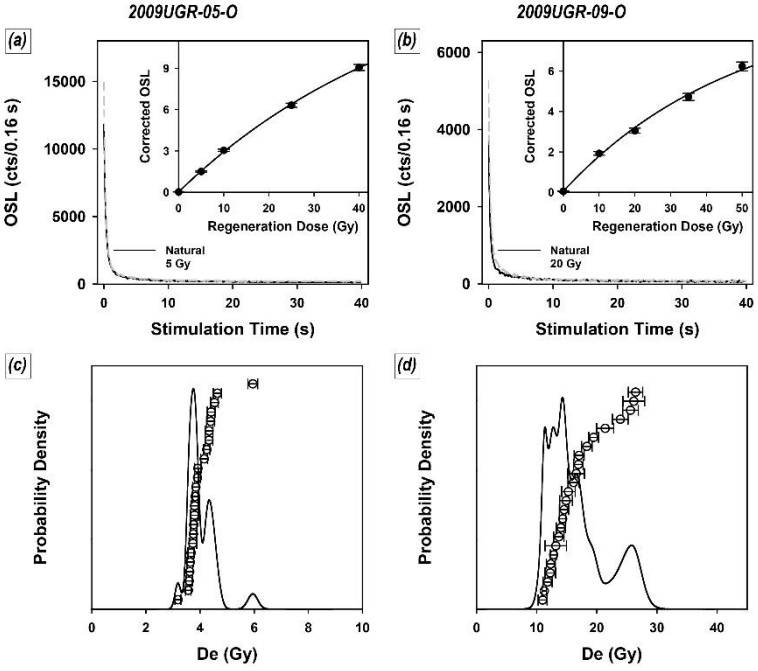

900

Figure ED4: Representative quartz OSL decay curves (a, b) and probability density graph (c, d) of Trench 4.

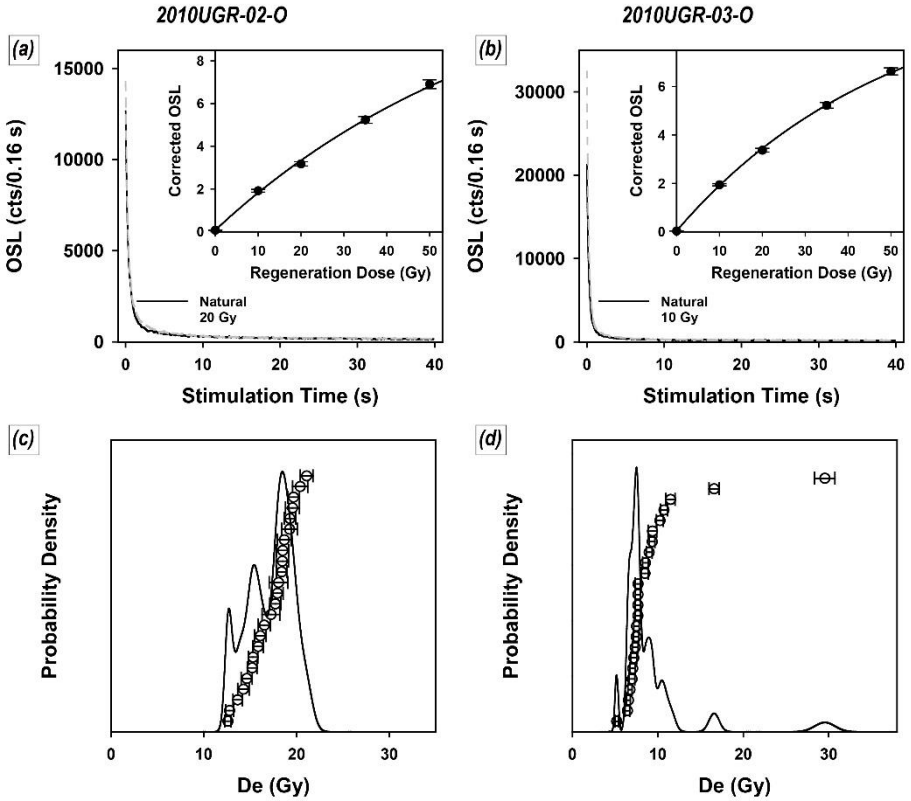

Figure ED5: Representative quartz OSL decay curves (a, b) and probability density graph (c, d) of Trench 5.

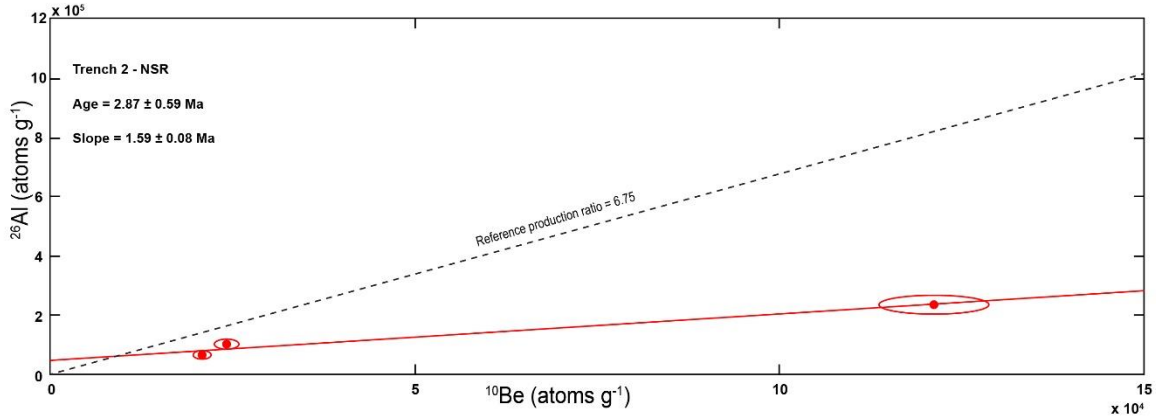

Figure ED6: ^{10}Be-^{26}Al isochron graph of coring samples in Trench 2.

Table ED1: Dose rates, equivalent doses, and luminescence ages of the samples from the Trench 1

Method	Sample code	Dose rate[a] (Gy/ka)	Water content[b] (%)	Equivalent dose (Gy)	Fading rate (g_{2days}, %/dec.)	Aliquots used (n)	age[c] (ka, 1σ SE)
Quartz OSL	1803BYG-01-O	3.26 ± 0.08	13	4.2 ± 0.2	-	24	1.3 ± 0.1
	1803BYG-02-O	3.54 ± 0.09	16	33 ± 1	-	24	9 ± 1
	1803BYG-03-O	3.00 ± 0.08	17	31 ± 1	-	24	10 ± 1
	1803BYG-05-O	3.16 ± 0.08	14	16 ± 1	-	24	4.9 ± 0.3
	1803BYG-06-O	3.37 ± 0.09	12	11 ± 1	-	24	3.2 ± 0.2
	1803BYG-13-O	4.02 ± 0.11	13	68 ± 4	-	24	17 ± 1
	1803BYG-14-O	3.31 ± 0.09	10	27 ± 1	-	24	8.1 ± 0.3
K-feldspar $pIRIR_{225}$	1803BYG-04-O	3.90 ± 0.09	18	537 ± 23	0.8 ± 0.3	12	146 ± 8
	1803BYG-07-O	4.36 ± 0.10	16	733 ± 31	0.7 ± 0.2	12	177 ± 7
	1803BYG-08-O	3.99 ± 0.09	18	558 ± 18	1.1 ± 0.3	24	151 ± 8
	1803BYG-09-O	4.21 ± 0.10	22	561 ± 21	1.0 ± 0.3	12	143 ± 7
	1803BYG-10-O	3.95 ± 0.10	20	581 ± 20	1.5 ± 0.3	12	164 ± 8
	1803BYG-11-O	4.12 ± 0.09	18	594 ± 19	1.0 ± 0.4	12	155 ± 8
	1803BYG-12-O	4.63 ± 0.11	15	613 ± 21	1.0 ± 0.3	12	142 ± 7

[a] Wet total dose rates. The activities of each radionuclide were converted to dose rates using the data presented by Liritzis et al. (2013). Cosmic ray dose rates were estimated using the method suggested by Prescott and Hutton (1994). The internal dose rate of K-feldspar was calculated assuming internal K content of 12.5 % and by using the methods proposed by Mejdahl (1987) and Readhead (2002). For deriving the total dose rates absorbed by K-feldspar, the internal dose rate of 0.736±0.04 Gy/ka was added to the external ones of each sample.

[b] Present water content.

[c] Fading-corrected ages in the case of K-feldspar

Table ED2: Dose rates, equivalent doses, and luminescence ages of the samples from the Trench 2

Method	Sample code	Dose rate[a] (Gy/ka)	Water content[b] (%)	Equivalent dose (Gy)	Aliquots used (n)	age[c] (ka, 1σ SE)
Quartz OSL	1810NSR-05-O	3.09 ± 0.08	18	9.9 ± 0.8	23	3.2 ± 0.3
	1810NSR-06-O	3.46 ± 0.09	14	12 ± 1	22	3.4 ± 0.4
	1810NSR-07-O	2.55 ± 0.06	19	47 ± 2	24	19 ± 1

[a] Wet total dose rates. The activities of each radionuclide were converted to dose rates using the data presented by Liritzis et al. (2013). Cosmic ray dose rates were estimated using the method suggested by Prescott and Hutton (1994).

[b] Present water content.

Table ED3: Dose rates, equivalent doses, and luminescence ages of the samples from the Trench 3

Method	Sample code	Dose rate[a] (Gy/ka)	Water content[b] (%)	Equivalent dose (Gy)	Fading rate (g_{2days}, %/dec.)	Aliquots used (n)	age[c] (ka, 1σ SE)
Quartz OSL	1903NS1R-10-O	3.67 ± 0.09	23	23 ± 1	-	24	6.4 ± 0.4
K-feldspar $pIRIR_{225}$	1903NS1R-02-O	4.01 ± 0.09	18	606 ± 22	1.8 ± 0.6	12	173 ± 11
	1903NS1R-03-O	4.11 ± 0.09	16	600 ± 16	2.4 ± 0.4	12	175 ± 9
	1903NS1R-08-O	4.55 ± 0.10	15	595 ± 18	0.6 ± 0.3	12	137 ± 6

[a] Wet total dose rates. The activities of each radionuclide were converted to dose rates using the data presented by Liritzis et al. (2013). Cosmic ray dose rates were estimated using the method suggested by Prescott and Hutton (1994). The internal dose rate of K-feldspar was calculated assuming internal K content of 12.5 % and by using the methods proposed by Mejdahl (1987) and Readhead (2002). For deriving the total dose rates absorbed by K-feldspar, the internal dose rate of 0.736±0.04 Gy/ka was added to the external ones of each sample.

[b] Present water content.

[c] Fading-corrected ages in the case of K-feldspar

Table ED4: Dose rates, equivalent doses, and luminescence ages of the samples from the Trench 4

Method	Sample code	Dose rate[a] (Gy/ka)	Water content[b] (%)	Equivalent dose (Gy)	Aliquots used (n)	age[c] (ka, 1σ SE)
Quartz OSL	2009UGR-05-O	3.11 ± 0.08	12	3.9 ± 0.1	24	1.3 ± 0.1
	2009UGR-06-O	2.97 ± 0.08	11	3.6 ± 0.1	24	1.2 ± 0.1
	2009UGR-07-O	3.44 ± 0.09	12	0.5 ± 0.1	24	0.15 ± 0.03
	2009UGR-08-O	3.41 ± 0.09	13	0.5 ± 0.1	24	0.15 ± 0.03
	2009UGR-09-O	2.75 ± 0.07	12	16.1 ± 0.9	24	5.9 ± 0.4

[a] Wet total dose rates. The activities of each radionuclide were converted to dose rates using the data presented by Liritzis et al. (2013). Cosmic ray dose rates were estimated using the method suggested by Prescott and Hutton (1994).

[b] Present water content.

Table ED5: Dose rates, equivalent doses, and luminescence ages of the samples from the Trench 5

Method	Sample code	Dose rate[a] (Gy/ka)	Water content[b] (%)	Equivalent dose (Gy)	Aliquots used (n)	age[c] (ka, 1σ SE)
Quartz OSL	2010UGR-01-O	3.19 ± 0.08	14	32 ± 3	23	10 ± 1
	2010UGR-02-O	3.47 ± 0.09	14	17 ±1	24	4.8 ± 0.2
	2010UGR-03-O	2.77 ± 0.07	21	7.9 ± 0.3	24	2.8 ± 0.1
	2010UGR-04-O	2.96 ± 0.07	17	7.6 ± 0.2	24	2.6 ± 0.1

[a] Wet total dose rates. The activities of each radionuclide were converted to dose rates using the data presented by Liritzis et al. (2013). Cosmic ray dose rates were estimated using the method suggested by Prescott and Hutton (1994).

[b] Present water content.

Data availability. All detailed age dating data are available in Tables 1~~2~~-4~~5~~, E~~D~~1-E~~D~~5. Questions or requests for original photomosaic of trenches can be sent to the corresponding author.

Author contributions. Conceptualization: SH, HCK, Funding acquisition: SM, Investigation: SM, HCK, SL, YBS, JHC, SJK, Project administration: SM, Supervision: SM, Validation: YBS, JGC, SJK, Visualization: SM, SJK, Writing – original draft preparation: SH, Writing – review & editing: SH, YBS, JHC, SM,

Competing interests. The authors declare that they have no conflicts of interest.

Financial support.
This research was supported by a grant (2022-MOIS62-001(RS-2022-ND640011)) of National Disaster Risk Analysis and Management Technology in Earthquake funded by Ministry of Interior and Safety (MOIS, Korea).

References

Ansari, K. and Bae, T.S.: Contemporary deformation and strain analysis in South Korea based on long-term (2000–2018) GNSS measurements, Int. J. Earth Sci. (Geol. Rundsch.), 109, 391–405, https://doi-org-ssl.oca.korea.ac.kr/10.1007/s00531-019-01809-4, 2020.

Argus, D.F., Gordon, R.G., Heflin, M.B., Ma, C., Eanes, R.J., Willis, P., Peltier, W.R., and Owen, S.E.: The angular velocities of the plates and the velocity of the Earth's centre from space geodesy, Geophys. J. Int., 18, 1-48, https://doi:10.1111/j.1365-246X.2009.04463.x, 2010.

Ashurkov, S.V., San'kov, V.A., Miroschnichenko, A.I., Lukhnev, A.V., Sorokin, A.P., Serov, M.A., and Byzov, L.M.: GPS geodetic constrains on the kinematics of the Amurian Plate, Russ. Geol. Geophys., 52, 239-249, https://doi.org/10.1016/j.rgg.2010.12.0172, 2011.

Atkinson, G.M., Finn, W.D.L. and Charlwood, R.G.: Simple computation of liquefaction probability for seismic hazard applications, Earthq. Spectra, 1, 107-123, https://doi.org/10.1193/1.1585259, 1984.

Balco, G., and Rovey, C.W.: An isochron method for cosmogenic-nuclide dating of buried soils and sediments. Am. J. Sci., 308, 1083–1114, https://doi.org/10.2475/1 0.2008.02, 2008.

Bird, P.: An updated digital model of plate boundaries, Geochem. Geophy. Geosy., 4, 1027, https://doi.org/10.1029/2001GC000252, 2003.

Bonilla, M. G., Mark, R. K., and Lienkaemper, J. J.: Statistical relations among earthquake magnitude, surface rupture length, and surface fault displacement, B. Seismol. Soc. Am., 74, 2379–2411, https://doi.org/10.1785/BSSA0740062379,1984.

Bronk Ramsey, C.: Methods for summarizing radiocarbon datasets, Radiocarbon, 59, 1809-1833, https://doi.org/10.1017/RDC.2017.108, 2017.

Buylaert, J.P., Jain, M., Murray, A.S., Thomsen, K.J., Thiel, C., and Sohbati, R.: A robust feldspar luminescence dating method for Middle and Late Pleistocene sediments, Boreas, 41, 435–451, https://doi.org/10.1111/j.1502-3885.2012.00248.x, 2012.

Buylaert, J.P., Murray, A.S., Thomsen, K.J., and Jain, M.: Testing the potential of an elevated temperature IRSL signal from K-feldspar, Radiat. Meas., 44, 560–565, https://doi.org/10.1016/j.radmeas.2009.02.007, 2009.

Calais, E., Dong, L., Wang, M., Shen, Z., and Vergnolle, M.: Continental deformation in Asia from a combined GPS solution, Geophys. Res. Lett., 33, L24319, https://doi.org/ 10.1029/2006GL028433, 2006.

Chang, C.-J., and Chang, T.W.: Movement History of the Yangsan Fault based on Paleostress Analysis, J. Eng. Geo., 8, 35-49, 1998.

Chang, C.-J.: Structural characteristics and evolution of the Yangsan fault, SE Korea, Ph.D. thesis, Kyungpook National University, Korea, 2002.

Chang, K.H., Woo, B.G., Lee, J.H., Park, S.O., and Yao, A.: Cretaceous and early Cenozoic stratigraphy and history of eastern Kyongsang Basin, S. Korea, J. Geol. Soc. Korea, 26, 471-487, 1990.

Cheon, Y., Cho, H., Ha., S., Kang, H.-C., Kim, J.-S., and Son, M.: Tectonically controlled multiple stages of deformation along the Yangsan Fault Zone, SE Korea, since Late Cretaceous, J. Asian Earth Sci., 170, 188-207, https://doi.org/10.1016/j.jseaes.2018.11.003, 2019.

Cheon, Y., Choi, J.-H., Choi, Y., Bae, H., Han, K.-H., Son, M., Choi, S.-J., and Ryoo, C.-R.: Understanding the distribution and internal structure of the main core of the Yangsan Fault Zone: Current trends and future work, J. Geol. Soc. Korea, 56, 61-640, https://doi.org//10.14770/jgsk.2020.56.5.619, 2020a.

Cheon, Y., Choi, J.-H., Kim, N., Lee, H., Choi, I., Bae, H., Rockwell, T.K., Lee, S.R., Ryoo, C.-R., and Choi, H.: Late Quaternary transpressional earthquakes on a long-lived intraplate fault: A case study of the Southern Yangsan Fault, SE Korea, Quatern. Int., 553, 132-143, https://doi.org/10.1016/j.quaint.2020.07.025, 2020b.

Cheon, Y., Ha, S., Lee, S., Cho, H, and Son, M.: Deformation features and history of the Yangsan Fault Zone in the Eonyang-Gyeongju area, SE Korea, J. Geol. Soc. Korea, 53, 95-114, http://doi.org/10.14770/jgsk.2017.53.1.95, 2017.

Choi, J.-H., Kim, Y.-S., and Klinger, Y.: Recent progress in studies on the characteristics of surface rupture associated with large earthquakes, J. Geol. Soc. Korea, 53, 129-157, https://doi.org/10.14770/jgsk.2017.53.1.129, 2017.

Choi, J.-H., Yang, S.-J., and Kim, Y.-S.: Fault zone classification and structural characteristics of the southern Yangsan fault in the Sangcheon-ri area, SE Korea, J. Geol. Soc. Korea, 45, 9-28, 2009.

Choi, S.-J., Ghim, Y.S., Cheon, Y., and Ko, K.: The First Discovery of Quaternary Fault in the Western Part of the South Yangsan Fault-Sinwoo Site, Econ. Environ. Geol., 52, 251-258, http://doi.org/10.9719/EEG.2019.52.3.251, 2019.

Choi, S.-J., Jeon, J.S., Song, G.Y., Kim, H.C., Kim, Y.H., Choi, B.Y., Chwae, W.C., Han, J.G., Ryoo, C.-R., Sun, C.-G., Jun, M.-S., Kim, G.-Y., Kim, Y. B., Lee, H. J., Shin, J. S., Lee, Y. S., and Kee, W.-S.: Active fault map and seismic hazard map, National Emergency Management Agency, Seoul, Seoul, 939 pp., 2012.

Crampin, S. and Gao, Y.: Earthquakes can be stress-forecast, Geophy. J. Int., 180, 1124-1127, https://doi.org/10.1111/j.1365-246X.2009.04475.x, 2010.

Delvaux, D., and Sperner, B.: New aspects of tectonic stress inversion with reference to the TENSOR program, in: New Insights into Structural Interpretation and Modelling, edited by Nieuwland, D. A., Geol. Soc., London Spec. Publ., 212, 75-100, https://doi.org/10.1144/GSL.SP.2003.212.01.06, 2003.

Delvaux, D., Moeys, R., Stapel, G., Petit, C., Levi, K., Miroshnichenko, A., Ruzhich, V., and San'kov, V.: Paleostress reconstructions and geodynamics of the Baikal region, Central Asia, Part 2. Cenozoic rifting, Tectonophysics, 282, 1-38, https://doi.org/10.1016/S0040-1951(97)00210-2, 1997.

DeMets, C., Gordon, R.G., Argus, D.F., and Stein, S.: Current plate motions, Geophys. J. Int., 101, 425-478, https://doi.org/10.1111/j.1365-246X.1990.tb06579.x, 1990.

DeMets, C., Gordon, R.G., Argus, D.F., and Stein, S.: Effect of recent revisions to the geomagnetic reversal time scale on estimates of current plate motions, Geophys. Res. Lett., 21, 191-2,194, https://doi.org/10.1029/94GL02118, 1994.

England, P., and Jackson, J.: Uncharted seismic risk, Nat. Geosci., 4, 348–349, https://doi.org/10.1038/ngeo1168, 2011.

Erlanger, E.D., Granger, D.E., and Gibbon, R.J.: Rock uplift rates in South Africa from isochron burial dating of fluvial and marine terraces, Geology, 40, 1019–1022. https://doi.org/10.1130/G33172.1., 2012.

Ge, J., Shi, X., Chen, H., Weldon, R., Walker, R., Li, T., Yang, H., Chen, J., Li, F., Wei, X., Yang, X., Bai, Z., Zhang, Y., Shu, Y., Liu, X., and Yan, Y.: Paleoseismology of the northern Kongur Shan Extensional System, NE Pamir: Implications for potential irregular earthquake recurrence, J. Geophys. Res.: Solid Earth, 129, e2023JB028371, https://doi.org/10.1029/2023JB028371, 2024.

Geller, R. J., Jackson, D. D., Kagan, Y. Y., and Mulargia, F.: Earthquakes Cannot Be Predicted, Science, 275, 1616-1616, https://doi.org/10.1126/science.275.5306.1616, 1997.

Granger, D. E.: A review of burial dating methods using ^{26}Al and ^{10}Be, in: In Situ-Produced Cosmogenic Nuclides and Quantification of Geological Processes: Geological Society of America Special Paper 415, edited by: Siame, L. L., Bourlès, D. L., and Brown, 1–16, https://doi.org/10.1130/2006.2415(01), 2006.

Granger, D.E., and Muzikar, P.F.: Dating sediment burial with in situ-produced cosmogenic nuclides: Theory, techniques, and limitations, Earth Planet. Sc. Lett., 188, 269-281, https://doi.org/10.1016/S0012-821X(01)00309-0, 2001.

Gurpinar, A.: The importance of paleoseismology in seismic hazard studies for critical facilities, Tectonophysics, 408, 23-28, https://doi.org/10.1016/j.tecto.2005.05.042, 2005.

Gwon, O., Park, K., Naik, S. P., Shin, H.-C., and Kim, Y. -S.: A study on the characteristics of fault activity in the southern part of the Ulsan fault using paleoseismic method, J. Geol. Soc. Korea, 57, 109-121, https://doi,org/10.14770/jgsk.2021.57.2.109, 2021.

Gwon, S., Cho, S., Park, D., Choi, W.-H., Nakao, R., Tanaka, T., and Inoue, D.: Microscopic analysis of fault rock using X-ray computed tomography from the Wolsan trench in the middle part of Yangsan fault, SE Korea, J. Geol. Soc. Korea, 56, 273-284, https://doi.org/10.14770/jgsk.2020.56.2.273, 2020.

Ha, S., Son, M., and Seong, Y.B.: Active Fault Trace Identification Using a LiDAR High-Resolution DEM: A Case Study of the Central Yangsan Fault, Korea, Remote Sens., 14, 4838, https://doi.org/10.3390/rs14194838, 2022.

Han, J.-W., Lee, S., Ha, S., Lee, C. H., Seong, Y. B., Kang, H.-C., Kim, M.-C., Gil, T., and Son, M.: A preliminary study on the Quaternary faulting along the northern part of Yangsan Fault and Yeongdeok Fault, in: 76th Annual Meeting of the Geological Society of Korea and 2021 Fall Joint Conference of the Geological Sciences, Jeju, Korea, 26-28 October 2021, 317, 2021.

Han, M., Kim, K.-H., Son, M., Kang, S.Y., and Park, J.-H.: Location of recent micro earthquakes in the Gyeongju area, Geophysics Geophys. Explor., 19, 97-104, https://doi.org/10.7582/GGE.2016.19.2.097, 2016.

Hansen, V., Murray, A., Buylaert, J.-P., Yeo, E.Y., and Thomsen, K.: A new irradiated quartz for beta source calibration, *Radiat. Meas., 81, 123*–127, https://doi.org/10.1016/j.radmeas.2015.02.017, 2015.

Heki, K., Miyazaki, S., Takahashi, H., Kasahara, M., Kimata, F., Miura, S., Vasilenko, N.F., Ivashchenko, A., and An, K.-D.: The Amurian Plate motion and current plate kinematics in eastern Asia, J. Geophys. Res., 104, 29, 147-29, 155, https://doi.org/10.1029/1999JB900295, 1999.

Hong, T. K., Lee, J., and Houng, S. E.: Long-term evolution of intraplate seismicity in stress shadows after a megathrust, Phys. Earth Planet. In., 245, 59–70, https://doi. org/10.1016/j.pepi.2015.05.009, 2015.

Hong, T. K., Lee, J., Park, S., and Kim, W.: Time-advanced occurrence of moderate-size earthquakes in a stable intraplate region after a megathrust earthquake and their seismic properties, Sci. Rep., 8, 13331, https://doi.org/10.1038/s41598-018-31600- 5, 2018.

Hong, Y., OH J.-S., Hong S.-C., and Shin J.: Geomorphological Development and Fault Activity of the Central-Southern Yangsan Fault (I): Developmental Characteristics and Distribution of the Quaternary Landforms, J. Korean Geomorphological Assoc., 28, 67-81. https://doi.org/10.16968/JKGA.28.1.67, 2021.

Hough, S., and Page, M.: Toward a consistent model for strain accrual and release for the New Madrid seismic zone, central United States, *J. Geophys. Res.*, 116, B03311. http://dx.doi.org/10.1029/2010JB007783, 2011.

Hough, S.E., Armbruster, J.G., Seeber, L., and Hough, J.F.: On the modified Mercalli intensities and magnitudes of the 1811–1812 New Madrid earthquakes, J. Geophys. Res., 105(B10), 23,839–23,864, https://doi.org/10.1029/2000JB900110, 2000.

Hwang, B.-H., Lee, J. D., and Yang, K.: Petrological study of the granitic rocks around the Yangsan Fault: Lateral displacement of the Yangsan Fault, J. Geol. Soc. Korea, 40, 161–178, 2004.

Hwang, B. H., Lee, J. D., Yang, K., and McWilliams, M.: Cenozoic strike-slip displacement along the Yangsan Fault, southeast Korean Peninsula, Int. Geol. Rev., 49, 768–775, https://doi.org/10.2747/0020-6814.49.8.768, 2007a.

Hwang, B. H., McWilliams, M., Son, M., and Yang, K.: Tectonic implication of A-type granites across the Yangsan Fault, Gigye and Gyeongju areas, southeast Korean Peninsula, Int. Geol. Rev., 49, 1094–1102, https://doi.org/10.2747/0020-6814.49.12.1094, 2007b.

Ikeya, M., Miki, T., and Tanaka, K.: Dating of a Fault by Electron Spin Resonance on Intrafault Materials, Science, 215, 1392-1393, https://doi.org/10.1126/science.215.4538.1392, 1982.

Jin, K., Kim, Y.-S., Kang, H.C. and Shin, H.C.: Study on developing characteristics of the Quaternary Gusan Fault in Uljin, Gyeongbuk, Korea, J. Geol. Soc. Korea, 49, 197-207, https://doi.org/10.14770/jgsk.2013.49.2.197, 2013.

Johnston, A.C., and Schweig, E.S.: The enigma of the New Madrid earthquakes of 1811–1812, Annu. Rev. Earth Pl. Sc., 24, 339-384, https://doi.org/10.1146/annurev.earth.24.1.339, 1996.

Kanamori, H.: The energy release in great earthquakes, J. Geophys. Res., 82, 2981–2987, https://doi.org.10.1029/JB082i020p02981, 1977.

Kang, H.-C., Cheon, Y., Ha, S., Seo, K., Kim, J.-S., Shin, H. C., and Son, M.: Geology and U-Pb Age in the Eastern Part of Yeongdeok-gun, Gyeongsangbuk-do, Korea, *J. Petrological Soc. Korea*, *27*, 153-171, https://doi.org/10.7854/JPSK.2018.27.3.15, 2018.

Kee, W.-S., Kim, Y.-H., Lee, H.-J., Choi, D.-L., Kim, B.-C., Song, K.-Y., Koh, H.-J., Lee, S.R., Yeon, Y.G., Hwang, S.-H., Sung, N.-H.: South eastern fault variable research and DB Construction, Korea Institute of Geoscience and Mineral Resources, Daejeon, 327 pp., 2009.

Khromovskikh, V. S.: Determination of magnitudes of ancient earthquakes from dimensions of observed seismodislocations, Tectonophysics, 166, 269-280, https://doi.org/10.1016/0040-1951(89)90219-9, 1989.

Kim, C.-M., Cheon, Y., Lee, T.-H., Choi, J.-H., Ha, S., and Jeong, J. O.: Long-Term Weakening Processes and Short-Term Seismic Slip Behavior of an Intraplate Mature Fault Zone: A Case Study of the Yangsan Fault, SE Korea, J. Geophys. Res-Sol Ea, 127, e2021JB023154, https://doi.org/10.1029/2021JB023154, 2022.

Kim, C.-M., Ha, S., and Son, M.: Evidence of coseismic slip recorded by Quaternary fault materials and microstructures, Naengsuri, Pohang, J. Geol. Soc. Korea, 56, 175-192, https://doi.org/10.14770/jgsk.2020.56.2.175, 2020a.

Kim, C.-M., Jeong, J. O., Gu, D., and Han, H.: Identification of materials in principal slip zones of faults by X-ray diffraction analysis using a small amount of sample, J. Geol. Soc. Korea, 53, 873-883, http://doi.org/10.14770/jgsk.2017.53.6.873, 2017a.

Kim, D.-E., and Seong. Y.B.: Cumulative Slip Rate of the Southern Yangsan Fault from Geomorphic Indicator and Numerical Dating, J. Kor. Geogr. Soc., 56, 201-213. https://doi.org/10.22776/KGS.2021.56.2.201, 2021.

Kim, D. E., and Oh. J.-S.: Landform Classification Using Geomorphons on the Middle Yangsan Fault System, Southeastern Korea, J. Korean Geogr. Soc., 54, 493-505, 2019.

Kim, D.H., Hwang, J.H., Park, K.H., and Song, K.Y.: Explanatory Note of The Pusan Sheet, 1:1:250,000, Korea Institute of Energy and Resources, Daejeon, 1998.

Kim, H.-U., and Bae, T.-S.: Monitoring of Possible Activities of Yangsan Fault Zone Using GNSS, Appl. Sci., 13, 1862, https://doi.org/10.3390/app13031862, 2023.

Kim, I.-S.: Origin and tectonic evolution of the East Sea (Sea of Japan) and the Yangsan fault system: a new synthetic interpretation, J. Geol. Soc. Korea, 28, 84-109, 1992.

Kim, K.-H., Ree, J.-H., Kim, Y., Kim, S., Kang, S.Y., and Seo, W.: Assessing whether the 2017 M_w 5.4 Pohang earthquake in South Korea was an induced event, Science, 360, 1007-1009, https://doi.org/10.1126/science.aat6081, 2018.

Kim, K.-H., Seo, W., Hang, J., Kwon, J., Kang, S.Y., Ree, J.-H., Kim, S., and Liu, K.: The 2017 M_L 5.4 Pohang earthquake sequence, Korea, recorded by a dense seismic network, Tectonophysics, 774, 228306, https://doi.org/10.1016/j.tecto.2019.228306, 2020b.

Kim, M.-C., Jung, S., Yoon, S., Jeong, R.-Y., Song, C.W., and Son, M.: Neotectonic crustal deformation and current stress field in the Korean Peninsula and Their Tectonic Implications: a review, J. Petrological Soc. Korea, 25, 169–193, https://doi.org/10.7854/JPSK.2016.25.3.169, 2016.

Kim, M.-J., and Lee, H.-K.: Long-term patterns of earthquakes influenced by climate change: Insights from earthquake recurrence and stress field changes across the Korean Peninsula during interglacial periods, Quaternary Sci. Rev., 321, 108369, https://doi.org/10.1016/j.quascirev.2023.108369, 2023

Kim, M.-J., and Lee, H.-W.: ESR dating of fault gouge - review, J. Geol. Soc. Korea, 56, 175-192, https://doi.org/10.14770/jgsk.2020.56.2.211, 2020.

Kim, N., Choi, J.-H., Park, S.-I., Lee, T.-H. and Choi, Y.: Cumulative offset analysis of the Central-Southern Yangsan Fault based on topography of Quaternary fluvial terrace, J. Geol. Soc. Korea, 56, 135-154, https://doi.org/10.14770/jgsk.2020.56.2.135, 2020c.

Kim, N., Park, S.-I., and Choi, J.-H.: Internal architecture and earthquake rupture behavior of a long-lived intraplate strike–slip fault: A case study from the Southern Yangsan Fault, Korea, Tectonophysics, 816, 229006, https://doi.org/10.1016/j.tecto.2021.229006, 2021.

Kim, T., Choi, J.-H., Cheon, Y., Lee, T.-H., Kim, N., Lee, H., Kim, C.-M., Choi, Y., Bae, H., Kim, S.-G., Ryoo, C.-R., and Klinger, Y.: Correlation of paleoearthquake records at multiple sites along the southern Yangsan Fault, Korea: Insights into rupture scenarios of intraplate strike-slip earthquakes, Tectonophysics, 854, 229817, https://doi.org/10.1016/j.tecto.2023.229817, 2023.

Kim, T., Lee, H., Kim, D. E., Choi, J. H., Choi, Y., Han, M., and Kim, Y. S.: Determination of the long-term slip rate of a fault in a slowly deforming region based on a reconstruction of the landform and provenance, Geomorphology, 461, 109286, https://doi.org/10.1016/j.geomorph.2024.109286, 2024.

~~Kim, Y. S. and Jin, K.: Estimated earthquake magnitude from the Yugye Fault displacement on a trench section in Pohang, SE Korea, J. Geol. Soc. Korea, 42, 79-94, 2006.~~

Kim, Y.-S., Jin, K., Choi, W.-H., and Kee, W.-S.: Understanding of active faults: A review for recent researches, J. Geol. Soc. Korea. 47, 723-752, 2011~~a~~.

~~Kim, Y. S., Kihm, J. H., and Jin, K.: Interpretation of the rupture history of a low slip rate active fault by analysis of progressive displacement accumulation: an example from the Quaternary Eupcheon Fault, SE Korea, J. Geol. Soc., 168, 273-288, https://doi.org/10.1144/0016-76492010-088, 2011b.~~

Kim, Y.-S., Kim, T., Kyung, J. B., Cho, C. S., Choi, J.-H., Choi, C. U.: Preliminary study on rupture mechanism of the 9.12 Gyeongju Earthquake, J. Geol. Soc. Korea, 53, 407-422, https://doi.org.10.14770/jgsk.2017.53.3.407, 2017b.

Ko, K., Choi, S.-J., Lee, T.-H., Gihm, Y. S., Kim, C.-M., Kim, K., and Cheon, Y.: A multidisciplinary approach to characterization of the mature northern Yangsan fault in Korea and its active faulting, Mar. Geophys. Res., 43, 21, https://doi.org/10.1007/s11001-022-09486-w, 2022.

Korea Meteorological Administration: 2022 yearbook, Korea Meteorological Administration, Seoul, 416 pp., 2022. Retrieved from https://www.kma.go.kr (archived on 6/March/2023).

Kreutzer, S.: calc_FadingCorr(): Apply a fading correction according to Huntley and Lamothe (2001) for a given g-value and a given tc. Function version 0.4.3, in Luminescence, edited by Kreutzer, S., Burow, C., Dietze, M., Fuchs, M.C., Schmidt, C., Fischer, M., Friedrich, J., Mercier, N., Philippe, A., Riedesel, S., Autzen, M., Mittelstrass, D., Gray, H.J., and Galharret, J.,

Comprehensive Luminescence Dating Data Analysis R package version 0.9.23, available at https://CRAN.R-project.org/package=Luminescence (last access: January 2024), 2023.

Kuwahara, Y., Choi, J.-H., Cheon, Y., and Imanishi, K.: Dependence of earthquake faulting type on fault strike across the Korean Peninsula: Evidence for weak faults and comparison with the Japanese Archipelago, Tectonophysics, 804, 228757, https://doi.org/10.1016/j.tecto.2021.228757, 2021.

~~Kyung, J. B.: Paleoseismological study and evaluation of maximum earthquake magnitude along the Yangsan and Ulsan Fault Zones in the Southeastern Part of Korea, Geophysics Geophys. Explor., 13, 187–197, 2010.~~

Kyung, J.B.: Paleoseismology of the Yangsan Fault, southeastern part of the Korean Peninsula, Ann. Geophys., 46, 983-996, http://hdl.handle.net/2122/999, 2003.

Lal, D.: Cosmic ray labeling of erosion surfaces: in situ nuclide production rates and erosion models, Earth Planet. Sc. Lett., 104, 424–439, https://doi.org/10.1016/0012-821X(91)90220-C, 1991.

Lee, C. H., Seong Y. B., Oh, J.-S., Kim. D. E.: Tectonic Geomorphology on Yugye-Bogyeongsa Area of Yangsan Fault Zone, J. Korean Geomorphological Assoc., 26, 93-106, https://doi.org/10.16968/JKGA.26.1.93, 2019.

Lee, H.-K., and Schwarcz, H. P.: ESR dating of the subsidiary faults in the Yangsan Fault System, Korea, Quaternary Sci. Rev., 20, 999–1003, https://doi.org/10.1016/S0277-3791(00)00055-X, 2001.

Lee, H.K., and Yang, J.S.: ESR dating of the Eupchon fault, south Korea, Quat. Geochronol., 2, 392–397, https://doi.org/10.1016/j.quageo.2006.04.009, 2003.

Lee, J., Rezaei, S., Hong, Y., Choi, J.-H., Choi, J.-H., Choi, W.-H., Rhee, K.-W., and Kim, Y.-S.: Quaternary fault analysis through a trench investigation on the northern extension of the Yangsan fault at Dangu-ri, Gyungju-si, Gyeongsangbuk-do, J. Geol. Soc. Korea, 51, 471-485, https://doi.org.10.14770/jgsk.2015.51.5.471, 2015.

Lee, K.: Historical earthquake data of Korean. J. Korea Geophys. Soc. 1, 3-22, 1998.

Lee, K., and Yang, W.-S.: Historical Seismicity of Korea, B.Seismol. Soc. Am., 96, 846-855, https://doi.org/10.1785/0120050050, 2006.

Lee, S.: Characteristics of the Quaternary Faults in SE Korea: Insight from the Yangsan Fault and Gokgang Fault, Ph.D. thesis, Pusan National University, Korea, 184 pp., 2023.

Lee, S., Han, J., Ha, S., Lim, H., Seong, Y. B., Choi, J.-H., Lee, C. H., Kim, S.-J., Kang, H.-C., Kim, M.-C., Lim, H., and Son, M.: Characteristics of the Quaternary faulting detected along the Yangsan Fault in Yugye- and Jungsan-ri, northern Pohang City, J. Geol. Soc. Korea, 58, 427-443, http://doi.org.10.14770/jgsk.2022.58.4.427, 2022.

Lee, Y., Cheon, Y., Ha, S., Kang, H.-C., Choi, J.-H., and Son, M.: Geometric and kinematic characteristics of the Quaternary fault at Seooe site, in Goseong-gun, Gyeongsangnam-do, J. Geol. Soc. Korea, 53, 115-127, https://doi.org/10.14770/jgsk.2017.53.1.115, 2017.

Lim, H., Ha, S., Ryoo, C.-R., Lee, T.-H., and Son, M.: Evidence of surface rupture in the southernmost part of the Yangsan fault and deterministic seismic hazard assessment: in the Busan metropolitan area, in: 76th Annual Meeting of the Geological Society of Korea and 2021 Fall Joint Conference of the Geological Sciences, Jeju, Korea, 26-28 October 2021, 275, 2021.

Liu, J., Ren, Z., Min, W., Ha, G., and Lei, J.: The advance in obtaining fault slip rate of strike slip fault-A review. Earthq. Res. Adv., 1, 100032. https://doi.org/10.1016/j.eqrea.2021.100032, 2021.

Liu, M., and Stein, S.: Mid-continental earthquakes: Spatiotemporal occurrences, causes, and hazards, Earth-Sci. Rev., 162, 364–386, https://doi.org/10.1016/j.earscirev.2016.09.016, 2016.

Mason, D.B.: Earthquake magnitude potential of the Intermountain Seismic Belt, USA, from surface-parameter scaling of late Quaternary faults. B. Seismol. Soc. Am., 86, 1487–1506, https://doi.org/10.1785/BSSA0860051487, 1996.

McCalpin, J.P.: Application of Paleoseismic Data to Seismic Hazard Assessment and Neotectonic Research, in: Paleoseismology, 2nd ed., edited by McCalpin, J.P., Academic Press-Elsevier, Burlington, USA, 1–106, https://doi.org/10.1016/S0074-6142(09)95009-4, 2009.

Min, Z., Hu, G., Jiang, X., Liu, S., and Yang, Y.: Catalog of Chinese Historic Strong Earthquakes From 23 AD to 1911, Seismological Press, Beijing, China, 514 pp., 1995.

Murray, A. S., and Wintle, A. G.: Luminescence dating of quartz using an improved single-aliquot regenerative-dose protocol, Radiat. Meas., 32, 57-73, https://doi.org/10.1016/S1350-4487(99)00253-X, 2000.

Murray, J., and Langbein, J.: Slip on the San Andreas Fault at Parkfield, California, over Two Earthquake Cycles, and the Implications for Seismic Hazard, B.Seismol. Soc. Am., 96, S283–S303, https://doi.org/10.1785/0120050820, 2006.

Naik, S. P., Rockwell, T. K., Jeong, S. H., Kim, Y. S., Shin, H. C., Choi, J. H., Ha, S., and Son, M.: Evidence for large Holocene earthquakes along the Yangsan fault in the SE Korean Peninsula revealed in three-dimensional paleoseismic trenches, Geol. Soc. Am. Bull., online publication, https://doi.org/10.1130/B37275.1, 2024.

O'Neill, C., Müller, D., and Steinberger, B.: On the uncertainties in hot spot reconstructions and the significance of moving hot spot reference frames, Geochem. Geophy. Geosy., 6, https://doi.org/10.1029/2004GC000784, 2005.

Obara, K., and Kato, A.: Connecting slow earthquakes to huge earthquakes. Science, 353, 6296, https://doi.org/10.1126/science.aaf1512, 2016.

Park, C., and Lee, G.: Analysis on Fault-Related Landforms in the Gyeongju Area of the Yangsan Fault Valley, J. Korean Geomorphological Assoc., 25, 19-30, https://doi.org.-/10.16968/JKGA.25.1.19, 2018.

Park, Y., Ree, J.-H., and Yoo, S.-H.: Fault slip analysis of Quaternary faults in southeastern Korea, Gondwana Res., 9, 118–125, https://doi.org/10.1016/j.gr.2005.06.007, 2006.

Patyniak, M., Landgraf, A., Dzhumabaeva, A., Abdrakhmatov, K. E., Rosenwinkel, S., Korup, O., Preusser, F., Fohmeister, J., Arrowsmith, J.R., and Strecker, M. R.: Paleoseismic record of three Holocene earthquakes rupturing the Issyk-Ata fault near Bishkek, North Kyrgyzstan, Bull. Seismol. Soc. Am., 107, 2721-2737, https://doi.org/10.1785/0120170083, 2017.

Powell, R. E., and Weldon II, R. J.: Evolution of the San Andreas fault, Annu. Rev. Earth Pl. Sc., 20, 431-468, https://doi.org/10.1146/annurev.ea.20.050192.002243, 1992.

Reimer, P., Austin, W., Bard, E., Bayliss, A., Blackwell, P., Bronk Ramsey, C., and Talamo, S.: The IntCal20 Northern Hemisphere Radiocarbon Age Calibration Curve (0–55 cal kBP), Radiocarbon, 62, 725–757, https://doi.org/10.1017/RDC.2020.41, 2020.

Reiter, L.: Earthquake Hazard Analysis: Issue and Insights. Columbia University Press, New York, USA, 254 pp., 1990.

Ryoo, C.-R., and Cheon, Y.: Characteristics of the Main Fault Zone Developed Along Yangsan Fault: On the Outcrop of Cheonjeon-ri, Dudong-myeon, Ulju-gun, Ulsan, Korea, J. Petrological Soc. Korea, 28, 347-357, https://doi.org/10.7854/JPSK.2019.28.4.347, 2019.

Ryoo, C.-R., Lee, B.-J., Cho, D.-L., Chwae, U.-C., Choi, S.-J., and Kim J.-Y.: Quaternary fault of Dangu-ri in Gyeongju Gangdong-myeon: Byeokgye Fault, in: Spring Joint Conference on East-North Asia Ore deposit of Cause of Formation, The Korean Society of Economic and Environmental Geology/The Korean Society of Mineral and Energy Resources Engineers/Korean Society of Earth and Exploration Geophysicists, 1999.

Sadler, P.: The Influence of Hiatuses on Sediment Accumulation Rates, GeoResearch Forum, 5, 15-40, 1999.

Schellart, W. P., and Rawlinson, N.: Convergent plate margin dynamics: New perspectives from structural geology, geophysics and geodynamic modelling, Tectonophysics, 483, 4-19, https://doi.org/10.1016/j.tecto.2009.08.030, 2010.

Seno, T., Sakurai, T., and Stein, S.: Can the Okhotsk plate be discriminated from the North American plate?, J. Geophys. Res.- Sol. Ea., 101(B5), 11305-11315, https://doi.org/10.1029/96JB00532, 1996.

Seno, T., Stein, S., and Gripp, A. E.: A model for the motion of the Philippine Sea plate consistent with NUVEL-1 and geological data, J. Geophys. Res.- Sol. Ea., 98(B10), 17941-17948, https://doi.org/10.1029/93JB00782, 1993.

Shimazaki, K., and Nakata, T.: Time-predictable recurrence model for large earthquakes, Geophys. Res. Lett., 7, 279-282, https://doi.org/10.1029/GL007i004p00279, 1980.

Sim, H., Song, Y., Son, M., Park, C., and Choi, W.: Reactivated Timings of Yangsan Fault in the Northern Pohang Area, Korea, Econ. Environ. Geol., 50, 97-104, https://doi.org/10.9719/EEG.2017.50.2.97, 2017.

Smith, B. R., and Sandwell, D. T.: A model of the earthquake cycle along the San Andreas Fault System for the past 1000 years, J. Geophys. Res., 111, B01405. https://doi.org/10.1029/2005JB003703, 2006.

Sohn, D.-H., Choi, B.-K., Kim, S., Park, S.-C., Lee, W.-J., and Park, P.-H.: Decaying Post-Seismic Deformation Observed on the Korean Peninsula Following the 2011 Tohoku-Oki Earthquake, Sensors, 21, 4493, https://doi.org/10.3390/s21134493, 2021.

Son, M., Song, C.W., Kim, M.-C., Cheon, Y., Cho, H., and Sohn, Y.K.: Miocene tectonic evolution of the basins and fault systems, SE Korea: dextral, simple shear during the East Sea (Sea of Japan) opening, J. Geol. Soc. London, 172, 664-680, https://doi.org/10.1144/jgs2014-079, 2015.

Song, C.W.: Study on the evolution of the Miocene Pohang Basin based on its structural characteristics, Ph.D. thesis, Pusan National University, Korea, 146 pp., 2015.

Song, Y., Ha, S., Lee, S., Kang, H.-C., Choi, J.-H., and Son, M.: Quaternary structural characteristics and paleoseismic interpretation of the Yangsan Fault at Dangu-ri, Gyeongju-si, SE Korea, through trench survey, *J. Geol.Soc. Korea*, *56*, 155–173, https://doi.org/10.14770/jgsk.2020.56.2.155, 2020.

Song, Y., Park, C., Sim, H., Choi, W., and Son, M.: Reactivated Timings of Yangsan Fault in the Sangcheon-ri Area, Korea, Econ. Environ. Geol., 49, 97-104, https://doi.org/10.9719/EEG.2016.49.2.97, 2016.

Song, Y., Sim, H., Hong, S., and Son, M.: K-Ar Age-dating Results of Some Major Faults in the Gyeongsang Basin: Spatio-temporal Variability of Fault Activations during the Cenozoic Era, Econ. Environ. Geol., 52, 449-457, https://doi.org/10.9719/EEG.2019.52.5.449, 2019.

Suzuki, Y., Nakata, T., Watanabe, M., Battulga, S., Enkhtaivan, D., Demberel, S., Odonbaatar, C., Bayasgalan, A., and Badral, T.: Discovery of Ulaanbaatar Fault: A new earthquake threat to the capital of Mongolia, Seismol. Soc. Am., 92, 437-447, https://doi.org/10.1785/0220200109, 2021.

Talwani, P.: On the nature of intraplate earthquakes, J. Seismol., 21, 47-68, https://doi.org/10.1007/s10950-016-9582-8, 2017.

Uchida, N., and Burgmann, R.: Repeating Earthquakes, Annu. Rev. Earth Pl. Sc., 47, 305–332, https://doi.org/10.1146/annurev-earth-053018-060119, 2019.

Wells, D. L., and Coppersmith, K. J.: New empirical relationships among magnitude, rupture length, rupture width, rupture area, and surface displacement, B. Seismol. Soc. Am., 84, 974–1002, https://doi.org/10.1785/BSSA0840040974, 1994.

~~Williams, R.T., Goodwin, L.B., Sharp, W.D. and Mozley, O.S.: Reading a 400,000 year record of earthquake frequency for an intraplate fault, P. Natl. Acad. Sci. USA, 114, 4893–4898. https://doi.org/10.1073/pnas.1617945114, 2017.~~

Woith, H., Petersen G.M., Hainzl, S., and Dahm, T.: Review: Can Animals Predict Earthquakes?, B. Seismol. Soc. Am., 108, 1031–1045, https://doi.org/10.1785/0120170313, 2018.

Wolin, E., Stein, S., Pazzaglia, F., Meltzer, A., Kafka, A., and Berti, C.: Mineral, Virginia, earthquake illustrates seismicity of a passive-aggressive margin, Geophys. Res. Lett., 39, L02305, https://doi.org/10.1029/2011GL050310, 2012.

Woo, J.-U., Rhie, J., Kim, S., Kang, T.-S., Kim, K.-H., and Kim, Y.H.: The 2016 Gyeongju earthquake sequence revisited: aftershock interactions within a complex fault system, Geophys. J. Int., 217, 58–74, https://doi.org/10.1093/gji/ggz009, 2019.

Woo, S., Lee, H., Han,R., Chon, C.-M., Son, M., and Song, I.: Frictional properties of gouges collected from the Yangsan Fault, SE Korea. J. Geol. Soc. Korea, 51, 569-584, https://doi.org//10.14770/jgsk.2015.51.6.569, 2015.

Wyss, M.: Cannot Earthquakes Be Predicted?, Science, 278, 487-490, https://doi.org/10.1126/science.278.5337.48, 1997.

Xu, S., Nieto-Samaniego, A.F., and Alaniz-Àlvarez, S.A.: Quantification of true displacement using apparent displacement along an arbitrary line on a fault plane, Tectonophysics, 467, 107-118, https://doi.org/10.1016/j.tecto.2008.12.004, 2009.

Yang, J.-S., and Lee, H.-K.: ESR dating of fault gouge from the Gacheon 1 site on the Yangsan fault zone, J. Geol. Soc. Korea, 48, 459-472, 2012.

Yang, J. S., and Lee, H. K.: Quaternary Fault Activity of the Yangsan Fault Zone in the Samnam-myeon, Ulju-gun, Ulsan, Korea, Econ. Environ. Geol., 47, 17-27, https://doi.org/10.9719/EEG.2014.47.1.17, 2014.